Reviews in Mineralogy & Geochemistry
Vol. 88 pp. 307-392, 2022

Mineral Inclusions in Lithospheric Diamonds

Thomas Stachel
Earth and Atmospheric Sciences
University of Alberta
Edmonton, AB, Canada
tstachel@ualberta.ca

Sonja Aulbach
Institut für Geowissenschaften
Goethe Universität Frankfurt
Frankfurt am Main, Germany
s.aulbach@em.uni-frankfurt.de

Jeffrey W. Harris
School of Geographical and Earth Sciences
University of Glasgow
Glasgow, UK
Jeff.Harris@glasgow.ac.uk

INTRODUCTION

Initially, it may seem extremely daunting to be sitting in front of several thousand carats of small diamonds, knowing that the likelihood of finding a diamond with a meaningful inclusion is about 1% of that parcel. Like other events in life, however, the joy of finding such material soon outweighs the perceived hardship. Mineral inclusions in diamond provide unique and pristine information about inner Earth, from depths of about 120 to just over 800 km and over 3.5 to 0.1 billion years of Earth history. Such is the scope and importance of inclusion research.

Once the inclusion-bearing diamonds have been collected, hopefully from a known source, an intricate set of procedures falls into place. A microscopic description of the physical features of the diamond and its valuable cargo are needed, a preliminary paragenesis is assigned based on inclusion color, and both diamond and inclusion are photographed in detail. Then comes the release of the µm-sized inclusion by crushing of the diamond host, the hope being that the mineral is recovered in one piece, an infrequent event. The next stage is mounting in epoxy and polishing, minimizing rounding of the inclusion surface *en route* to quarter µm perfection. When this stage is complete, the researcher can afford to relax as modern-day analytical techniques are non-destructive (electron microprobe) or dig only small holes in the perfect inclusion surface (ion microprobe and to a lesser degree, laser ablation-based micro-sampling).

In this chapter, we present results of the above procedures for minerals included in diamonds that originate in the lithospheric mantle. A comprehensive review of the mineral chemistry of inclusions, based on an already largely saturated database of almost 5000 inclusion analyses, was previously presented by Stachel and Harris (2008) and is not repeated here. Instead, the two main sections of the review focus on detailed comparisons of the major and trace element compositions of peridotitic and eclogitic suite inclusions with the equivalent minerals in cratonic xenoliths.

1529-6466/22/0088-0006$10.00 (print)
1943-2666/22/0088-0006$10.00 (online)
http://dx.doi.org/10.2138/rmg.2022.88.06

A history of inclusion discovery in lithospheric diamonds

When John Evelyn was advised by his parents in 1642 that an extended European tour would be better than fighting on the Royalist's side in the English Civil War (1642–1651), a connection between this sojourn and the probable first description of a mineral inclusion in diamond might be considered distinctly tenuous. Nevertheless, on Friday, September 29th, 1645 his diary records that he was in Venice and he wrote, "I went to see the collection of a noble Venetian Signor Rugini: he has a stately Palace richly furnished, …. but above all was a diamond which had growing in it a faire ruby" (de Beer 1955). It is not surprising that he identified a ruby, a mineral known from ancient times. However, since ruby is exceptionally rare as an inclusion in diamond, the inclusion was most likely a peridotitic garnet.

Another 17th century traveler, Jean Baptist Tavernier, noted black material in some Indian diamonds he bought, referring to them as "l'herbe pourrie", translated as either "rotten weed" or "decomposed vegetable matter" (Tavernier 1676). The burning of a diamond by Lavoisier in 1772 and similar quantitative experiments with charcoal convinced the French scientist that these two substances were distinct forms of carbon. When graphite was further shown to be a third form of carbon, the origin and formation of diamond was linked to processes involving biogenic matter and gases, a concept that lasted for most of the 19th century. Göppert (1864) outlines the beliefs of over twenty scientists published between 1816 and 1860. The majority view was that diamond formation was linked to biogenic matter, although water, topaz and gold were surmised as other inclusions. One author had a different view, suggesting that diamond formation was the result of compression of carbonic acid in Earth, which caused carbon to crystallize as diamond. This rather perceptive view of diamond formation was not appreciated by the monograph's author, a botanist and paleontologist. Brewster (1861) examined fifty Indian diamonds and remarked that some had small cavities having "shapes that resembled those of insects and lobsters" (see below).

If one steps back in time for a moment and assumes a scientific knowledge base of the mid-19th century, Figures 1 to 4 illustrate what the early scientists may have been looking at. Figure 1 shows graphite clusters in a diamond from Sierra Leone exhibiting a 'plant-like' impression. The realistic, encapsulated flying insect inclusion in Figure 2 is from the Karowe Mine in Botswana, the head and feelers being the result of some minute inclusion, which also caused two disproportionately large graphite-filled cleavage fractures to create the wings. The very rounded outline of the clear inclusion in Figure 3 might easily confirm the presence of water or gas within that diamond. Finally, Figure 4 would reinforce some of these initial observations as vegetable matter (graphite flakes) occurring on the interfacial surfaces between the water or gas inclusions and the diamond.

With the discovery of the first primary diamond deposits in South Africa in 1870, inclusion identification was still by observation only, and the new igneous environment did not have an immediate impact on research thinking. Boutan (1886) divided inclusions into crystalline and non-crystalline, and post-1870 research proposed hematite (iron glance), ilmenite and pyrite as inclusions. Lewis and Bonney (1897) considered that compressed gas was responsible for the common yellow color of diamonds from Kimberley. Bauer (1904) believed he had recognized fluid enclosures in diamond and, from their behavior when heated, considered the liquid to consist of either carbon dioxide and water or a saline solution. They also mention diamond as an inclusion.

With a new century came the understanding that the minerals found in diamond were linked to the mineralogy of the kimberlite rock and its xenoliths. In perhaps the shortest letter ever to be published in the periodical Nature (14 column lines long), Sutton (1907) reasonably argued the first identification of garnet (color unspecified) inside a South African diamond. Additionally, refractive index work on inclusions by Wagner (1914) identified pyrope and

Figure 1. An octahedral diamond from Sierra Leone showing a graphite cluster in the central portion of the diamond.

Figure 2. An 'insect'-shaped inclusion in a Botswana diamond. See text for details.

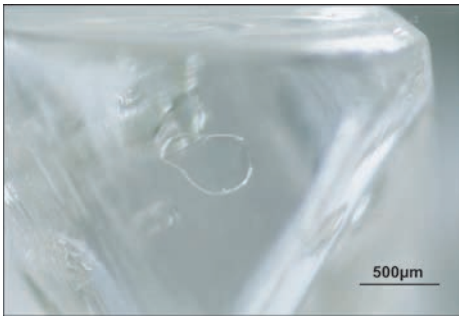

Figure 3. The rounded nature of this colorless inclusion might easily be considered as a liquid by a 19th century observer.

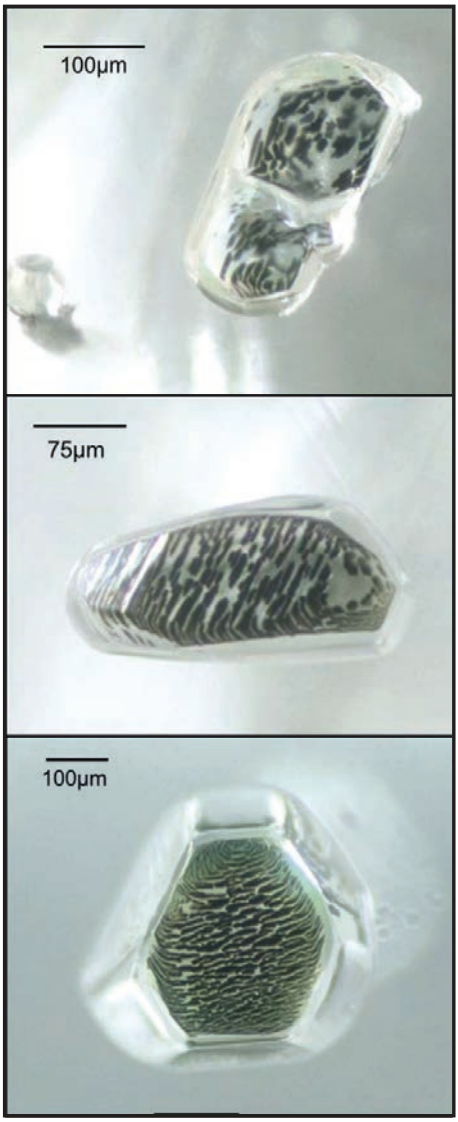

Figure 4. The presence of graphite crystals on {111} diamond/inclusion interfaces may have helped reinforce the presence of 'vegetable matter' in diamond to early inclusion researchers.

recorded the presence of (chrome) diopside in a diamond. Sutton (1921) listed garnet, ilmenite, pyrite, and mentions olivine for the first time as definite inclusions and notes zircon, mica and cognate graphite as probable inclusions. Sutton also studied epigenetic material in diamond fractures proposing calcite, an apophyllite mineral and pectolite. Magnetite was identified as an inclusion by Spencer (1924). The book on diamonds by Williams (1932) listed the known inclusion minerals up to that time and provided clear evidence of diamond as an inclusion: a mauve stone embedded in a colorless one. Williams concludes, as might be expected from the evidence at hand, that diamond was a phenocryst in kimberlite.

The first color micro-photographs of a suite of inclusions, mostly in polished diamonds, were described by Gübelin (1952). The inclusion in the sixth diamond in the color set likely resolves why zircons were commonly noted by previous authors as an inclusion in diamond, as the color of that mineral looks very much like the typical pale orange of an eclogitic garnet. The connection to zircon may also have been influenced by the typical honey color of zircons recovered from kimberlite heavy media concentrate. Two colorless inclusions were visually identified as quartz, a rare mineral in diamond, though they were likely the much more commonly found colorless mineral, olivine. Apart from crystalline inclusions, this work also captured photographic detail of fractures within diamonds containing dark/black material. For example, what the author called hematite 'iron-roses' look very much like typical sulfide inclusions within their rosette fractures. Graphite was identified by experiment, but much of the other dark material was considered as original magma. There were also observations and descriptions about diamond and cloud-like masses as inclusions.

Diamonds containing clouds were specifically examined by Giardini and Melton (1975). Similar to Gübelin, these authors considered such inclusions as gaseous. This is because the four, six or twelve sided cavities of 1 to 5 μm size contained no solid material when broken or polished through. Subsequent studies have shown this not to be the case (Weiss et al. 2022). Clouds range in color from white to mid-grey with an overall shape that can be irregular but is more often distinctly cuboid or star-shaped and visually aligned with the shape of the diamond. In the first case, the sides of the cube are aligned at right-angles to the fourfold direction of the diamond and in the second orientation, the six arms of the star cloud end at the apices of the octahedron, if that is the enclosing diamond shape.

The identification of an olivine inclusion by Mitchell and Giardini (1953) using X-ray diffraction techniques quickly developed into the principal way of defining inclusions in diamond. Orlov (1959) and Futergendler (1960) used this procedure to document the newly discovered (in 1954) Siberian diamonds, and the latter author reviewed her inclusion work over the second half of the 1950s. Futergendler first identified enstatite and chrome spinel, and from both authors other documented inclusions were olivine, chrome diopside, garnet and diamond. With Orlov, some cell parameters and refractive indices are given and inclusions are divided into syngenetic and epigenetic, the latter being serpentine, as a pseudomorph after olivine, red quartz and red iron hydroxide both filling diamond fractures. Much of Orlov's inclusion work can be found in his translated book (Orlov 1977). Also, orientation studies between diamond and some of the principal inclusions were developed by Futergendler and Frank-Kamenetsky (1961), a subject fully considered in Angel et al. (2022).

Eppler (1961) studied the specific gravity and refractive indexes of some inclusions. From the associated description to his Figure 4, the previously common descriptions of ilmenite as an inclusion are most likely chrome spinel. Also identified were a high Mg# (molar 100Mg/(Mg+Fe)) olivine, a garnet of a composition approaching pyrope, the aforementioned ilmenite (likely chrome spinel) and apatite. He also remarked upon gaseous cloud-like inclusions, black expansion fractures around minerals, and considered that graphite and quartz were not likely inclusions.

From large batches of diamond samples from all the South African mines then operated by De Beers (and with one stone from the DRC), Sharp (1966) selected 89 diamonds containing black inclusions. After diamond crushing, brassy-colored non-diamond material was collected and individually examined by X-ray powder diffraction. Apart from a single cohenite (from a Jagersfontein diamond), pyrrhotite was identified as the dominant phase. Cell parameters indicated that two inclusions were nearly stoichiometric (i.e., showed no Fe deficiency) and therefore troilite. Most of the identified specimens were intergrown with pentlandite and to a lesser extent pyrite. Although there was some uncertainty about whether pyrite was primary, Sharp (1966) had found most of the minerals in the typical sub-solidus re-equilibration sequence of sulfide inclusions in diamond.

Harris (1968a,b) outlined criteria for recognizing whether inclusions in diamond were syngenetic or epigenetic. These works were based principally on the nature of the inclusions and their response to X-rays. Of the syngenetic inclusions, rutile and coesite were new identifications along with a dispersed dark cloud of microcrystalline olivine. Epigenetic inclusions were grouped into pseudomorphs after primary inclusions (goethite, quartz and possibly mica), fractures surrounding inclusions (graphite, pyrrhotite and pentlandite), and material in surface fractures (calcite, hematite, kaolinite, sellaite and xenotime).

Although commercial electron microprobe analyzers (EMPA) were available from the late 1950s, their use in determining the chemistry of inclusions in diamond only began in the late 1960s. This development essentially eliminated the need for X-ray techniques in inclusion recognition and came at a time when there was a growing awareness of the mineralogical and chemical links between inclusions in diamond and the equivalent minerals in peridotitic and eclogitic xenoliths found in kimberlites. The earliest EMPA study was completed by Meyer (1968), on a suite of inclusion garnets. Subsequent work by Meyer and Boyd (1972) separated garnets into peridotitic and eclogitic types, with inclusion assemblages further emphasizing the two principal growth environments for diamond. At this time, EMPA did not find many new inclusion minerals, although kyanite, ilmenite and zircon are examples, but instead rather precisely defined the chemistry of the existing mineralogies.

During the 1970s two major inclusion research centres emerged, one in South Africa through John Gurney at the University of Cape Town, the other through Nick Sobolev at the Siberian Branch of the Russian Academy of Sciences in Novosibirsk. Part of the inclusion research at Cape Town was linked to a prospecting program established by De Beers Consolidated Mines (organized by Barry Hawthorne and managed by Jeff Harris), who, over a ten-year period starting in 1970/71, provided representative inclusions for analysis from each of the De Beers mines in South Africa and Botswana. Similar independent inclusion studies were conducted in Novosibirsk on diamonds from the developing Siberian mines and linked to xenolith and xenocryst studies, providing important new insights into the crystal chemistry of inclusions. Much of the work on southern African localities, but also studies from other localities around the world, can be found in the 1st to 4th IKC Proceedings volumes (1975–1989 and references therein), where, for example, such rare inclusions as kyanite, sanidine, albite, phlogopite, zircon and moissanite are identified by EMPA and linked to a diamond paragenesis. Much of the early results of the Novosibirsk group were reviewed in a seminal book by Sobolev (1977; translated from the Russian edition of 1974).

With the southern African work, additional projects involving inclusions were set in place. For example, one was the determination of inclusion abundance tables and the relationship between inclusions and specific diamond shapes for some of the mines (Harris and Gurney 1979). A second project led to the first successful determination of genesis ages for diamond. Although by the mid-to-late 70s the eruption ages of several diamondiferous kimberlites were known (Davis 1977), the question still remained as to whether diamond was a phenocryst or xenocryst in the rock that brought it to the surface. The purity of diamond excluded any kind of dating analysis but the visual characteristics of the inclusions indicated a probably syngenetic growth with the diamond, and some of those minerals contained radioactive isotopes. Whilst the first studies used U–Pb in sulfides (Welke et al. 1974; Kramers 1979), the most successful work was started by Richardson et al. (1984), by determining the Sm–Nd isotopes in aliquoted harzburgitic garnet inclusions from the De Beers Pool and Finsch mines in South Africa. This work showed beyond doubt that diamonds were xenocrysts in kimberlite and easily justified the collection of 200 inclusion-bearing diamonds from both sources for the analyses. The Sm–Nd chronometer was then applied to date separate aliquots of eclogitic garnet and clinopyroxene inclusions (Richardson 1986) and, over the subsequent 20 years, to determine diamond ages in southern Africa, Russia and Australia (reviewed in Smit et al. 2022). With the considerable improvement in analytical precision, the Sm–Nd dating technique can now obtain an age from an array formed by single garnet or clinopyroxene inclusions (Koornneef et al. 2017; Gress et al. 2021).

Other dating techniques followed; the principal one being Re–Os isotopes from sulfide inclusions, first developed by Pearson et al. (1998) in diamonds from the Koffiefontein mine in South Africa specifically to date single diamonds. Results confirmed a xenocrystal origin for diamond but also, where comparison was possible, gave similar ages to those obtained from the silicates, indicating that the common dates were not coincidences (see Table 9 in Stachel and Harris 2008). The use of Ar–Ar isotopes from peridotitic or eclogitic clinopyroxene inclusions, although initially considered to be a genesis dating technique (see Burgess et al. 1989), became more useful in determining diamond eruption ages, with particular importance in diamond prospecting (see, for example, Phillips et al. 2018).

From the mid-1980s, therefore, not only had many different inclusion minerals been assigned to the peridotitic and eclogitic growth environments, or to the minor websteritic suite (Gurney et al. 1984), but also, inclusions were providing important information about mantle evolution. A significant consequence of the first two diamond dating programs, for example, was that the results generally correlated with tectonothermal events which had affected the lithospheric mantle where the diamonds occurred; a subject more fully considered by Smit et al. (2022). Also, the discovery and subsequent study of eclogitic inclusions in lamproite-hosted diamonds at Argyle, in Australia (Sobolev 1985, Jaques et al. 1989) led to the first proposal that the mantle source for a predominantly eclogitic diamond deposit was generated during subduction (in this case along the Kimberley Craton margin). Additionally, inclusion chemistry linked to HPHT experimental work enabled the temperature and pressure of inclusion formation to be determined (see Boyd and Gurney 1986; Nimis 2022), and broader inclusion studies began to explore the relationship between mineralogy and particularly the chemistry of inclusions and the carbon and nitrogen isotopes and nitrogen abundances of the host diamonds (see Stachel et al. 2022).

Returning specifically to the inclusions, a significant review of the two principal parageneses was provided by Meyer (1987) and for all three parageneses by Stachel and Harris (2008). Examples of further studies that have added to our inclusion knowledge are the finding of rare single crystals of primary graphite in diamond from the Panda kimberlite in Canada (Glinnemann et al. 2003) and a thorough study of rare phlogophite inclusions, identified in peridotitic and eclogitic diamonds from Siberia, Arkhangelsk and Venezuela (Sobolev et al. 2009). Thus, inclusions in diamonds seemed to firmly place diamond genesis in the subcratonic lithospheric mantle.

However, after four crystalline isotropic reddish-brown inclusions of magnesio-wüstite (now more commonly called ferropericlase) were recovered from four diamonds from the Koffiefontein mine in South Africa in the early 1970s (later studied by Cardoso 1980), this belief began to be queried. It was the recovery of a lower mantle inclusion assemblage of low-nickel enstatite (retrogressed bridgmanite) and a ferropericlase in a single diamond from the Orroroo kimberlite dykes in South Australia (Scott Smith et al. 1984) that established a whole new dimension to studies of inclusions in diamond. Thus were born sublithospheric and lower mantle diamond studies, a subject covered by Walter et al. (2022).

In conclusion to this historical overview of cratonic diamonds the reader is referred to Table 1, which updates the inclusion compilation of Stachel (2014) with subsequent discoveries.

The inclusion–diamond relationship

The research on the geochemistry of inclusions in diamond captured in the database underpinning this review generally relied on sampling of run-of-mine diamonds between 1.8 and 3.5 mm in size (corresponding to round aperture Diamond Trading Company (DTC) sieve sizes +5 to −11), although in some rare instances inclusions were recovered from diamonds

measuring less than 1.1 mm (DTC sieve size –1; e.g., Stachel et al. 2006). Based on the examination of over 1 million diamonds ~2 mm in size mined from nine kimberlites in South Africa and Botswana, the abundance of diamonds with visually identifiable mineral inclusions is 1.0% (see Table 1 of Stachel and Harris 2008). The size of studied mineral inclusions commonly is about 100 μm in longest dimension, although there are exceptions both to smaller and larger sizes. Our observations suggest an only minor increase in inclusion size towards larger diamonds and for the same inclusion mineral, the chemical composition does not significantly change with diamond size.

Disequilibrium among non-touching inclusions is occasionally observed, reflecting incorporation during diamond growth in chemically evolving environments (e.g., Griffin et al. 1988; Bulanova 1995; Wang 1998). Based on multiple lines of evidence (reviewed, e.g., in Gurney 1989 and Stachel and Luth 2015), disequilibrium between non-touching inclusions is nevertheless considered the exception rather than the rule.

Inclusions exhibit an often cubo-octahedral shape, irrespective of mineral symmetry or paragenesis (Harris et al. 2022). For many years, this characteristic was considered to reflect syngenetic growth with that of the host diamond (e.g., Harris 1968a; Bulanova 1995). This hypothesis was recently queried by Nestola et al. (2014), who observed an absence of an overall preferred orientation of inclusions in diamond indicating a protogenetic origin. Occurrence of both syngenetic and protogenetic relationships was subsequently documented through a combination of cathodoluminescence imaging and crystallographic orientation (EBSD) data (Davies et al. 2018). Based on small inclusion sizes (see above) and fast diffusion speeds in hot mantle environments, pre-existing host-rock minerals are nevertheless expected to generally equilibrate during fluid-mediated diamond growth events and thus the term "synchronous" inclusion was introduced (Nestola et al. 2017, 2019a; Pamato et al. 2021). That a lack of syngeneity does not necessarily preclude inclusion-based diamond dating is established in detail in Smit et al. (2022).

Table 1. Mineral inclusions in cratonic diamond.

Peridotitic
Common: Cr-pyrope, Forsteritic olivine, Enstatite, Cr-diopside, Mg-chromite, Fe–Ni sulphides.
Rare: Coesite*, Mg-ilmenite, Magnesite, Calcite, Native Fe, Zircon, Phlogopite, Yimengite.
Eclogitic
Common: Grossular–Almandine–Pyrope, Omphacitic Clinopyroxene, Fe-sulphides.
Occasional: Rutile, Coesite*, Kyanite.
Rare: Corundum, Ilmenite, Magnetite, Fe–Mg-chromite, Phlogopite, K-feldspar, Titanite, Staurolite, Zircon, Moissanite, Calcite, Dolomite.
Websteritic
Common: Almandine–Pyrope, Diopside–Augite, Enstatite.
Occasional: Coesite*, Olivine.
Rare: Phlogopite, Goldschmidtite
Origin Uncertain
Common: Graphite (mostly epigenetic to all parageneses)
Rare: Primary graphite, Diamond, Perovskite, Amphibole, Apatite, Eskolaite, Sr-titanate, Monazite.

Notes: * Refers to a mineral inclusion where an original structure is inferred.
See text for most of the epigenetic mineralogy.

Inclusion suites and parageneses

A first order division of mantle-derived diamonds is based on their origin in either the lithospheric mantle (our topic) or the sublithospheric mantle, the latter including the convecting upper mantle, the transition zone and the lower mantle (reviewed in Walter et al. 2022). Correcting for an extreme overrepresentation of sublithospheric diamonds in the literature, Stachel and Harris (2008) estimated that about 99% of diamonds produced worldwide ultimately derive from the lithospheric mantle and only about 1% from sublithospheric sources. The subsequent recognition that the CLIPPIR subpopulation of large, irregular, nitrogen-free (Type II) diamonds largely or entirely derives from transition zone to lower mantle environments (Smith et al. 2016) suggests that the estimate for sublithospheric diamonds needs to be increased to about 2% and the proportion of lithospheric diamonds decreased to 98%. Based on their mineral inclusions, lithospheric diamonds are conventionally subdivided into two main suites, peridotitic and eclogitic, plus a minor websteritic or pyroxenitic (websterites are a subclass of pyroxenites) suite (Meyer 1987; Gurney 1989; Stachel and Harris 2008). Based on 2844 diamonds with analyzed inclusions, Stachel and Harris (2008) derived relative abundances of 65% for the peridotitic, 33% for the eclogitic and 2% for the websteritic suite.

Peridotitic suite. Based on a primitive mantle Mg# of 89–90 (see McDonough and Sun 1995; their Table 4), olivine, orthopyroxene and clinopyroxene inclusions from depleted cratonic peridotite substrates[1] have Mg# ≥ 90, with infrequent Mg# values between 90–85 indicating increasingly melt-modified peridotitic substrates, which become transitional to websterites (Viljoen et al. 2018). In addition to their more magnesian character, peridotitic inclusions are separated from the eclogitic inclusion suite by Cr_2O_3 in garnet > 1 wt% (Schulze 2003) and molar Cr# (100Cr/(Cr+Al)) in clinopyroxene ≳7–10 (Stachel and Harris 2008). The peridotitic inclusion suite may be further subdivided into harzburgitic (to dunitic), lherzolitic, and wehrlitic parageneses, based principally on the groundbreaking work on garnet classification using Cr and Ca abundances by Sobolev et al. (1969, 1973). In this review, we employ the updated garnet classification scheme of Grütter et al. (2004) for this purpose. It should be noted that classification of peridotites based on garnet compositions is distinct from classification based on petrographic modes (Streckeisen 1976): garnet chemistry tracks equilibration with (1) orthopyroxene only (harzburgitic paragenesis), (2) clinopyroxene only (wehrlitic paragenesis), or (3) both pyroxenes (lherzolitic paragenesis), whilst petrographically defined boundaries are based on 5 vol% of either clinopyroxene (for the harzburgite/lherzolite distinction) or orthopyroxene (for the lherzolite/wehrlite distinction). Consequently, using garnet chemistry, highly depleted rocks may classify as lherzolites in spite of very minor (< 1 vol%) clinopyroxene contents. However, in contrast to xenolith studies, classification based on mineral modes is not feasible in inclusion research.

The minerals encountered as peridotitic suite inclusions in diamond are given in Table 1 and here we will exclusively focus on the common inclusion types (garnet, olivine, orthopyroxene, clinopyroxene and spinel), with the exception of sulfides that are discussed elsewhere in this volume (Smit et al. 2022). A table with inclusion abundance counts for lithospheric diamonds is given by Stachel and Harris (2008; their Table 2).

Eclogitic and websteritic/pyroxenitic suites. Eclogites are metamorphic rocks with a broadly basaltic composition, composed predominantly of jadeite-rich clinopyroxene and grossular-almandine-rich garnet (cf. Figs. 31, 32 in section *Eclogitic–Pyroxenitic Substrates*). In one more formal definition of eclogite, the clinopyroxene has $Al/(Al + Fe^{3+}) > 0.5$ on the M1 site and $0.2 \leq Na/(Na + Ca) < 0.8$ on the M2 site (Clark and Papike 1968). Conversely,

[1] In this review, we use the term "substrate" to refer to the rock in which diamond crystallised and which may have been the source of protogenetic and synchronous inclusions. The chemical composition and/or mineralogy of this rock may evolve subsequent to diamond formation, but this later modified diamond source did not form the substrate for diamond precipitation.

garnet–clinopyroxene rocks with jadeite-poor clinopyroxene are classified as pyroxenite, which, *sensu* Streckeisen (1976), encompasses all ultramafic rocks with <40 vol% olivine. There are gradations between garnet clinopyroxenites, which can be mineralogically and texturally similar to mantle eclogite, and websterites containing additional orthopyroxene ± olivine.

The assignment of silicate inclusions in diamond to the eclogitic suite is relatively straightforward and based on low Cr_2O_3 (< 1 wt%; see above) at elevated CaO contents in garnet, and low Cr_2O_3 and elevated Al_2O_3 contents in clinopyroxene (Gurney 1984; Grütter et al. 2004; Stachel and Harris 2008). In contrast, the websteritic inclusion suite, with compositions intermediate between the peridotitic and eclogitic suites, is less well defined, and relies on elevated Cr# and Mg#, and low Ca# in garnet, and/or the presence of orthopyroxene (Deines et al. 1993; Stachel and Harris 2008). Eclogitic and pyroxenitic garnet occurring as inclusions, as xenocrysts or in xenoliths can be grouped, based on Cr and Ca contents and Mg#, into classes G3 (eclogitic), G4 (eclogitic and pyroxenitic) and G5 (pyroxenitic) (Grütter et al. 2004). More recent work aimed at distinguishing Cr-poor garnet sourced from granulite and orogenic (crustal) eclogite vs. mantle eclogite recognized Ti/Si and Mg/Fe as useful discriminants (Hardman et al. 2018). The classification used here follows Aulbach and Jacob (2016) by employing a simplified version of the definition of Clark and Papike (1968), whereby cpx with $0.2 \leq Na/(Na+Ca) < 0.8$ classifies as eclogitic and that with lower ratios as pyroxenitic. This translates into distinctive bulk-rock compositions and is therefore not controlled by a pressure-dependent change in mineral chemical composition.

In addition, using a combination of major and trace elements, gabbroic eclogites with positive Eu anomalies indicative of high normative plagioclase modes (Eu/Eu* = chondrite-normalized $Eu/(Sm \times Gd)^{0.5} > 1.05$; Rudnick and Fountain 1995) are distinguished from basaltic eclogites with lower Eu/Eu*. The latter are classified into high-Ca, high-Mg and low-Mg eclogites. High-Ca eclogites have garnet with Ca# (molar $100Ca / (Ca + Fe^{total} + Mg + Mn)) > 20$, high-Mg eclogites garnet with $Ca\# \leq 20$ and $Mg\# > 60$, and low-Mg eclogites garnet with $Ca\# \leq 20$ and $Mg\# \leq 60$ (cf. Fig. 32a in section *Eclogitic–Pyroxenitic Substrates*). This classification contains petrogenetic information, reviewed below, but relies on the availability of both major and trace element compositions for both garnet and clinopyroxene. Also, these groupings do not typically have sharp distinctions, especially when samples from various localities with their own endemic compositional ranges are considered.

Inclusion minerals associated with the eclogitic and websteritic suites are given in Table 1 and again, our focus is on the common minerals (garnet and clinopyroxene) with the exception of sulfides, which are discussed by Smit et al. (2022).

Origin and evolution of subcratonic lithospheric mantle

As previously discussed, diamonds are principally associated with peridotitic and eclogitic substrates occurring in subcratonic lithospheric mantle. Through dating of inclusions following pioneering developments by Richardson et al. (1984) and Pearson et al. (1998) (for a review and full references see Smit et al. 2022) it emerged that formation of diamonds in harzburgitic substrates principally occurred in the Paleoarchean (Gurney et al. 2010; Shirey and Richardson 2011). Formation of lherzolitic diamonds preferentially occurred in the Paleoproterozoic but extends through the Mesoproterozoic and, with diamonds from the Victor Mine (Aulbach et al. 2018), even into the Neoproterozoic. For individual diamonds with presumably lherzolitic sulfides from Koffiefontein and Jagersfontein, even Mesozoic formation ages are observed (Pearson et al. 1998; Aulbach et al. 2009). Probably as a consequence of younger formation ages, lherzolitic diamonds are not exclusively restricted to undisturbed Archean lithospheric mantle but also occur in areas impacted by younger tectonothermal events (Shirey et al. 2002; Richardson and Shirey 2008; Smit et al. 2014a; Stachel et al. 2018b) or underpinned by entirely post-Archean lithospheric mantle (e.g., Banas et al. 2007; Hunt et al. 2009; Czas et al. 2020;

Liu et al. 2021). Episodic addition of eclogitic diamonds to the subcratonic lithospheric mantle was associated with subduction along craton margins immediately following the presumed onset of modern style Wilson cycles at about 3 Ga (Helmstaedt et al. 2010; Shirey and Richardson 2011) and likely continues to the present, with the youngest eclogitic diamonds dated at 0.14 (± 0.09) Ga (Timmerman et al. 2017).

The formation of the most important diamond substrate, cratonic peridotites, is associated with intense primary melt depletion (Jordan 1978; Boyd 1989; Herzberg 2004) that reached up to the point of orthopyroxene exhaustion from the melting residues, i.e., requiring up to about 40% melt extraction (Walter 1999; Bernstein et al. 2007). These large degrees of melt extraction are presumed to relate to 100–300 °C higher mantle potential temperatures in the Archean (Labrosse and Jaupart 2007; Korenaga 2008; Aulbach and Arndt 2019a). The very low FeO of some cratonic peridotites (filtered for orthopyroxene addition and refertilization), which requires melt extraction at pressures > 5 GPa, has been used among other arguments to infer melting associated with ascending mantle plumes (e.g., Boyd 1989; Griffin et al. 1999b; Aulbach 2012). Based, for example, on Cr/Al ratios (Stachel et al. 1998) and concentrations of mildly incompatible trace element contents including HREE (Canil 2004; Pearson and Wittig 2008), a principally low-pressure origin in the Archean equivalent of oceanic ridges and/or arc mantle is favoured by others (reviewed in Brey and Shu 2018 and Pearson et al. 2021), which implies a metamorphic origin for cratonic garnet peridotites from Cr-spinel peridotite precursors. Suggested modes of emplacement into the subcratonic lithosphere then involve imbrication associated with subduction (Helmstaedt and Schulze 1989; Kesson and Ringwood 1989), or lateral compression and thickening (Jordan 1978; Wang et al. 2018; Pearson et al. 2021) or vertical attaching (Herzberg and Rudnick 2012; Perchuk et al. 2020).

Irrespective of the exact mode of origin, in several cratons (e.g., Kaapvaal, Yakutia, Tanzania) the composition of cratonic peridotites points to enrichment in silica (i.e., enrichment in orthopyroxene; Boyd 1989; Kesson and Ringwood 1989; Kelemen et al. 1998). Major element relationships (Al/Si, Mg/Si) of cratonic peridotites indicate involvement of high-temperature aluminous pyroxene in this process, inconsistent with Si enrichment through infiltration of siliceous melts in cold supra-subduction zones (Aulbach 2012). Also, the absence of detectable perturbations in $\delta^{18}O$ values of orthopyroxene-enriched cratonic peridotites clearly precludes slab-derived melts as the principal agent of Si enrichment (Regier et al. 2018) and points to melt–rock reactions involving mantle-derived melts instead (e.g., Kelemen et al. 1992; Koornneef et al. 2009; Tomlinson and Kamber 2021). For the Kimberley area of the Kaapvaal Craton, orthopyroxene enrichment in the lithospheric mantle has been linked to the 2.7 Ga Ventersdorp large igneous province (Branchetti et al. 2021), which agrees well with the model of Si enrichment with komatiite infiltration (Tomlinson and Kamber 2021). More subtle metasomatic enrichment of principally trace elements (cryptic metasomatism; Dawson 1984) in Kaapvaal cratonic peridotites was attributed to percolation of small-volume melts of the carbonatite-kimberlite spectrum, peaking between 3.3 and 2.7 Ga and then tapering off in the Mesoproterozoic (Shu and Brey 2015). As a final important stage of metasomatic overprint of the Kaapvaal Craton lithospheric mantle, Simon et al. (2007) identified localized clinopyroxene ± garnet re-enrichment, likely associated with kimberlite magmatism < 200 Ma.

Mantle eclogites and associated inclusions in diamond are widely interpreted as representing various parts of subducted oceanic crust, which inherited major element, trace element and isotopic signatures from low-pressure accumulation-differentiation processes of igneous protoliths, seawater alteration and subsequent dehydration and partial melting (MacGregor and Manton 1986; Beard et al. 1996; Jacob 2004; Stachel et al. 2004). Strong indices for a subduction origin of inclusions and xenoliths comprise non-mantle oxygen isotope compositions, implying low temperature crustal fractionation, and Eu anomalies, requiring the participation of plagioclase during protolith formation (Schulze et al. 2003; Jacob 2004;

Stachel et al. 2018a). Moreover, sulfide inclusions have yielded a range of mass-dependently fractionated S isotope compositions, with $\delta^{34}S$ from −13 to +14‰, similar to sediments and altered oceanic crust (Chaussidon et al. 1987; Eldridge et al. 1991). Finally, mass-independently fractionated S isotope compositions reflect processes unique to the O_2-poor Archean atmosphere, which were incorporated first into sediments and, after subduction, into sulfides trapped by diamond (Farquhar et al. 2002; Thomassot et al. 2009; Smit et al. 2019a). Apart from such signatures of a low-pressure origin and the stable isotope evidence, direct formation from mafic melts in the mantle is precluded because major and trace element relationships are inconsistent with the participation of garnet, which is on the liquidus of mafic melts at depths from which eclogites are entrained (Aulbach and Arndt 2019b). The occurrence of eclogite with low-pressure signatures in the cratonic lithosphere, combined with age constraints (Smit et al. 2022), indicates emplacement during two principal processes: (1) Archean amalgamation of cratonic nuclei into larger cratonic masses, with closure of intervening ocean basins and (2) subsequent accretion/collision at craton margins, best exemplified by the Slave craton.

Databases

For the present review, we compiled two databases for inclusions in diamond of all suites from the literature, one focusing on major element compositions (8412 inclusion analyses), the other on trace element compositions (949 inclusion analyses). For the presented data, a blanket detection limit of 0.02 wt% was assumed for major element oxides. For trace elements, collated analytical tables in the literature typically only report data above the specific limits of detection. These databases are available for download at https://doi.org/10.7939/DVN/EJUE1G (major element database) and https://doi.org/10.7939/DVN/581P99 (trace element database).

Peridotitic inclusions and xenolith minerals. For comparison of inclusion compositions with the same mineral phases in cratonic peridotites, we assembled a further database of minerals in well-equilibrated mantle xenoliths, including 967 samples from on-craton kimberlite localities (used in plots presented here), 909 being garnet peridotites. This database is not yet in a publication ready state but can be obtained from us on request. Mineral analyses of olivine, orthopyroxene, clinopyroxene, garnet or spinel were filtered for analytical totals between 98.5 and 101.5 (98.5–102.0 for garnet and 97.5–102.0 for spinel) and for cation per formula unit ranges that match accepted bounds for these mineral species. To assess differences and similarities in the trace element composition of inclusion and xenolith/xenocryst garnets, we compiled an additional database with trace element compositions of 152 harzburgitic and 281 lherzolitic garnets from xenoliths (or in a few instances occurring as xenocrysts) in on-craton kimberlites. For both xenolith databases, a paragenesis was assigned based on garnet major element chemistry (Grütter et al. 2004), which for the major element database in a few instances was revised based on assignments in the original publications (where garnets with "lherzolitic" compositions sometimes come from pyroxenite xenoliths). Of the 843 peridotitic garnets that pass the analytical filters described above, 679 (80.5%) derive from lherzolites (classified as G1 = megacrysts ($n = 64$), G9 = lherzolitic ($n = 460$), and G11 = high-TiO_2 peridotitic ($n = 155$)), 154 (18.0%) derive from harzburgites (with 105 of the G10 garnets classifying as "diamond facies" (G10D)), and 12 (1.4%) derive from wehrlites (G12). Only samples with an assigned harzburgitic or lherzolitic paragenesis were used in this review. Textural information (allowing to separate, e.g., strongly deformed varieties) is generally not available for these samples.

For the inclusion database, orthopyroxenes and clinopyroxenes with Mg# < 90 recovered from diamonds from the Voorspoed Mine were excluded from the peridotitic data set because of their compositionally unique character related to intense melt metasomatism (Viljoen et al. 2018).

Eclogitic inclusions and xenolith minerals. For comparison with their xenolithic counterparts, only garnet and/or clinopyroxene-bearing diamonds are considered. The database comprises reported eclogitic and websteritic diamonds with 23 touching clinopyroxene–garnet

pairs and 249 non-touching pairs, 567 unpaired clinopyroxenes, and 906 unpaired garnet inclusions. Multiple non-touching inclusions per mineral and diamond are not counted individually but were averaged instead. However, touching inclusions were not averaged with non-touching ones as they may have re-equilibrated in response to changing pressure–temperature conditions, contrary to non-touching inclusions.

The xenolith database encompasses on-craton samples for which both major and trace element compositions are reported for both garnet and clinopyroxene, and excluding those where trace element compositions were affected by kimberlite contamination evident in anomalous Ba and Nb concentrations (cf., Aulbach and Jacob 2016). Cut-off values for contamination are estimated using mineral–melt distribution coefficients and concentrations in the contaminant, typically kimberlite, which determine how much Ba and Nb can be incorporated in garnet and clinopyroxene under equilibrium conditions. Garnet/kimberlite distribution coefficients for Ba of 0.0002 and for Nb of 0.0008, and clinopyroxene/kimberlite distribution coefficients for Ba of 0.001 and for Nb of 0.0002 are taken from Girnis et al. (2013). Combined with Ba and Nb concentrations in primitive kimberlites of 1250 and 260 ppm, respectively (Becker and Le Roex 2006), this yields maximum values of 0.25 ppm for Ba and 0.052 ppm for Nb in garnet, and of 1.25 ppm for Ba and 0.208 ppm for Nb in clinopyroxene at equilibrium. Allowing for metasomatism by more incompatible trace element enriched melts, we apply cut-offs for Ba in garnet and clinopyroxene of 0.5 and 1.5 ppm, respectively, and for Nb of 0.5 and 1 ppm, respectively. For a comparison of mineralogy, only xenoliths for which at least clinopyroxene and garnet major element data are reported are considered, which is the case for 1907 eclogite and 544 pyroxenite xenoliths. For a comparison of compositions, diamond-absent xenoliths are only considered when REE data are available, allowing full classification (695 samples), whereas diamond-bearing xenoliths (n = 251) are retained regardless of trace-element data availability (cf. Table 3 in section *Eclogitic–Pyroxenitic Substrates*). Cratons with corresponding data coverage encompass Kaapvaal, Zimbabwe, West Africa, India, Siberia, Slave, Sask, Superior, the North Atlantic craton in West Greenland, and the East European Platform (references in Appendix Table 1).

Values below the detection limit are often not given and can therefore not be counted for calculation of average or median compositions, which implies that these are maxima. Since this applies only to a small proportion of the data for elements considered here, the resultant bias is considered minor.

MAJOR ELEMENT COMPOSITION OF PERIDOTITIC SUITE INCLUSIONS AND COMPARISON WITH CRATONIC PERIDOTITE XENOLITH MINERALS

Olivine

Of the 1468 analysed peridotitic olivine inclusions in diamond, the majority (79%) cannot be assigned to a specific paragenesis due to an absence of coexisting garnet or clinopyroxene, 16% are harzburgitic, 5% are lherzolitic and a single inclusion (equivalent to 0.07%) is of wehrlitic paragenesis. The olivine inclusions are high in forsterite content, with a median Mg# of 92.8 (mean is 92.7 ± 1.3; 1 sigma). Olivine from cratonic garnet peridotites is lower in Mg# (median value of 91.8, mean of 91.7 ± 1.3). Comparing the Mg# of harzburgitic (median and mean of 93.1) and lherzolitic (median and average of 91.8) olivine inclusions, harzburgitic inclusions are more magnesian (Mg# difference is 1.3; Fig. 5). The same distinction is seen for harzburgitic (median is 92.8, average is 92.9) and lherzolitic (median is 91.6, average is 91.5) olivines in cratonic garnet peridotites (average difference is 1.3; Fig. 5). For both parageneses, equality of means in Mg# of olivines included in diamond and contained in xenoliths cannot be rejected, based on a two tailed Student's t-test for two independent samples, assuming

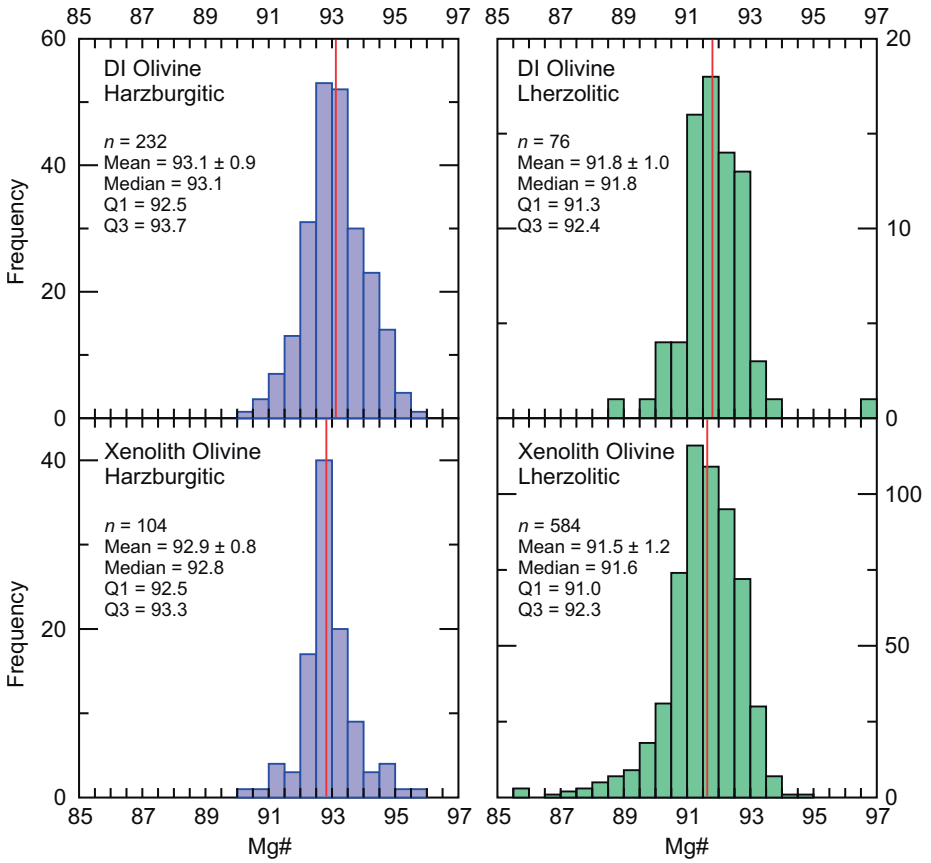

Figure 5. Histograms of molar Mg# (100Mg / (Mg + Fe)) of olivine included in diamond (DI, **top**) and from cratonic garnet peridotite xenoliths (**bottom**). The paragenesis of olivine inclusions is derived from coexisting garnet or the presence of clinopyroxene (lherzolitic). The harzburgitic paragenesis is shown on the **left**, the lherzolitic paragenesis on the **right**. The majority (n = 1157) of olivine inclusions are of unspecified paragenesis (not shown), due to an absence of coexisting garnet or clinopyroxene. Their mean Mg# (92.8 ± 1.2) is the same as that of the combined data set for harzburgitic and lherzolitic inclusions (92.8 ± 1.1), indicating that peridotitic olivines of unspecified paragenesis represent a mixture of harzburgitic and lherzolitic olivines, in proportions similar to the 3:1 ratio for olivines of known paragenesis. For each set, the number of analyzed olivines (n), the mean (± 1 standard deviation), the median value and the interquartile range (as middle values of the lower half (Q1) and the upper half (Q3) of the data set) are given as well. The median value is also indicated as a **red line** in each histogram.

unequal variances and an alpha value of 5%. Olivine Mg# is widely interpreted to gauge the degree of depletion of the protoliths of subcratonic lithospheric mantle (Boyd 1989; Herzberg 2004; Bernstein et al. 2007; Pearson and Wittig 2014) with typically only minor subsequent modification. The observation of equal means then suggests that, on the paragenesis level, diamond substrates and diamond-free garnet peridotites experienced effectively the same depletion history. Equality of means on the paragenesis level is reconciled with a higher Mg# of inclusion olivines relative to xenolith olivines based on very different relative proportions of the harzburgitic and lherzolitic parageneses, with 75% of inclusions with an assigned paragenesis being harzburgitic, as opposed to 15% of olivines from garnet harzburgite xenoliths.

A long-recognized difference between olivine included in diamond and from garnet peridotite xenoliths is a higher Cr content of the former (Meyer and Boyd 1972; Meyer 1987). Peridotitic olivine inclusions have a median Cr_2O_3 content of 0.05 wt% (mean is 0.06 ± 0.08 wt%), with an interquartile range of 0.03–0.14 wt% and a maximum value of 1.36 wt%. Olivine in cratonic garnet peridotites has a median Cr_2O_3 content of 0.03 wt% (mean is 0.03 ± 0.02 wt%), with an interquartile range from below the limit of detection (< 0.02 wt%) to 0.05 wt%, with a maximum value of 0.12 wt%. Higher Cr in inclusion olivines has been related to incorporation of Cr^{2+} (Meyer and Boyd 1972) during crystallization at reducing conditions and at high temperature (Li et al. 1995). High Cr, however, is not a universal characteristic of olivine inclusions and only 10% have $Cr_2O_3 > 0.10$ wt%.

Orthopyroxene

As with olivine inclusions, the majority of the 417 analysed peridotitic orthopyroxene inclusions (57%) are of unspecified paragenesis, 32% are harzburgitic and 11% are of lherzolitic paragenesis. Inclusion orthopyroxene is almost pure endmember enstatite, with a median Mg# of 94.1 (mean is 94.0 ± 1.9)[2]. These Mg# values are 1.3 higher than the median and mean for olivine inclusions in diamond (see above). Orthopyroxene in cratonic garnet peridotites is less magnesian than inclusions (median Mg# of 92.9, mean of 92.8 ± 1.1). On the paragenesis level, harzburgitic orthopyroxene inclusions (median value of 94.9, mean of 94.8 ± 1.2) are more magnesian than lherzolitic inclusions (median Mg# of 92.8, mean of 92.4 ± 1.9; Fig. 6). The harzburgitic inclusion dataset is strongly biased by a large number (n = 59) of highly magnesian orthopyroxenes from De Beers Pool (the combined production of the Kimberley Mines), and after removing this sample set, the median Mg# drops to 94.1 (mean of 94.2 ± 1.1; Fig. 6). These paragenesis level values are very similar to harzburgitic (median Mg# of 93.8, mean of 93.9 ± 0.7) and lherzolitic (median Mg# of 92.7, mean of 92.6 ± 1.0; Fig. 6) orthopyroxenes from cratonic garnet peridotites. A two tailed Student's t-test for two independent samples, assuming unequal variances and an alpha value of 5%, however, rejects the hypothesis of equal means for both the harzburgitic and lherzolitic inclusion and xenolith orthopyroxenes. Based on the nevertheless high similarity of inclusion and xenolith orthopyroxene on the paragenesis level, the lower Mg# of xenolith orthopyroxenes for the combined peridotitic data sets largely reflects a much lower proportion of the harzburgitic paragenesis, which makes up only 16% (as opposed to 75% of inclusions). This matches the observation made for olivine inclusions.

Among minor elements, NiO in orthopyroxene is higher in inclusions in diamond (median value is 0.13 wt%, mean is 0.13 ± 0.03 wt%) compared to cratonic garnet peridotites (median value is 0.09 wt%, mean is 0.07 ± 0.05 wt%). There is no variation in NiO with paragenesis: for inclusions of known lherzolitic and harzburgitic paragenesis the median NiO content is 0.13 wt% and the mean is 0.14 ± 0.03 wt%; for xenoliths the two parageneses have the same median and mean as the combined peridotitic orthopyroxene dataset. Given the similarity in Mg# of orthopyroxene inclusions and in xenoliths on the paragenesis level and the similarity of NiO in olivine inclusions (median NiO is 0.36 wt%, mean is 0.36 ± 0.05 wt%) and in xenoliths (median NiO is 0.38 wt%, mean is 0.36 ± 0.08 wt%), this observation cannot be interpreted as a bulk rock signal but suggests a temperature control on Ni in orthopyroxene instead, similar to Ni in garnet (Griffin et al. 1989a). Indeed, a blurred positive correlation (r^2 = 0.2, not illustrated) between temperature of last equilibration (enstatite in clinopyroxene-based estimates; Brey and Köhler 1990) and NiO content is observed for our database of 189 orthopyroxene analyses from cratonic garnet lherzolite xenoliths.

[2] As previously noted, excluded from the peridotitic data set is a suite of "lherzolitic" orthopyroxenes (and clinopyroxenes) from Voorspoed (Kaapvaal Craton) derived from strongly melt-metasomatised substrates, which shows characteristics, such as a mean Mg# of 88.9 and mean MnO content of 0.28 wt%, that are clearly transitional to the websteritic suite (see Viljoen et al. 2018 for a detailed discussion).

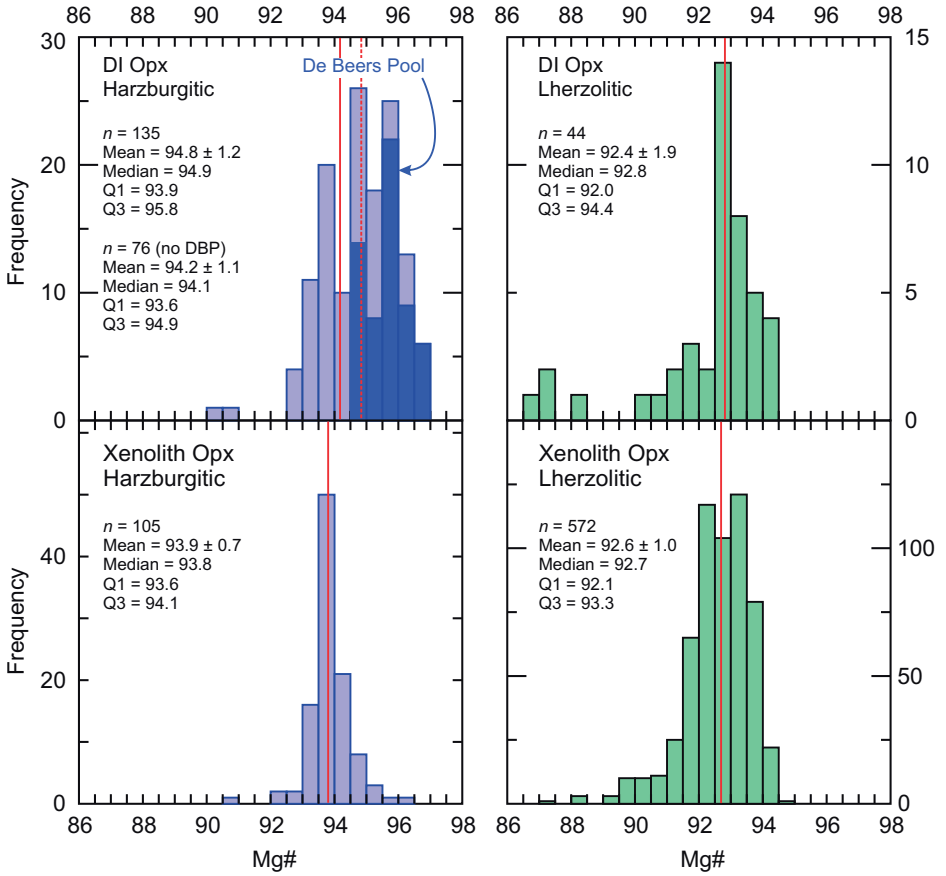

Figure 6. Histograms of molar Mg# (100Mg / (Mg + Fe)) of orthopyroxene included in diamond (DI, **top**) and from cratonic garnet peridotite xenoliths (**bottom**). The harzburgitic paragenesis is shown on the **left**, the lherzolitic paragenesis on the **right**. As with olivine inclusions, the majority (n = 235) of orthopyroxene inclusions are of unspecified paragenesis (not shown), due to an absence of coexisting garnet or clinopyroxene, but again their mean Mg# (94.1 ± 1.3) is very similar to that of the combined data set for harzburgitic and lherzolitic inclusions (93.8 ± 2.2). For each set, the number of analyzed olivines (n), the mean (±1 standard deviation), the median value and the interquartile range (as middle values of the lower half (Q1) and the upper half (Q3) of the data set) are given as well. For harzburgitic orthopyroxene inclusions, samples from De Beers Pool (shown in **dark blue**) are highly overrepresented and, due to their highly magnesian character, bias the dataset. Therefore, a second set of statistical parameters is given that excludes the De Beers Pool orthopyroxenes (labelled "no DBP"). The median value is also indicated as a red line in each histogram. For harzburgitic inclusions, the higher median value including the De Beers Pool data is shown as a **dashed line**. 'De Beers Pool' is the pooled diamond production from the four mines in Kimberley: Bultfontein, De Beers, Dutoitspan, Wesselton.

Due to their incompatible behavior during mantle melting, Na and Ti were efficiently removed from the Archean melting residues that now form subcratonic lithospheric mantle (O'Hara et al. 1975; McDonough and Rudnick 1998). This is well reflected in harzburgitic orthopyroxene inclusions, where over 50% of analyses for Na_2O and TiO_2 are below the limit of detection (≤ 0.02 wt%). For inclusions of the lherzolitic paragenesis (and presumably lherzolitic inclusions contained in the "unspecified peridotitic" group), metasomatic re-enrichment of the diamond substrates is documented in maximum Na_2O contents of

Table 2. Comparison of selected major elements in lherzolitic clinopyroxenes included in diamond (DI) and from cratonic garnet peridotite xenoliths.

	Mg#		TiO_2		Cr_2O_3		Al_2O_3		Na_2O		K_2O	
	DI	Xenolith	DI	Xenolith	DI	Xenolith	DI	Xenolith	DI	Xenolith	DI	Xenolith
Min	88.4	86.9	≤ 0.02	≤ 0.02	≤ 0.02	0.17	0.05	0.36	0.18	0.24	≤ 0.02	≤ 0.02
Q1	91.9	91.3	≤ 0.02	0.05	0.81	1.02	0.89	1.61	0.67	1.38	0.05	≤ 0.02
Median	92.8	92.3	0.05	0.13	1.08	1.37	1.42	1.96	1.17	1.63	0.10	0.03
Q3	93.5	93.4	0.10	0.26	1.64	1.73	2.12	2.28	1.90	1.92	0.18	0.05
Max	96.4	96.4	1.85	0.65	15.6	3.96	5.83	5.65	10.10	3.76	1.68	0.26

Notes: Interquartile ranges given as middle values of the lower half (Q1) and the upper half (Q3) of the data sets. Because of strongly non-normal distributions and common outliers, means and standard deviations are not quoted. A blanket detection limit of ≤ 0.02 wt% is assumed for all oxides analysed and to avoid biasing the data set, values below the limit of detection were not omitted but treated as ½ the detection limit instead. Mg# is given as Mg / (Mg+Fe) × 100

0.57 wt% and maximum TiO_2 contents of 0.29 wt%. For orthopyroxene from cratonic garnet peridotites, the metasomatic re-enrichment of Na and Ti can be much more intense (Fig. 7). From the xenolith data set, a positive correlation between Na and Ti is apparent, which on a cation basis has a slope of about 2, consistent with a coupled substitution of the type $2Na^{1+}$-$^{VI}Ti^{4+}$ (Cameron and Papike 1981). Using the 95th percentile values for Na_2O (≤ 0.16 wt%) and TiO_2 (≤ 0.06 wt%) of orthopyroxene inclusions as upper cutoffs, which in combination encompass 93% of the inclusion data set, permits (empirical) definition of a diamond inclusion field for orthopyroxenes. Forty two percent of orthopyroxenes from cratonic garnet peridotites fall outside this inclusion field, indicating that substantive metasomatic re-enrichment of Na and Ti is much more widespread in xenolith samples.

Clinopyroxene

Lherzolitic clinopyroxene inclusions (n = 148) are Cr_2O_3-rich, with contents typically near 1 wt%. Their median Mg# (92.8) is the same as that of lherzolitic orthopyroxene inclusions and mildly elevated relative to clinopyroxene from cratonic garnet lherzolites (92.3; Table 2). Compositional differences between inclusion and xenolith clinopyroxenes are evident for Al, Ti, Na, but largely overlapping compositional ranges preclude the definition of compositional cut-offs between the two groups (Table 2). Al_2O_3 in inclusions shows a strongly right (towards higher Al) skewed distribution with a mode at 0.8 wt% (median value 1.42 wt%) whereas xenolith-derived clinopyroxene displays a near-normal distribution with a mode at 1.8 wt% (median value 1.96 wt%; see Fig. 8). Inclusion clinopyroxenes also have lower median and 25th percentile (Q1) values in TiO_2 and Na_2O contents (Table 2). The strongest compositional difference exists for K_2O, where the inclusion distribution shows a tail up to 1.68 wt%, whereas xenolith clinopyroxenes do not exceed 0.26 wt% (Fig. 9). The occurrence of strong to extreme metasomatic enrichment in potassium is a unique characteristic of inclusions, which also have a higher median value and interquartile range (Q1 and Q3 values Table 2), but nevertheless, the bulk of clinopyroxenes from diamonds and cratonic garnet lherzolites overlap in K_2O content (Fig. 9).

Garnet

The "classical" Cr_2O_3 versus CaO diagram (Sobolev et al. 1973; Gurney and Switzer 1973; Gurney 1984; Grütter et al. 2004; Fig. 10), with fields separating the three principal peridotitic parageneses, harzburgitic

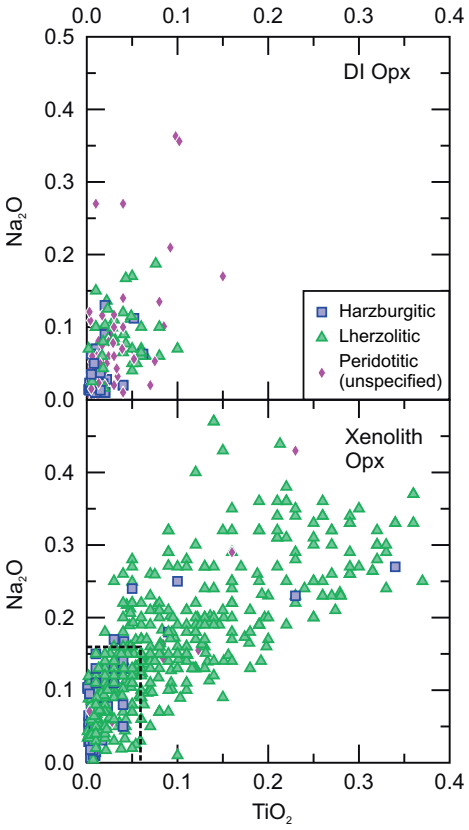

Figure 7. Co-variations of Na_2O and TiO_2 (wt%) in orthopyroxene included in diamond (DI, **top**) and from cratonic garnet peridotite xenoliths (**bottom**). The **dashed box** in the bottom diagram is based on the 95th percentile in Na_2O and TiO_2 contents of inclusion orthopyroxenes.

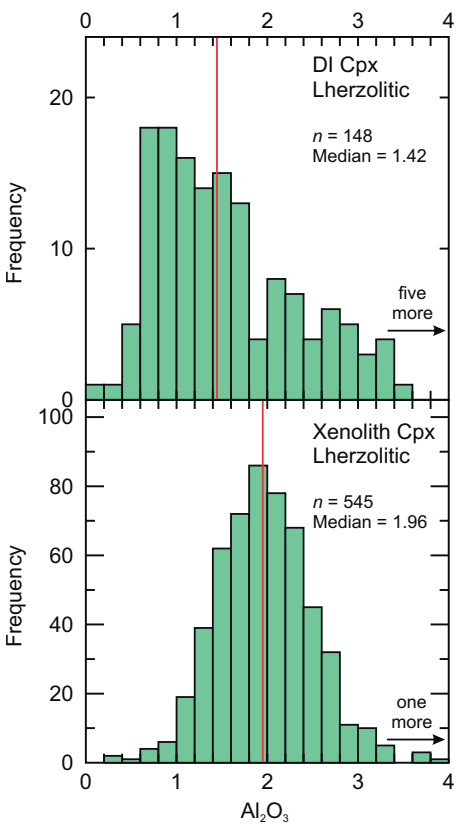

Figure 8. Histogram of Al_2O_3 content (wt%) in lherzolitic clinopyroxene included in diamond (DI, **top**) and from cratonic garnet peridotite xenoliths (**bottom**). A few outliers, five inclusions with Al_2O_3 up to 5.8 wt% and one xenolith clinopyroxene with Al_2O_3 of 5.7 wt%, exceed the shown range. Median values are indicated as **red lines**.

(-dunitic), lherzolitic and wehrlitic, is widely used in assessing the compositions of mantle-derived garnets. For our database (n = 1175), 81% of inclusion garnets are of harzburgitic paragenesis, 18% are lherzolitic and 1% are wehrlitic. Ultra-depleted harzburgitic and dunitic diamond substrates are represented by garnets with CaO contents < 1.8 wt% (Grütter et al. 1999; Fig. 10), which applies to 38% of peridotitic inclusions (or 47% of garnets classified as harzburgitic). In evaluating these relative proportions, it should, however, be noted that the published garnet inclusion data set is strongly biased towards a few well studied locations, with about 40% of analyses in our database being derived from only four occurrences (De Beers Pool, Finsch and Premier (Cullinan Mine) on the Kaapvaal Craton and Victor on the Superior Craton), with a clear under-representation of inclusion garnets from Yakutian occurrences (9%). For that reason, we consider the original proportion of 85% harzburgitic (-dunitic) or "G10" garnet inclusions established by Gurney (1984), using a much smaller data set, to be still equally valid. Garnets from cratonic peridotite xenoliths (n = 843) show an exactly inverse relationship in the proportions of the harzburgitic (18% in our database) and lherzolitic (81%) parageneses, with again 1% of garnets with wehrlitic compositions (Fig. 10). Ultra-depleted (< 1.8 wt% CaO) xenolith garnets are rare (2% of all peridotitic and 13% of harzburgitic garnets).

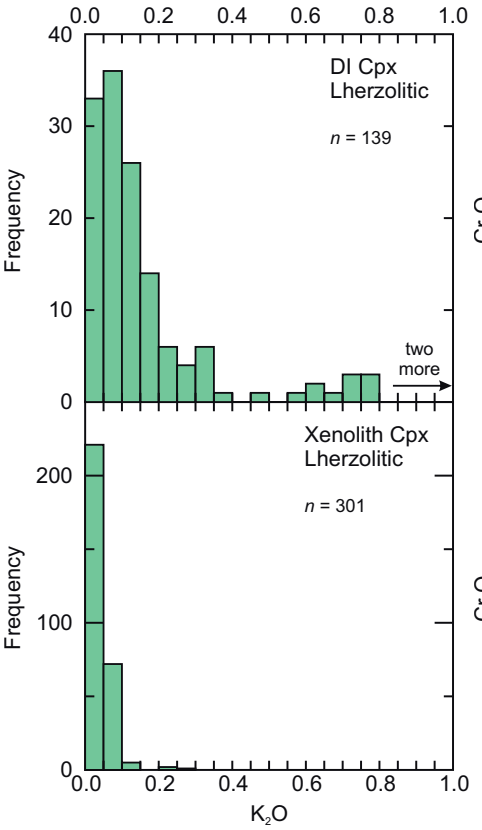

Figure 9. Histogram of K_2O content (wt%) in lherzolitic clinopyroxene included in diamond (DI, **top**) and from cratonic garnet peridotite xenoliths (**bottom**). Two outliers, inclusion clinopyroxenes with K_2O of 1.57 and 1.68 wt%, exceed the shown range.

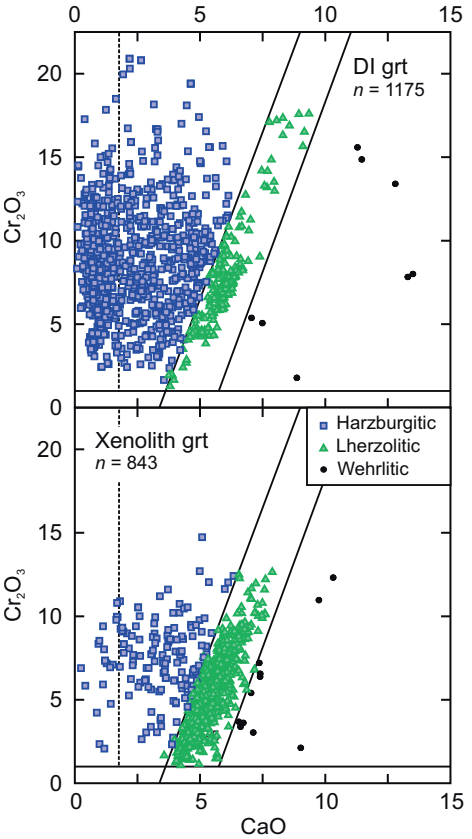

Figure 10. Cr_2O_3 versus CaO (wt%) in peridotitic garnet included in diamond (DI, **top**) and from cratonic xenoliths (**bottom**). Fields for the different peridotitic parageneses (harzburgitic, lherzolitic and wehrlitic) and cut-off towards eclogitic garnets at 1 wt% Cr_2O_3 are from Grütter et al. (2004). Ultra-depleted harzburgitic and dunitic garnets fall to the left of the **dashed line** at 1.8 wt% CaO (Grütter et al. 1999). The total number of analyzed peridotitic garnets is given for both inclusions in diamond and xenoliths.

Calcium intercept values (calculated after Grütter et al. 2004) are a one-dimensional measure of how far a garnet is removed in Ca content from the harzburgite–lherzolite division, which intersects the *x*-axis in a Cr_2O_3–CaO plot (Fig. 10) at 3.375 wt% CaO. In garnet compositional space, the transition to Ca intercept values below 3.375 is considered petrologically equivalent to the exhaustion of clinopyroxene from the residues during primary melt depletion and corresponds to about 20% melt removal (Jaques and Green 1980; Kushiro 1994). Further decreasing Ca intercept values of garnet document increasing degrees of primary melt depletion, progressing to the exhaustion of orthopyroxene in the residues at about 40% melt extraction (Jaques and Green 1980; Bernstein et al. 2007 and references therein). For harzburgitic garnets, Ca intercept values, therefore, are a measure of the primary chemical depletion of their substrates (see Grütter et al. 1999 for a detailed discussion).

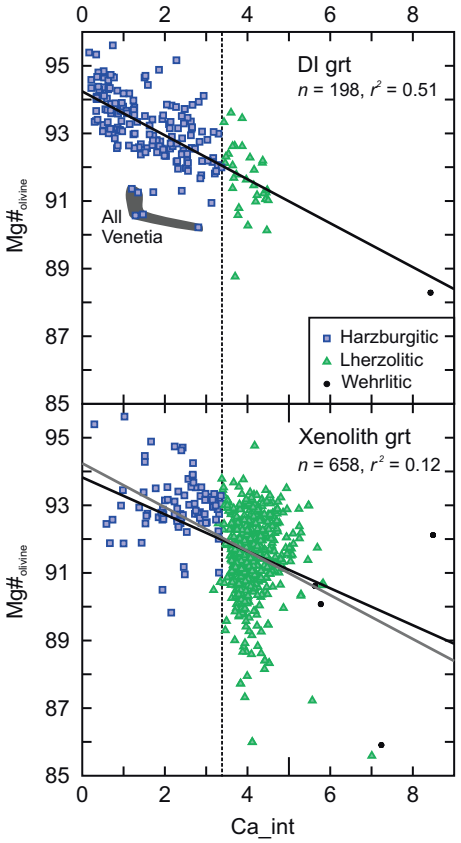

Figure 11. Olivine Mg# versus Ca intercept value (Ca_int) of coexisting garnets included in diamond (DI, **top**) and from cratonic peridotite xenoliths (bottom). Ca intercept values measure how far a garnet is removed from the harzburgite–lherzolite division (see Fig. 10) shown as a **dashed line** with a Ca intercept value of 3.375 (for details of calculation, see Grütter et al. 2004). Linear regressions (**black lines**) are given for both the inclusion- and xenolith-based datasets. Five harzburgitic garnet–olivine inclusion pairs that fall distinctly below the regression line are derived from Venetia Mine diamonds, for which crystallization following modification of their mantle substrates through the 2.05 Ga Bushveld large igneous province was inferred (Richardson et al. 2009). For comparison purposes, the inclusion-based regression is shown as a **dark grey line** in the xenolith garnet plot (**bottom**).

Correspondingly, Mg# and Ca intercept values are negatively correlated for both inclusion and xenolith garnets (not shown). Garnet Mg# is, however, controlled by temperature-dependent Mg–Fe partitioning with olivine, orthopyroxene and clinopyroxene and hence only provides a distorted image of bulk rock Mg#. Pairing garnet Ca intercept values with the Mg# of coexisting olivines (Fig. 11; see also Eaton et al. 2009, their Fig. 4) sidesteps this distortion problem, with the drawback of greatly reducing the data set for inclusions (from 1175 individual garnets to 198 garnet–olivine pairs). Despite some scatter, regression of the inclusion data set yields a clear linear trend ($r^2 = 0.51$; Fig. 11), with olivine Mg# increasing from 92.0 at the transition from lherzolitic to harzburgitic garnets (Ca intercept value = 3.375) to 94.2 for Ca-free garnets. Note that for the lherzolitic paragenesis some deviation from this linear trend is expected, as (1) varying degrees of primary melt depletion prior to the point of exhaustion of clinopyroxene in the protoliths would not be reflected in the Ca intercept values of garnet and (2) metasomatic addition of clinopyroxene to original harzburgitic melting residues may have occurred. In spite of that, including only harzburgitic garnet–olivine pairs results in an indistinguishable regression line ($y = 94.2 - 0.62x$ versus $y = 94.2 - 0.65x$ for the entire data set) but with a lower r^2 (0.31). For the xenolith data set, the same trend of decreasing Mg# with increasing Ca intercept values is visible but with much more scatter (Fig. 11). For the lherzolitic paragenesis, the variation in olivine Mg# at a given garnet Ca intercept value visually appears more pronounced than for the inclusion data set. Given the equality of mean Mg# of lherzolitic olivines inside and outside of diamond (see above), this apparently increased variability likely only reflects a much larger number of analyzed lherzolitic xenoliths compared to inclusion pairs. Highly similar median and mean Mg# values of lherzolitic garnets inside and outside diamond (inclusions: median = 83.0 and mean = 83.3 ± 2.8; xenolith garnets: median = 83.4, mean = 83.1 ± 2.2) support this interpretation. The overlapping trends in olivine Mg# versus garnet Ca intercept value document that peridotitic diamond substrates and cratonic garnet peridotites followed the same melt depletion path, with the key difference that carbon-bearing fluids preferentially react with the cpx-absent, depleted peridotitic substrates during mineralization events that produce diamond.

As a consequence of intense primary melt depletion, Na and Ti contents in peridotitic diamond substrates and cratonic peridotites are expected to be very low (see above). For harzburgitic garnets included in diamond and from cratonic peridotite xenoliths, median Na_2O and TiO_2 contents are indeed at or below the limit of detection (≤ 0.02 wt%; averages are not reported because of strongly non-normal distributions), with concentrations above the limit of detection being considered to indicate secondary metasomatic re-enrichment (Figs. 12 and 13). For the lherzolitic paragenesis, median contents are above the limit of detection for TiO_2

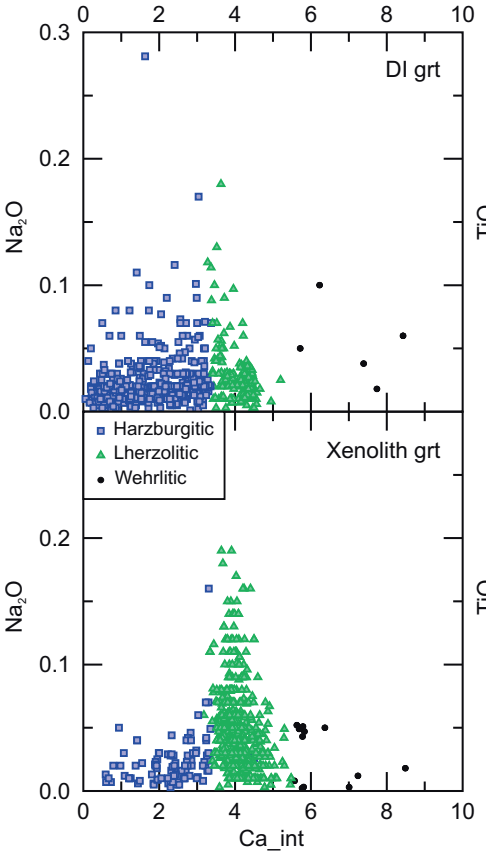

Figure 12. Na_2O content (wt%) versus Ca intercept value (Ca_int; see Fig. 11 for explanation) for peridotitic garnets included in diamond (**top**) and from cratonic xenoliths (**bottom**).

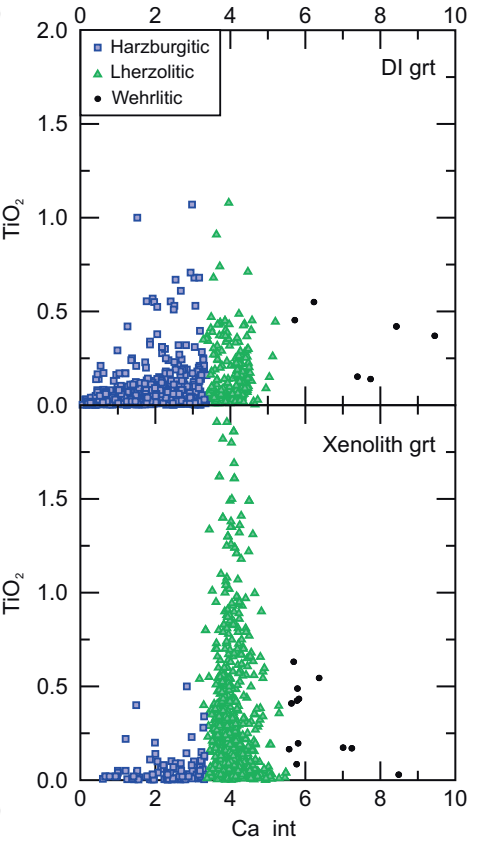

Figure 13. TiO_2 content (wt%) versus Ca intercept value (Ca_int; see Fig. 11 for explanation) for peridotitic garnets included in diamond (DI, **top**) and from cratonic xenoliths (**bottom**). For the harzburgitic paragenesis, comparison of the upper and lower diagrams gives the impression of higher TiO_2 contents in inclusions compared to xenolith garnets. This impression, however, relates to the much higher number of harzburgitic inclusion garnets analysed for TiO_2 (n = 864 versus n = 134 for xenolith garnets), with median values for both inclusions and xenolith garnets being ≤ 0.02 wt% (i.e., below the limit of detection) and Q3 values (middle value of the upper half of the data set) being nearly identical (0.06 wt% for inclusions and 0.05 wt% for xenolith garnets).

(0.13 wt% for inclusions and 0.24 wt% for xenolith garnets) and for xenolith garnets also for Na_2O (median of 0.04 wt%). In this work, we repurpose $Na_2O \leq 0.02$ wt% (below the limit of detection) and $TiO_2 \leq 0.04$ wt% from our previous work (Stachel and Harris 2008) to represent upper-limit thresholds for garnets included in diamond and from xenoliths, above which cratonic lherzolites are considered enriched in Na and Ti by secondary metasomatism.

On that basis, Figures 12 and 13 document widespread metasomatic modification of the harzburgitic and lherzolitic substrates of both inclusion and xenolith garnets. Maximum Na_2O concentrations in garnet are 0.31 wt% (a harzburgitic inclusion outside the range of Figure 12) and 0.19 wt% (xenoliths) and extreme TiO_2 values reach 1.08 wt% (inclusions) and 1.91 wt% (xenoliths). For xenolith garnets there is a clear positive correlation of Na with Ti ($r^2 = 0.67$; Figure not shown), which is barely discernible for inclusions ($r^2 = 0.15$). A slope of Na versus Ti of about 0.2 (on a cation basis) indicates that Na likely is fully accommodated by the substitution mechanism $^{VIII}M^{2+} + {}^{VI}Al^{3+} = {}^{VIII}Na^{1+} + {}^{VI}Ti^{4+}$ (Bishop et al. 1976). The strong excess of Ti over Na reflects additional substitution mechanisms of the type $2\,{}^{VI}Al^{3+} = {}^{VI}Ti^{4+} + {}^{VI}M^{2+}$ or $^{VI}Al^{3+} + {}^{IV}Si^{4+} = {}^{VI}Ti^{4+} + {}^{IV}Al^{3+}$ (Ackerson et al. 2017).

Intense metasomatic addition of Ti is particularly common for lherzolitic xenolith garnets, with 25% of samples containing > 0.5 wt% TiO_2 (Q3 value), as opposed to only 2.4% of inclusions. A large set of pressure–temperature estimates for well-equilibrated cratonic garnet lherzolites (n = 372) allows the relationship of Ti-metasomatism and temperature of last equilibration to be assessed. This relationship indicates that TiO_2 contents > 0.5 wt% (the above quoted Q3 value for lherzolitic xenolith garnets), with one exception, are restricted to temperatures > 1130 °C (Fig. 14). A comparable data set does not currently exist for inclusions in diamond but the observed paucity of inclusion garnets with TiO_2 > 0.5 wt% documents that the style of high-temperature, Ti-rich ("melt") metasomatism (Griffin and Ryan 1995) documented in one quarter of lherzolite xenoliths either did not significantly impact diamond

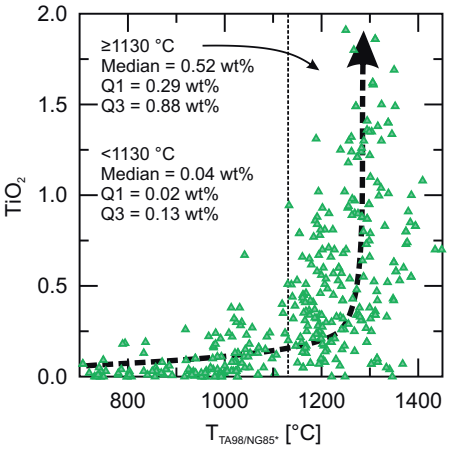

Figure 14. TiO_2 content (wt%) in xenolith garnets versus temperature of last equilibration (°C) of their cratonic lherzolite hosts. Temperature is calculated using the enstatite in clinopyroxene thermometer of Taylor (1998) in combination with the garnet–orthopyroxene Al exchange barometer of Nickel and Green (1985) (with Al in the M1 site of orthopyroxene calculated after Carswell and Gibb 1987). With a single exception, TiO_2 contents in garnet remain relatively low (≤ 0.02 to 0.40 wt%) at equilibration temperatures below 1130 °C. At higher temperatures, a large range in TiO_2 contents is observed (from 0.04 to 1.91 wt%), consistent with the melt metasomatic trend of Griffin and Ryan (1995). For the low- and high-temperature groups, median values and interquartile ranges (as middle values of the lower half (Q1) and the upper half (Q3) of the data sets) are given as well.

substrates or only occurred in a different, much milder form (note footnote 1 in section *Introduction* here). Given that typical temperatures of diamond formation in peridotitic substrates are estimated at 1130 ± 120 °C (Stachel and Luth 2015; see also Nimis 2022), this near absence of Ti metasomatism of diamond substrates is not a temperature effect but either indicates an increasing abundance of Ti-rich melt metasomatism in the more recent geological past (Mesoproterozoic to Phanerozoic) and/or a diamond unfriendly effect of such metasomatism that renders affected potential substrates infertile.

Mg-chromite

Low Al contents and consequent high bulk rock Cr/Al ratios cause spinel to persist to diamond-stable pressures in cratonic peridotites and, in particular, in peridotitic diamond substrates (Doroshev et al. 1997; Klemme 2004; Ziberna et al. 2013). Of the 1001 peridotitic spinel inclusions in diamond in our database, most (97%) are associated with neither garnet nor clinopyroxene and hence are of unspecified peridotitic paragenesis. Based on the observation that only 9% of the Mg-chromite inclusions with an assigned paragenesis are lherzolitic and 91% are harzburgitic, a mostly harzburgitic paragenesis may also be assumed for the inclusions with unspecified paragenesis. Based on high pressure experiments, spinel, in equilibrium with garnet and orthopyroxene, at the pressure–temperature conditions of the graphite–diamond transition along a typical cratonic geotherm, should have a molar Cr# (100Cr/(Cr+Al)) of ≥ 80 (Doroshev et al. 1997; Girnis and Brey 1999; Klemme 2004). In good agreement with these experimental outcomes, the median Cr# of spinel inclusions in diamond is 86.8 (mean = 86.6 ± 3.5) and the few samples of unspecified peridotitic paragenesis falling towards lower Cr# (Fig. 15) likely represent orthopyroxene-free (i.e., dunitic) assemblages, for which spinel + olivine remains stable for all lithospheric pressures.

For comparison of spinels from cratonic garnet peridotite xenoliths with inclusions in diamond, we excluded all xenolith spinels with Cr# < 60 because of a likely shallow garnet facies (< 100 km, see Klemme 2004) or retrograde origin. Despite this cut-off, the Cr# of spinel from garnet peridotites (median 80.5, mean 78.8 ± 6.8) is lower than that of inclusions. The Mg# of all but two (0.02%) spinel inclusions is > 50 (median = 69.1, mean = 68.9 ± 5.2) and compared to xenolith spinels (median Mg# = 62.6, mean = 61.6 ± 6.0) higher by about 6–7. Besides bulk rock composition, the Mg# of spinel depends on the temperature dependent exchange of Mg–Fe with olivine (O'Neill and Wall 1987); elevated Mg# for inclusion spinels may thus, at least partially, represent a temperature (depth) effect. Combined with high Cr#, spinel Mg# generally >50 allows classification as Mg-chromite. The ferric iron number (Fe^{3+}# = 100Fe^{3+} / (Fe^{2+} + Fe^{3+}); calculated from stoichiometry after Droop 1987) of spinel inclusions (median Fe^{3+}# = 15.9, mean = 15.7 ± 7.4; Fig. 16) is lower than that of xenolith spinels (median = 18.8, mean = 19.6 ± 7.6).

Overall low Fe^{3+}# in both inclusions and xenolith spinels is consistent with the moderately reducing conditions observed in the deep lithospheric mantle (Frost and McCammon 2008; Stagno et al. 2013; Luth et al. 2022). In view of the almost exclusively harzburgitic association of inclusion spinel, focusing on garnet harzburgites only, the Cr# (median = 83.1, mean = 82.8 ± 4.2) and Mg# (median = 63.9, mean = 64.2 ± 4.3) in xenolith spinel increases whilst the Fe^{3+}# (median = 18.1, mean = 17.5 ± 6.9) decreases slightly, but still not to the levels observed for inclusions (Figs. 15 and 16). TiO_2 contents are generally similarly low in both inclusions (median = 0.09 wt%; no mean reported for strongly non-normal distribution) and xenolith spinels (median = 0.10 wt%) but elevated 75th percentile values (Q3 = 0.22 wt% for inclusions and 0.33 wt% for xenolith spinels) indicate that moderate metasomatic re-enrichment of Ti is relatively widespread.

Key observations and conclusions

The principal distinction between diamond substrates and the cratonic mantle roots as sampled by garnet peridotite xenoliths is the well-established, much higher proportion of harzburgite (-dunite) to lherzolite (-wehrlite) in the former (~85:15%; Gurney 1984) compared to the latter (18:82% in our xenolith database). Potentially dunitic mineral assemblages, indicated by CaO contents in garnet < 1.8 wt%, are common diamond substrates (~38%) but rarely documented in xenoliths (~2%). This latter discrepancy may be somewhat enhanced by sampling bias during xenolith collection, as garnet- and/or clinopyroxene-rich peridotites are more likely to be picked. Using mineral Mg# as an indicator of source depletion through melt extraction again documents the overall more depleted character of diamond substrates relative to the deep (garnet-facies) cratonic lithospheric mantle represented in the xenolith record. Olivine, because of its very high modal abundance in cratonic peridotites (72 vol% as mean and median value; Pearson et al. 2004), is the most robust proxy for this purpose, as its Mg# effectively becomes independent of temperature and instead equivalent to bulk rock Mg#. The observation that on the paragenesis level olivine inside and outside of diamond has statistically indistinguishable means in Mg#, therefore, has fundamental implications: (1) that the major element composition of inclusions is imposed by the substrate and not by the diamond forming medium and (2) that widespread Fe-rich metasomatism of the lithospheric mantle did not occur subsequent to diamond formation, which is focused in the Paleoarchean for harzburgitic substrates and the Paleoproterozoic–Mesoproterozoic for lherzolitic substrates. The latter conclusion precludes neither metasomatism by small melt fractions/fluids subsequent to diamond formation, as such events have limited impact on bulk rock Mg#, nor localized metasomatic shifts in Mg#.

A distinguishing feature between inclusions and xenolith minerals lies in the higher Cr content and Cr/Al ratio of garnet and Mg-chromite in diamond. The extensive melt depletion events that characterize the protoliths of subcratonic lithospheric mantle did not affect the Cr content of the melting residues but efficiently removed Al (from primitive mantle to average cratonic harzburgite, Cr contents remain constant but about 90% of Al is removed; e.g., McDonough and Rudnick 1998, their Table 1). Higher Cr contents for inclusions are not limited to garnets with very low Ca intercept values and high Mg# (in fact, the highest Cr contents are associated with harzburgitic garnets with relatively low Mg# of 84–86) but occur equally for mildly subcalcic and even for lherzolitic garnets. This suggests that the almost exclusive restriction of Cr_2O_3 contents greater than 13 wt% to inclusion garnets is not a consequence of higher degrees of primary melt depletion being restricted to diamond substrates.

Nevertheless, the systematic offset to higher Cr contents, as best seen for spinel inclusions, may, at least partially, represent a source signal. Cr is not usually considered as a mobile element during mantle metasomatism but high pressure (4–6 GPa) experiments indicate an order of magnitude increase in the solubility of Cr in hydrous fluids associated with increased salinity (addition of 1.3–3 wt% of KCl; Klein-BenDavid et al. 2011). These authors consider that during percolation of such saline high-pressure fluids, Cr could dissolve from the peridotitic wall rocks without significantly affecting their high Cr concentrations. The ability of such saline fluids to impose their high-Cr characteristics on garnet inclusions in diamond, however, is likely limited, given that their mean Cr# (100Cr/(Cr+Al)) is only 7.5 (high-density fluid compilation of Weiss et al. 2022) compared to Cr# of 38–65 for the unusually Cr_2O_3-rich (> 13 wt%) garnet inclusions discussed here. In contrast, enrichment of Al in cratonic peridotites is frequently observed and possibly relates to fluids derived from recycled sediments (e.g., Rapp et al. 2017). Consequently, widespread but relatively mild re-enrichment in Al may have decreased Cr/Al ratios and increased modal garnet in cratonic peridotites sampled as xenoliths, with this effect being strongest for rocks with extreme primary Al depletion (very high Cr/Al ratios). This type of metasomatism may be responsible

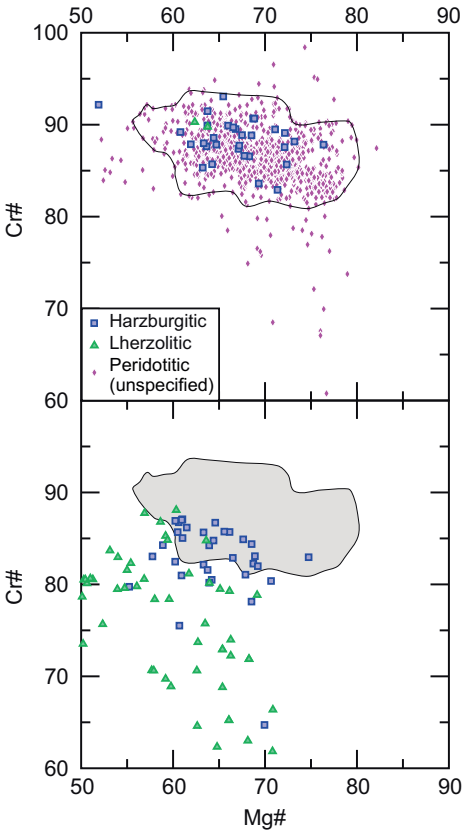

Figure 15. Molar Cr# (100Cr / (Cr + Al)) versus molar Mg# (100Mg / (Mg + Fe^{2+}), with Fe^{2+} calculated from total Fe based on stoichiometry; Droop 1987) for peridotitic Mg-chromites included in diamond (DI, **top**) and from cratonic garnet (-spinel) peridotite xenoliths (**bottom**). The **grey area** in the bottom diagram corresponds to the outline of the area of common spinel inclusions in diamond in the upper diagram (cf., Fipke et al. 1995). The paragenesis of Mg-chromite inclusions is derived from coexisting garnet or the presence of clinopyroxene (lherzolitic), in their absence the paragenesis is unspecified.

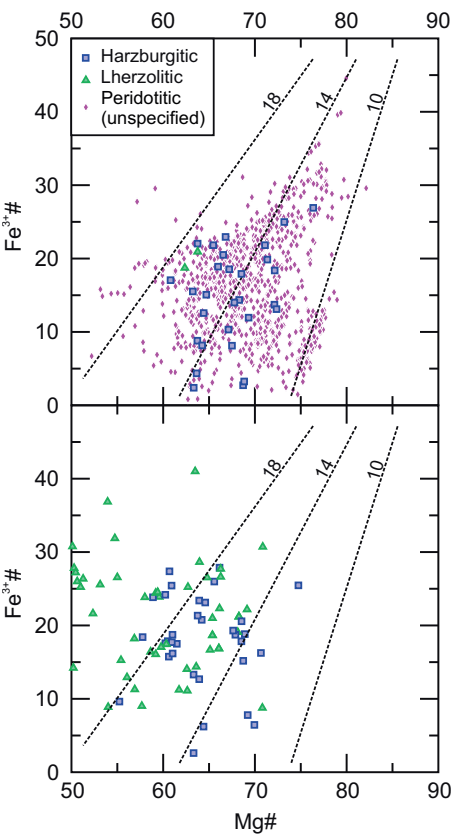

Figure 16. Molar Fe^{3+}# (100Fe^{3+}/ (Fe^{2+} + Fe^{3+})) versus molar Mg# (100Mg / (Mg + Fe^{2+})) for peridotitic Mg-chromites included in diamond (DI, **top**) and from cratonic garnet (-spinel) peridotite xenoliths (**bottom**). Fe^{2+} and Fe^{3+} were calculated from total Fe content based on stoichiometry (Droop 1987). The **dashed lines** and associated numbers indicate approximately constant total iron content (FeO^{total} in wt%).

for both the lower average and maximum Cr contents in xenolith-hosted garnet and spinel; it may have affected diamond substrates as well, just to a lesser degree.

An alternate explanation relates to the pressure and temperature dependence of the distribution of Cr between garnet and spinel (Doroshev et al. 1997; Grütter et al. 2006). Experiments demonstrated inclusion-like high Cr/Al ratios for coexisting Cr-pyrope and Cr-spinel in harzburgite at high pressures and temperatures (> 5 GPa and > 1200 °C; Malinovsky and Doroshev 1975; Girnis and Brey 1999). High Cr/Al inclusion compositions are accordingly interpreted as indicative of some diamond growth occurring over a wide range of temperatures, elevated above a cratonic geotherm during high-temperature thermal perturbations (Girnis et al. 1999; Grütter 2006).

The most sensitive indicators of metasomatism on the major-minor element level are Na, Ti and, for clinopyroxene, K. In orthopyroxene, clinopyroxene and garnet, metasomatic enrichment of Na and Ti in both inclusions and xenoliths is most prominent in the lherzolitic paragenesis and very intense Ti-rich metasomatism is almost entirely restricted to lherzolite xenoliths. Intense Ti metasomatism (leading to > 0.5 wt% TiO_2 in garnet) is restricted to temperatures of last equilibration in excess of 1130 °C, i.e., occurs above the hydrous solidus of lherzolite along typical cratonic geotherms (e.g., Wyllie and Ryabchikov 2000). Since equilibration temperatures of > 1130 °C are frequently observed for inclusions, the almost complete absence of evidence of intense Ti-metasomatism in inclusions (mild Ti-metasomatism is more frequent) likely relates to either a diamond unfriendly character of such metasomatism or an increase in Ti-metasomatic intensity or frequency after the formation of most peridotitic diamonds in the Archean-Mesoproterozoic. The opposite is true for potassic metasomatism documented in clinopyroxene, where only fairly moderate levels of enrichment are seen in xenoliths ($K_2O \leq 0.26$ wt%) whilst clinopyroxene inclusions show a tail in their frequency distribution of up to 1.68 wt% K_2O. This type of metasomatism may relate to potassic brines that are frequently observed as high-density fluid inclusions in fibrous diamonds (Izraeli et al. 2001; Weiss et al. 2022). That evidence for such metasomatism is best preserved inside diamond may relate to reactivation of potassic mantle metasomes and migration to shallower mantle in the course of transient heating events (e.g., Waters and Erlank 1988; Tappe et al. 2008). The overall low abundance of strongly potassic clinopyroxene inclusions suggests that potassic brines may be one medium of diamond formation in peridotitic substrates, but not the dominant one.

TRACE ELEMENT COMPOSITION OF PERIDOTITIC SUITE INCLUSIONS AND COMPARISON WITH CRATONIC PERIDOTITE XENOLITH MINERALS

Garnet

To our knowledge, the first REE pattern for peridotitic garnet was obtained by Philpotts et al. (1972), via isotope dilution thermal ionization mass spectrometry on separated minerals from a phlogopite garnet lherzolite xenolith (GSFC #187) from Roberts Victor (Kaapvaal Craton). From today's perspective, the reported humped REE_N pattern with a prominent peak at Dy would be considered anomalous.

The two common types of REE_N patterns of garnet from cratonic peridotites, *normal* and *sinuous* or *sinusoidal*, were first reported by Shimizu (1975): (1) garnets from three sheared (mosaic-porphyroclastic texture) lherzolite xenoliths from kimberlites in Lesotho showed steep positive slopes in the $LREE_N$ and fairly flat MREE–HREE at ≥10 times chondritic abundance, similar to garnets from eclogite xenoliths and megacrysts (hence the term "*normal*" patterns), (2) garnets from three granular (coarse texture) lherzolite xenoliths from Lesotho and the Kimberley area had sinusoidal patterns, with a prominent peak at Sm_N–Eu_N and an upward kink in slope near Er_N. For inclusions in diamond, similar sinusoidal REE_N pattern were subsequently reported by Shimizu and Richardson (1987) for harzburgitic garnets in diamonds from Kimberley and Finsch, while normal REE_N patterns were first observed for lherzolitic garnet inclusions from Akwatia, Ghana (Stachel and Harris 1997).

REE_N patterns of garnet inclusions of harzburgitic and lherzolitic paragenesis. Since the pioneering work of Shimizu and Richardson (1987), the number of REE analyses of garnet inclusions has risen considerably as ion microprobes enjoyed wider use, with 223 harzburgitic and 72 lherzolitic garnets in our database (see Fig. 17). These analyses clearly establish sinusoidal REE_N patterns as the hallmark of both harzburgitic and lherzolitic inclusion garnets. On average, the degree of sinuosity, however, is more pronounced for harzburgitic garnets (see median, 10^{th} and 90^{th} quartile patterns in Fig. 17).

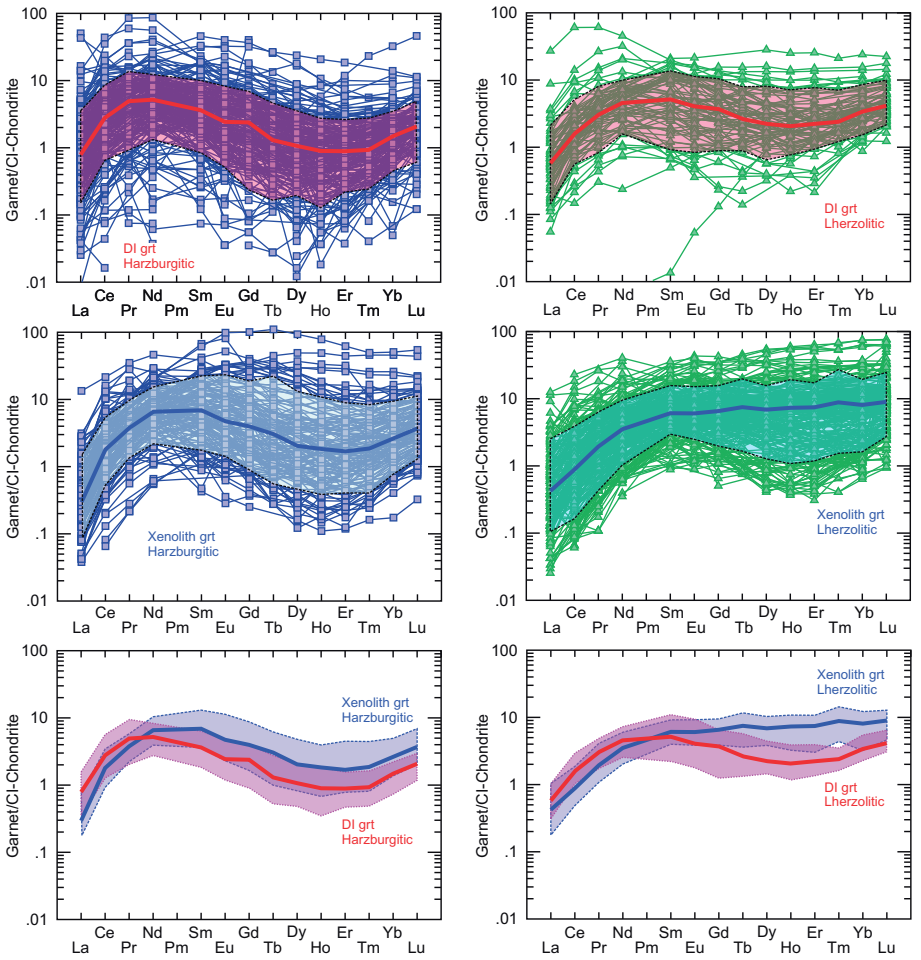

Figure 17. Chondrite-normalized REE patterns for harzburgitic (n = 223) and lherzolitic (n = 72) garnet inclusions in diamond (DI, **top**) and harzburgitic (n = 152) and lherzolitic (n = 280) garnets from xenoliths (**middle**). **Thick red or blue lines** are median values, transparent fields are ranges from the 10th to 90th percentile. The **two bottom plots** compare the median patterns and interquartile ranges (i.e., 25th to 75th percentile) of inclusion (**red**) and xenolith (**blue**) garnets of harzburgitic and lherzolitic paragenesis. CI-chondrite composition is from McDonough and Sun (1995).

In detail, the range of REE_N patterns displayed by peridotitic garnet inclusions is much more complex than apparent from Figure 17. Based on overall shape and the presence and position of a peak in the $LREE_N$–$MREE_N$, we identified 10 types of REE_N patterns, which due to uncertainties in the classification of garnet analyses that do not include the LREE praseodymium (Pr) were assigned into 12 classes. The REE_N patterns for these classes are shown in Appendix Figure 1 and the frequency of their occurrence for garnets of the harzburgitic and lherzolitic paragenesis is shown in Figure 18. Patterns with peaks at Ce, Pr, Nd, Sm and Eu are all sinusoidal. Non-sinusoidal patterns are either V-shaped with a peak at La, show steep *positive* or nearly *flat* slopes from $LREE_N$ to $HREE_N$, or classify as *normal* (rise in $LREE_N$, flat and superchondritic MREE–HREE). *Abnormal* patterns fit none of these categories and typically are "noisy" with multiple peaks. For harzburgitic garnets, sinusoidal patterns peaking at Nd are clearly dominant (Fig. 18). Including patterns with a peak at Nd

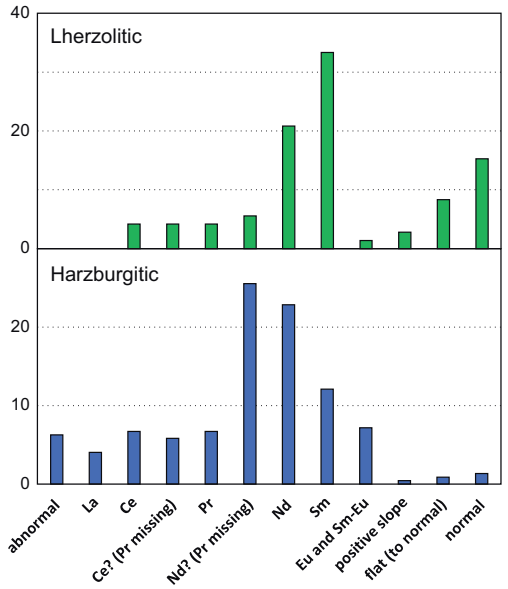

Figure 18. The relative abundance (in %) of the various inclusion garnet REE_N patterns, calculated separately for the harzburgitic and lherzolitic parageneses (based on 295 peridotitic garnets: 223 harzburgitic and 72 lherzolitic). The classes from Ce to Eu represent the different peak positions for sinusoidal REE_N patterns. The groups Ce? and Nd? show peaks at these elements but since the neighboring LREE Pr was not analyzed, a true peak at Pr cannot be excluded – hence the question marks. REE_N patterns peaking at La are V-shaped. Other types (1) show positive slopes from $LREE_N$ to $HREE_N$, (2) are nearly flat, or (3) show a positive slope within the $LREE_N$ but nearly flat $MREE_N$–$HREE_N$ (normal patterns). Patterns that fit none of these categories are classified as abnormal. REE_N patterns for all groups are shown in Appendix Figure 1.

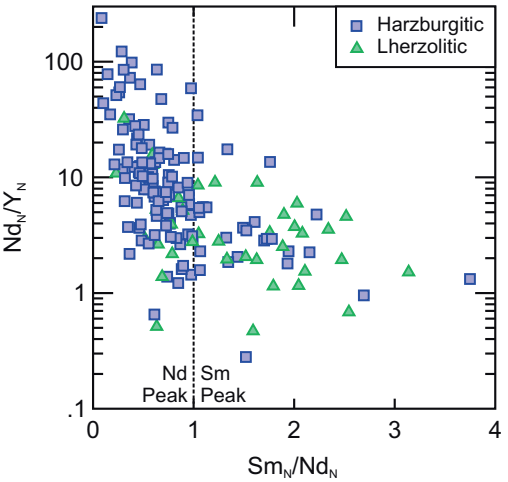

Figure 19. Chondrite-normalized ratios of Nd/Y and Sm/Nd for inclusion garnets with REE_N patterns peaking (1) at Nd (77% harzburgitic), (2) at Nd? (Pr missing, 93% harzburgitic) and (3) at Sm (with about equal abundance of harzburgitic and lherzolitic garnets). Garnets with REE_N patterns peaking at Nd ($Sm_N/Nd_N < 1$) have a much steeper slope in the MREE (high Nd_N/Y_N) than samples with a peak at Sm ($Sm_N/Nd_N > 1$).

with Pr not analyzed, 49% of harzburgitic garnets peak at Nd. By contrast, 33% of lherzolitic garnets peak at Sm and only 21% at Nd (27% including the peaks at Nd with Pr missing) and 15% of lherzolitic garnets show normal patterns, as opposed to 1% of harzburgitic garnets (Fig. 18). The transition between the two most important REE_N patterns, peak at Nd (including samples with Pr missing) to peak at Sm, is associated with a decrease in the degree of sinuosity, measured as the Nd_N/Y_N ratio ($MREE_N$ slope) in Figure 19.

Other trace elements. Other commonly and reliably analyzed trace elements in garnet inclusions are Sr, Nb, Ti, Hf, Zr and Y (in sequence of increasing compatibility; Fig. 20). Whilst Sr concentrations are higher in harzburgitic garnets (median value of 2.4 ppm, compared to 0.67 ppm for lherzolitic garnets; likely controlled by the absence/presence of clinopyroxene, see Stachel et al. 2004), the patterns for the remaining elements are nearly parallel but

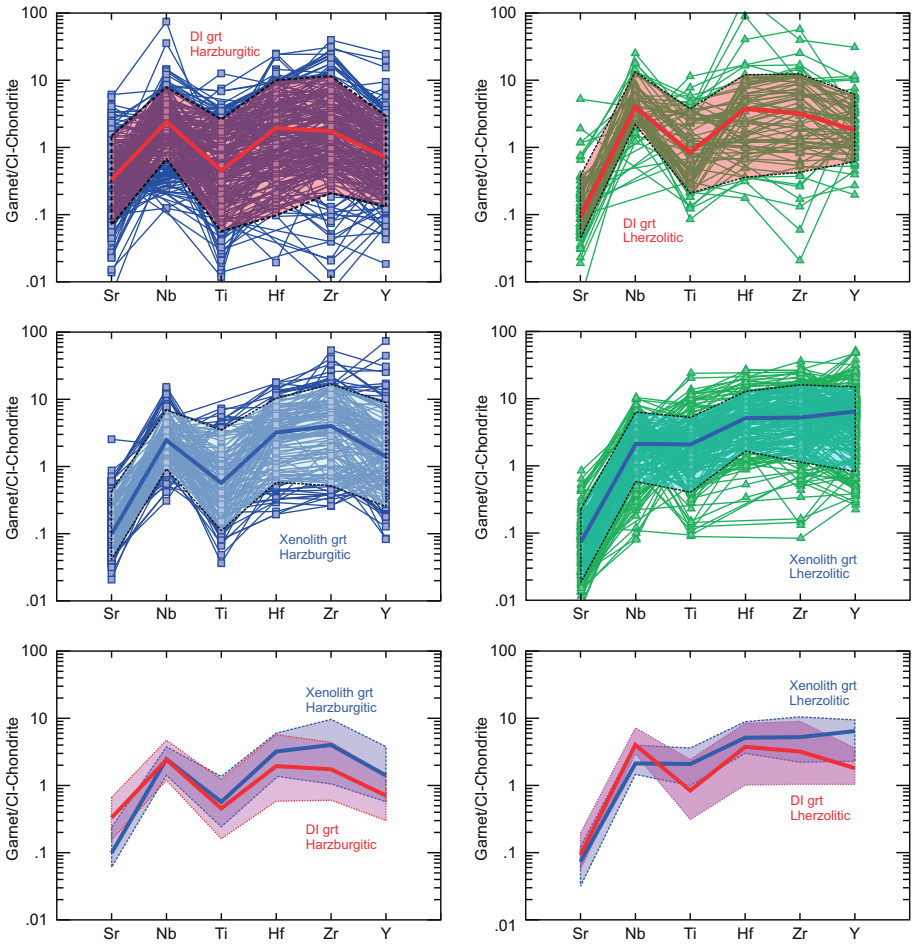

Figure 20. Chondrite-normalized patterns for large ion lithophile (Sr) and high field strength elements (Nb, Ti, Hf, Zr and Y) in harzburgitic and lherzolitic garnet inclusions in diamond (**top**) and from cratonic garnet peridotite xenoliths (**middle**). Compatibility in garnet (based on garnet–melt partition coefficients; e.g., Green 1994) increases from left to right. **Thick red or blue lines** are median values, transparent fields are ranges from the 10th to 90th percentile. The **two bottom diagrams** compare the median patterns and interquartile ranges (i.e., 25th to 75th percentile) of inclusion (**red**) and xenolith (**blue**) garnets of harzburgitic and lherzolitic paragenesis.

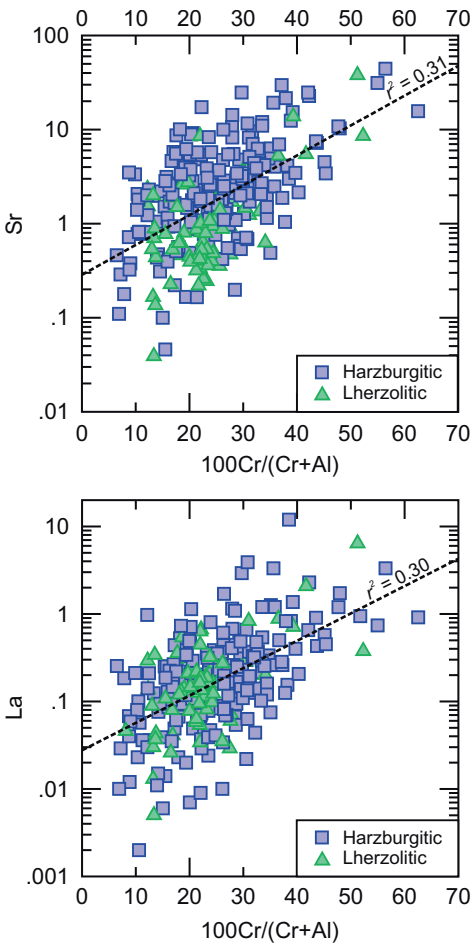

Figure 21. Sr (**top**) and La (**bottom**) in ppm versus molar Cr# (100Cr / (Cr + Al)) for peridotitic garnet inclusions in diamond. The **dashed lines** are linear regressions with the coefficient of determination (r^2) being indicated.

with higher concentrations in lherzolitic garnets (Fig. 20). Both parageneses show distinct negative anomalies for Sr and Ti (subchondritic median values), flat and typically superchondritic Nb, Hf and Zr, and slightly depressed Y_N (with a subchondritic median for harzburgitic garnets).

Correlations with major elements. Griffin et al. (1999a) highlighted the usefulness of garnet Cr# as a measure for the degree of chemical depletion of cratonic peridotites. In addition to possible metasomatic modification (e.g., Burgess and Harte 1999; Grütter and Menzies 2017), the interpretation of garnet Cr# is, however, complicated by the pressure-controlled exchange of Cr and Al between spinel and garnet (in spinel–garnet peridotites, garnet Cr# is a geobarometer; Grütter et al. 2006). In garnet, increasing Cr# is accompanied by broad trends of enrichment in strictly incompatible trace elements such as Sr and the LREE (Fig. 21).

A more unambiguous indicator in garnet of the degree of primary melt extraction from its source protolith is its position relative to the lherzolitic trend in a Cr/Ca plot, which can be expressed as the Ca intercept value (Grütter et al. 2004; see above) or more simply but less accurately, as the Ca# (molar 100Ca/(Ca+Mg+Fe)). In addition to primary melt depletion, garnet Ca intercept values (or Ca#) also track secondary metasomatic modification of the diamond substrates. Figure 22 shows a positive correlation between the Yb content and Ca# of garnet. To interpret this correlation as a straightforward geochemical trend may, however, be misleading as crystal chemical controls have to be considered as well. For eclogites, increasing partitioning of REE into garnet with increasing Ca content was recognized by Harte and Kirkley (1997). In a study of trace element partitioning between mantle minerals and silico-carbonate melts, Girnis et al. (2013) confirmed these findings and observed a strong increase in garnet–melt partition coefficients for REE with Ca#. This effect renders HREE like Yb and Lu incompatible in strongly subcalcic garnets (Girnis et al. 2013). Figure 22 shows a predicted trend for Yb in garnet, based purely on the crystal chemical effect imposed by varying the Ca# number from 15 (approximately equivalent to the lherzolite/harzburgite boundary) to 0. The predicted effect is over an order of magnitude stronger than the observed correlation in the inclusion data set, suggesting that either the crystal chemical effect was overestimated by Girnis et al. (2013) or that other effects (e.g., bulk rock chemistry) partially compensate the crystal chemically predicted strong HREE depletion in low-Ca garnets.

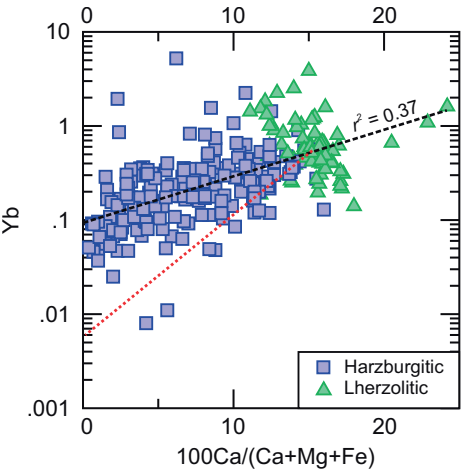

Figure 22. Yb (ppm) versus molar Ca# (100Ca / (Ca + Mg + Fe)) for peridotitic garnet inclusions in diamond (DI). The **black dashed line** is a linear regression with the coefficient of determination (r^2) being indicated. The **red stippled line** is a hypothetical trend, showing how garnet should evolve away from compositions at the lherzolite/harzburgite boundary (Ca# of ~15) towards highly subcalcic, harzburgitic–dunitic compositions, based on trace element partitioning with a silico-carbonatitic melt of constant composition (using the X_{Ca} dependent *D*-value for Yb of Girnis et al. 2013).

Comparison with garnet from cratonic peridotites. In cratonic peridotites, harzburgitic garnets inside and outside of diamond share overall similar, sinusoidal REE_N patterns (Fig. 17). On average, xenolith garnets, however, have higher MREE and HREE, resulting in a shift of the peak from Nd (for inclusion garnets) to Sm for the median REE_N pattern. Sr contents in xenolith garnets tend to be lower and Zr and Y contents higher than in inclusions garnets (Fig. 20). Distinct Nd and Sr isotope composition of harzburgitic garnets included in diamond and from concentrate were first reported by Richardson et al. (1984) and are discussed in detail by Smit et al. (2022).

For lherzolitic garnets, differences are even more pronounced: xenolith garnets have significantly higher contents in the MREE–HREE from Gd onwards, resulting in normal REE_N patterns for median and 25th and 75th quartile compositions, as opposed to sinusoidal patterns for the median and interquartile range of lherzolitic garnet inclusions in diamond (Fig. 17). Lherzolitic xenolith garnets generally also lack the pronounced negative Ti_N anomalies characteristic for inclusion garnets and on average have higher Y contents (Fig. 20).

Clinopyroxene

Shimizu (1975) not only defined the two principal types of REE_N patterns of peridotitic garnet but also characterized the REE_N patterns of associated clinopyroxene: (1) clinopyroxene occurring together with garnet with normal REE_N in the three studied sheared lherzolite xenoliths showed mildly fractionated REE_N patterns with about 10× chondritic LREE and chondritic to mildly subchondritic HREE, similar to clinopyroxene in eclogite xenoliths and megacrysts. (2) Clinopyroxene in equilibrium with garnet with sinusoidal REE_N in three coarse lherzolites was found to have much more fractionated LREE–HREE, falling from ~20–30 chondritic LREE to about 0.4× chondritic HREE.

Types of REE_N patterns. The two groupings introduced by Shimizu (1975) largely hold for peridotitic clinopyroxene inclusions in diamond. For inclusions, the mildly fractionated group is characterized by *humped* patterns peaking at Nd_N (Fig. 23), with La_N/Sm_N between 0.3 and 2.5 with a median value of 0.6. Two clinopyroxenes associated with the humped

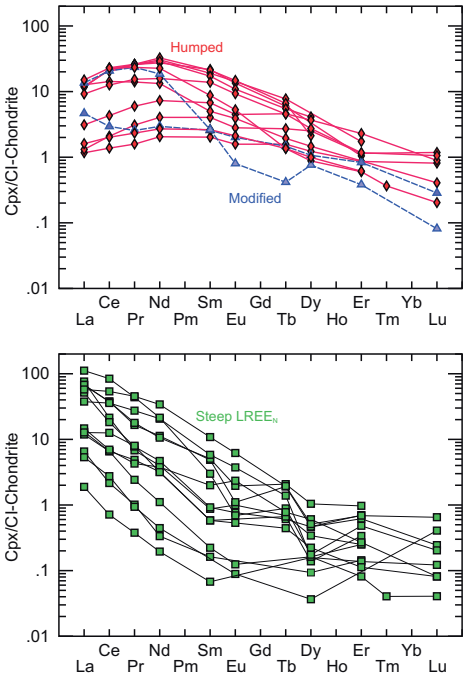

Figure 23. Chondrite-normalized REE patterns for peridotitic clinopyroxene inclusions in diamond. **Top**: mildly fractionated humped patterns (peaking at Nd_N) and similar modified patterns, distinct through either additional enrichment in La and Ce or a trough in the $MREE_N$ (Sm–Tb). **Bottom**: clinopyroxenes with steep $LREE_N$ slopes and fairly unfractionated Dy_N/Lu_N.

group show *modified* patterns, which by comparison with the humped patterns show enrichment of La and Ce in one case and enriched LREE and a trough in $MREE_N$ in the other. In slight contrast to the xenolith data of Shimizu (1975), the key distinguishing criterion of the second group are steep negative $LREE_N$ slopes (*steep-LREE$_N$*) and not necessarily a high LREE–HREE ratio (Fig. 23). La_N/Sm_N ranges between 4.6 and 87 with a median value of 22.

Clinopyroxene inclusions with humped REE_N patterns coexist with garnets with normal patterns (n = 2 for inclusion database), characterized by steep positive slopes in the $LREE_N$. This coexistence matches observations made for peridotite xenoliths beyond the limited sample set of Shimizu (1975), with, e.g., the occurrence of clinopyroxene with humped patterns together with garnet with normal patterns being characteristic for the Type 1 garnet lherzolites of Grégoire et al. (2003). Clinopyroxene inclusions with steep $LREE_N$ coexist with garnets with sinusoidal or positively sloped REE_N (n = 4), the latter characterized by a less positive slope in the LREE compared to garnets with normal REE_N patterns. Clinopyroxene with steep $LREE_N$ (but with a peak at Ce) and garnets with sinusoidal or positively sloped REE_N patterns also characterize the Type 2 garnet lherzolites of Grégoire et al. (2003).

In major/minor element composition, clinopyroxenes with humped REE_N patterns have lower Mg# (87.9–93.1, median of 90.6) and higher TiO_2 contents (0.04–0.23 wt%, median of 0.10 wt%) than clinopyroxenes with steep-$LREE_N$ (Mg# 91.5–94.8, median of 92.8; TiO_2 < 0.02–0.05 wt%, median of 0.03).

Olivine

Olivine is the last of the three peridotitic inclusion minerals that have received attention for trace element studies. Following up on an initial study (De Hoog et al. 2010) on trace elements in olivine from peridotite xenoliths and their application to thermobarometry, De Hoog et al. (2019) analyzed 10 trace elements in 36 olivine inclusions in diamonds from Akwatia, Ghana with an ion microprobe. They found that the contents of Ca and Na and their ratios with Al can be used in combination to constrain the paragenesis (harzburgitic versus lherzolitic) of peridotitic olivine inclusions, while Ti in olivine may be employed as a tracer of metasomatic re-enrichment of diamond substrates. Based on new reference materials and recent advances in the analysis of trace elements in olivine via LA-ICPMS (Bussweiler et al. 2019), we expect a large increase in trace element data for olivine inclusions over the coming years. Only such an expanded data set will allow us to conclusively assess whether the paragenetic fields defined by De Hoog et al. (2019) on the basis of Akwatia inclusions can be applied universally.

Discussion of trace elements in peridotitic inclusions

Normalization to primitive (J4) garnet and cpx. To derive the trace element characteristics of the rock a mineral derives from, normalization to CI-chondrite or primitive mantle is of limited use, as the derived patterns are strongly determined by the degree of compatibility of the studied trace elements in the available lattice sites. To overcome this problem, Stachel et al. (1998) instead suggested normalization to minerals that are well equilibrated in a bulk rock with a primitive mantle-like composition and chose high-temperature sheared garnet-lherzolite xenolith J4 from Jagersfontein (Jagoutz and Spettel, unpublished data; Wolff-Boenisch 1994). Since then, other samples with near-primitive compositions have been recognized (e.g., Vitim xenolith 313-105 of Ionov et al. 2005) but despite offering a more complete range of analyzed trace elements, their bulk rock REE patterns are neither a perfect match for primitive nor for depleted MORB-source mantle. For that reason, we carefully re-analyzed mineral separates from J4 using laser ablation sector field ICPMS (Appendix Table 2) and continue the use of J4 garnet and clinopyroxene for normalization purposes.

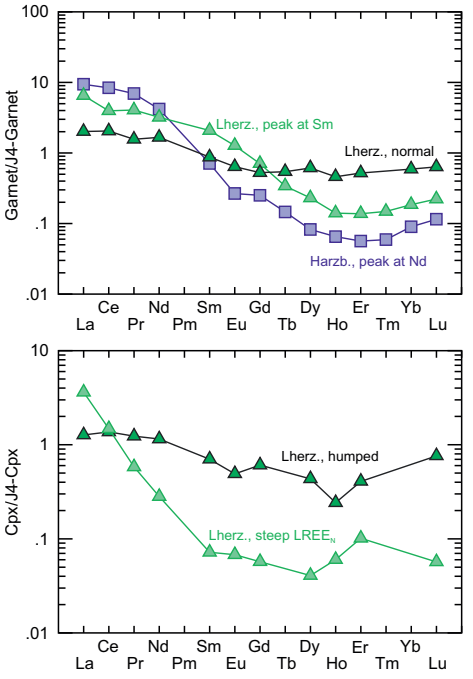

Figure 24. Median REE contents of the principal garnet (**top**) and clinopyroxene (**bottom**) groups, normalized to REE concentrations of the same minerals in a well equilibrated garnet lherzolite xenolith with a primitive mantle-like bulk composition (J4 from Jagersfontein; major and trace element mineral compositions in Appendix Table 2). Based on their chondrite normalized REE_N patterns (Fig. 18 and Appendix Figure 1), the three principal garnet groups shown are: (1) harzburgitic garnets peaking at Nd, (2) lherzolitic garnets peaking at Sm and (3) lherzolitic garnets with normal REE_N. The two principal types of chondrite-normalized clinopyroxene REE patterns are (1) humped and (2) steep $LREE_N$.

For simplicity, for J4-normalization we only use the median patterns of the principal REE_N pattern types (see Fig. 18 and Appendix Fig. 1): harzburgitic garnet inclusions peaking at Nd, lherzolitic garnet inclusions peaking at Sm, and lherzolitic garnet inclusions with normal REE_N patterns. Normalization to primitive garnet reveals that harzburgitic garnets with strongly sinusoidal patterns reflect sources with REE contents steadily decreasing from mildly enriched LREE through the MREE to a trough in the HREE at Er, with increasingly less-depleted HREE from Er to Lu, overall resulting in a V-shaped REE_{J4} pattern (Fig. 24). On the other end of the spectrum, normal REE_N patterns of lherzolitic garnet inclusions, which are dominant among garnets from lherzolite xenoliths (Fig. 17), represent sources with near-primitive trace element compositions similar to J4 (Fig. 24). Lherzolitic garnet inclusions with REE_N patterns peaking at Sm fall in between these two endmembers, with near primitive LREE concentrations, a less prominent drop towards Er_{J4} than for harzburgitic garnets, and a shallower increase towards Lu_{J4}. Given the higher distribution coefficients for LREE in clinopyroxene relative to garnet (e.g., Johnson 1998), minor relative depletion of LREE in lherzolitic relative to harzburgitic garnets may partially relate to metamorphic equilibration with clinopyroxene for the lherzolitic paragenesis.

For lherzolitic substrates, the median values of the two principal pattern types in clinopyroxenes, humped and steep-$LREE_N$, may be used to assess the validity of the garnet-based findings. HREE concentrations in clinopyroxene inclusions in diamond generally are low (in part below detection), resulting in noisy median HREE patterns. In addition, Yb analyses in clinopyroxene via SIMS appear to frequently suffer from an analytical problem (possibly an unrecognized interference) and hence are not reported in a number of studies. This drawback relative to garnet inclusions is compensated by higher and therefore more accurately determined LREE concentrations (e.g., La is approximately 1–100 × chondritic in abundance, compared to 0.03–15 × chondritic for garnet inclusions). Normalized to J4-clinopyroxene, inclusions with humped REE_N patterns also reveal a near-primitive composition (Fig. 24). This agrees well with the observation that such clinopyroxenes occur together with garnets with normal REE_N patterns. Clinopyroxene with steep $LREE_N$ patterns shows enrichment in LREE and steep negative slopes towards the MREE, when normalized to J4 (Fig. 24). Overall, this fits with the observation made for lherzolitic garnets with sinusoidal patterns peaking at Sm but suggests a more continuous negative slope from La–Sm in the diamond substrates than indicated by these garnets. Due to the problems outlined above, the HREE patterns of clinopyroxenes are considered less informative than those of garnet and not further discussed here.

Considering the well-established origin of cratonic peridotites as residues of intense melt extraction events in the Archean (*see above*), the LREE-enriched character of peridotitic diamond substrates appears counterintuitive. Based on REE patterns of unmodified MORB residues (e.g., Sharma and Wasserburg 1996), the positive slope within the $HREE_{J4}$ from Tm to Lu, observed for garnets with chondrite-normalized patterns peaking at Nd and Sm (Fig. 24), fits the steep positive $LREE_N$–$HREE_N$ slopes in such residues. The common negative slopes from La_{J4}–Er_{J4} then are a consequence of metasomatic re-enrichment in incompatible trace elements, first recognized as a universal process in lithospheric peridotites by Frey and Green (1974). From harzburgitic garnets, through lherzolitic garnets with sinusoidal REE_N and associated clinopyroxenes with steep-$LREE_N$ patterns, to lherzolitic garnets with normal REE_N and associated clinopyroxenes with humped REE_N patterns, the signature of primary depletion becomes increasingly obliterated and eventually completely erased in the J4-normalized mineral trace elements patterns (and hence the bulk rocks). The decrease in Mg# and increase in TiO_2 for the transition from clinopyroxenes with steep-$LREE_N$ to humped patterns implies that this metasomatic progression is not limited to trace elements but falls in the categories of "enrichment in major–minor–trace elements without modal change" or "modal metasomatism" of Harte (1983, 1987).

Fluid versus melt metasomatism. Having established (1) that garnets with sinusoidal REE_N patterns, when normalized to a primitive garnet composition, document preferential re-enrichment in LREE and (2) that the progression from sinusoidal towards normal REE_N patterns (or from V-shaped to primitive J4-normalized patterns) increasingly also involves addition of moderately incompatible trace elements and major/minor elements, raises the question what metasomatic agent(s) drive this re-enrichment process. Trace element signatures, in particular ratios of strongly to mildly incompatible elements (LREE/HREE, Zr/Y, Sm/Hf), have long been used to make a first order division between fluid- and melt-driven metasomatism (Stosch and Lugmair 1986; Shimizu and Richardson 1987; Griffin and Ryan 1995; Stachel et al. 1998; Viljoen et al. 2014). Griffin and Ryan (1995) empirically developed a widely used diagram of Y versus Zr (Fig. 25), with vectors for low-temperature phlogopite (fluid) metasomatism (high Zr/Y) and high-temperature melt metasomatism (intermediate Zr/Y). These two trends emerge from a field for "depleted" garnets near the origin, where a distinction is no longer possible (approximately at Y < 5 ppm and Zr < 20 ppm).

For inclusion garnets exceeding this threshold, harzburgitic garnets mostly fall onto or close to the fluid metasomatic trend whilst lherzolitic garnets generally have lower Zr/Y, compatible with melt metasomatic re-enrichment of their substrates. A notable exception is the large population of

lherzolitic garnet inclusions from the Victor Mine in Canada, which mainly displays Zr/Y ratios indicative of fluid metasomatism or intermediate between fluid and melt metasomatism (Fig. 25). Excluding Victor garnets, this overall distribution was linked (Stachel and Harris 1997; Stachel and Luth 2015) to harzburgitic diamond substrates mostly residing below their hydrous solidus (thus permitting percolation of fluids only), while lherzolitic diamonds form generally above the hydrous (± carbonated) solidus (allowing for the percolation of melt). Geothermobarometric data for lherzolitic inclusions in diamonds from Victor indicate their derivation from just below the hydrous lherzolite solidus, consistent with their comparatively high Zr/Y.

For the study of garnets included in diamond, however, Y and Zr generally are not sensitive enough as tracers of metasomatism and 70% of garnets fall below the threshold of Y < 5 and Zr < 20 ppm. This is in stark contrast to cratonic peridotite xenoliths, where only 29% of garnets fall below the Y and Zr threshold. This much higher proportion among inclusions of garnets below the threshold again highlights the overall much more depleted nature of peridotitic diamond substrates compared to the xenolith and xenocryst sample. Despite their low Y and Zr, garnets below the threshold nevertheless are almost invariably affected by metasomatic re-enrichment. Garnets reflecting the intense primary melt depletion characteristic for cratonic peridotites should have trace element patterns with $LREE_N/MREE_N \ll 1$ (see above), a signature that is virtually absent among inclusion garnets even below the Y and Zr threshold. Of the inclusion garnets below the threshold, only 7% have $Nd_N/Y_N < 1$, and one sample (0.5%) has $Nd_N/Y_N < 0.1$. Xenolith garnets below the threshold show a very similar picture, with only 11% having $Nd_N/Y_N < 1$ and 0.7% < 0.1. With over 2/3 of garnet inclusions being depleted below the threshold in Y–Zr space, it is evident that diamond formation usually is associated with mild metasomatic events, reflecting low fluid–rock or melt–rock ratios. Note that low

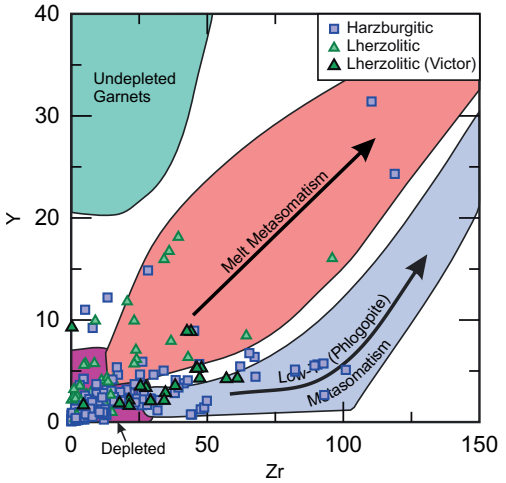

Figure 25. Y versus Zr (ppm) in peridotitic garnet inclusions in diamond. Compositional fields and trends are from Griffin and Ryan (1995). The major melt extraction event that preceded the formation of subcratonic lithospheric mantle in the Archean is reflected in Y and Zr contents of garnets falling into the depleted field (shown in **purple**). Secondary metasomatic re-enrichment may occur (1) through fluids at low (subsolidus) temperatures, associated with high Zr/Y (**blue field**) or (2) through melts (supersolidus conditions), associated with lower Zr/Y (**red field**). The bulk of inclusion garnets falls into the depleted field, but for garnets where Zr and Y contents are sufficiently high (Y ≥ 5 ppm and Zr ≥ 20 ppm) to assign a trend, fluid metasomatism dominates for harzburgitic garnet inclusions and melt metasomatism for lherzolitic inclusions. Assuming an average cratonic model geotherm, this observation is consistent with harzburgitic substrates in the lithospheric mantle generally residing at pressure–temperature conditions below their solidus and lherzolitic substrates residing mostly at supersolidus conditions (see main text for a more detailed discussion). An exception is formed by lherzolitic garnets in diamonds from the Victor Mine, for which geothermobarometric results indicate formation below the wet lherzolite solidus.

fluid/melt–rock ratios do not imply diamond formation under fluid-limited conditions: protracted diamond growth involving multiple metasomatic pulses evidently involves sufficiently high ratios of fluid/melt–diamond to preclude widespread Rayleigh fractionation of stable isotopes and nitrogen in diamond (Howell et al. 2020; Stachel et al. 2022).

On the level of mineral inclusions, the effects of multiple metasomatic events cannot be separated using only trace elements but require radiogenic isotope approaches. For example, based on unsupported (low Rb) highly radiogenic Sr in harzburgitic garnet inclusions, Richardson et al. (1984) proposed that a melt metasomatic event affected the harzburgitic diamond substrates beneath the Kimberley area of the Western Kaapvaal Craton within 300 m.y. before diamond formation (at about 3.3–3.2 Ga).

Fluids as metasomatic agents. The concept of fluid-driven metasomatism of lithospheric mantle was widely popularized by Bailey (1982) and two key arguments support the involvement of supercritical CHO fluids in mantle metasomatism, particularly of harzburgitic substrates: (1) As discussed above, extremely high ratios of strongly to moderately incompatible trace elements and a negligible metasomatic effect on both moderately incompatible trace elements (Ti, Y, HREE) and major elements (e.g., Mg#, Ca, Al and Cr) clearly are not compatible with melt involvement. (2) The average cratonic model geotherm (40 mW/m^2; Hasterok and Chapman 2011) intersects the carbonated, hydrous solidus of harzburgite (Wyllie 1987) at ~1300 °C. This implies that with the exception of the deepest regions ($\gtrsim$180 km) located near the lithosphere–asthenosphere boundary, harzburgite in the lithospheric mantle is impermeable to melt percolation, as migration along grain boundaries causes both thermal and compositional equilibration, which inevitably leads to freezing of melts in subsolidus substrates.

The range in composition of possible metasomatic fluids can be considerably narrowed by examining a few basic constraints:

1. *The fluid must be stable in equilibrium with peridotite*. This constraint is not met for CO_2-rich fluids, which may occur only on the oxidizing side of the EMOD/G (enstatite + magnesite = olivine + diamond/graphite; Eggler and Baker 1982) buffer. Along cratonic geotherms throughout the entire peridotitic lithospheric mantle, CO_2 is buffered through carbonation reactions involving olivine ± pyroxene (Wyllie and Huang 1976; Brey et al. 1983). Depending on the redox conditions, H_2O-rich and CH_4-rich fluids can both be stable in equilibrium with peridotite. Excluding a subgroup of unusually oxidized samples from the Slave craton, the xenolith record for the depth range 140–180 km has a main range in $\Delta\log fO_2$ (FMQ), i.e., the oxygen fugacity in log unit difference relative to the FMQ buffer, of ~ −3 to −1.5 (see, e.g., Luth and Stachel 2014). For the average conditions of diamond formation (~1140 °C/5 GPa, based on garnet–olivine thermometry; Stachel and Luth 2015), this fO_2 range implies that CHO fluids are at the water maximum, with water contents ranging between 85 and 98 mol% (calculated using GFluids of Zhang and Duan 2010; see Fig. 1 of Stachel et al. 2017). Matjuschkin et al. (2019) showed that on the reducing side of the water maximum (lower end of the main range considered here), GFluids may significantly underestimate CH_4 contents but this does not affect the principal conclusion that the xenolith record over the 140–180 km depth range is centered at fO_2 conditions corresponding approximately to the water maximum.
2. *The fluid must be able to percolate through peridotite at low fluid:rock ratios*. High dihedral angles for both CO_2–olivine and CH_4–olivine (Watson et al. 1990; Wyllie 1992; Ferrando et al. 2017) preclude efficient percolation of such fluids through the lithospheric mantle. The dihedral angle for aqueous fluid–olivine decreases with increasing pressure (Watson et al. 1990), permitting efficient percolation at pressures ≥ 3 GPa (Mibe et al. 1998). Added salinity decreases dihedral angles of aqueous fluids with olivine even further (Huang et al. 2019).

3. *The fluid must dissolve and transport the chemical components associated with mantle metasomatism*. Low solubility of trace elements such as REE is well documented for CO_2-rich fluids under mantle conditions (e.g., Meen et al. 1989). An experimental study of trace element solubility in CH_4-rich fluids is still outstanding but given the non-polar character of the symmetrical CH_4 tetrahedron, CH_4 fluids are expected to be poor solvents. In contrast, the solubility of solids in aqueous fluids increases strongly with pressure and is on the wt% level at mantle conditions (e.g., Ayers et al. 1997). At diamond stable conditions (≥ 4 GPa), trace element partitioning between peridotite minerals and aqueous fluids is similar to partitioning with silicate melts, with strong LREE/HREE fractionation (Fig. 26), and about 36 wt% (15 mol%) dissolved solids in the fluid at subsolidus conditions (1000 °C, 5–6 GPa; Kessel et al. 2015).

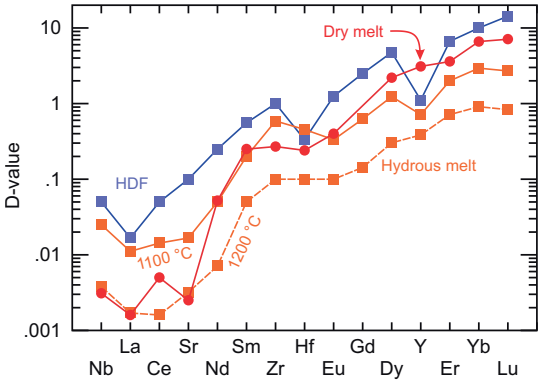

Figure 26. Trace element distribution coefficients (D-values) between garnet and possible metasomatic agents ranging from hydrous high-density fluids (HDF) through hydrous melts to "dry" melts. The 6 GPa experiments for HDF (1000 °C; 64 wt% H_2O) and hydrous melts (1100 and 1200 °C; 39 and 24 wt% H_2O, respectively) are from Kessel et al. (2015), the experiments for garnet in equilibrium with dry Hawaiian olivine tholeiite are from Johnson (1998). The experiments of Kessel et al. (2015) suggest that trace element partitioning into garnet decreases by about an order of magnitude from HDF to hydrous melt significantly above the solidus (1200 °C). Overall slopes and predicted LREE/HREE fractionations are, however, quite similar for all four sets of partition coefficients. Element order reflects increasing compatibility in the garnet structure (after Green 1994).

In conclusion, (1) the redox state recorded in mantle xenoliths from the main portion of the lithospheric diamond stability field falls at or near the water maximum, (2) H_2O is the only CHO fluid species with a sufficiently low dihedral angle with olivine to readily percolate along grain boundaries and (3) aqueous fluids also are the only CHO species with the ability to dissolve incompatible trace elements in the required quantities. The high load of dissolved solids carried by aqueous fluids at the pressure–temperature conditions inside the diamond stability field justifies using the term "high-density fluid" (HDF; Klein-BenDavid et al. 2007; Weiss et al. 2022) instead. Research on primary fluid inclusions in fibrous, clouded and coated diamonds indicates that for peridotitic substrates, hydrous HDFs generally range from potassium-rich brines to Mg-carbonatitic, while in eclogitic substrates an evolution from saline through low-Mg carbonatitic to silicic HDFs is observed (Weiss et al. 2015, 2022). The carbonatitic and silicic inclusions are transitional between hydrous HDFs and hydrous melts. For example, inclusions representing an original carbonate melt with molar $100H_2O / (H_2O + CO_2)$ of only 5–20, were recognized in cuboid diamonds of unknown paragenesis from Udachnaya (Zedgenizov et al. 2004). Fluid inclusion-rich diamonds are often interpreted as having grown at high levels of carbon supersaturation in the HDF, to be genetically linked to

kimberlite or proto-kimberlite magmatism, and to be typically of similar age as the transporting host kimberlite (e.g., Boyd et al. 1987; Gurney et al. 2010; Weiss et al. 2011). On that basis, the HDFs observed in clouded and fibrous diamonds may represent a growth medium that is distinct from that for generally much older (Gurney et al. 2010; Smit et al. 2022) smooth-faced monocrystalline diamonds. The discovery of rare but compositionally highly similar, saline to carbonatitic hydrous HDFs as inclusions in gem-quality monocrystalline diamonds from Kankan, Finsch, Voorspoed and Venetia (Weiss et al. 2014; Jablon and Navon 2016), however, clearly established a much wider role of HDFs in diamond formation, both with respect to diamond types and time. We emphasize, however, that the presence of HDFs as inclusions in some smooth-faced monocrystalline diamonds does not automatically imply that all diamonds formed from HDFs or that the types of HDFs observed in diamond are the principal agents of mantle metasomatism. These conjectures will have to be validated or disproven through future research and will be discussed further below.

Melts as metasomatic agents. Hydrous silicate, silico-carbonate and carbonate melt compositions have all been suggested as agents of mantle metasomatism, based on studies of very distinct aspects of subcratonic lithospheric mantle:

1. A group of peridotite xenoliths with fertile compositions—often displaying "sheared" textures, equilibration temperatures that exceed the local conductive geotherm, and evidence for rim-ward enrichment in Fe, Ti, Zr, Y and Ga in constituent minerals—document re-fertilization in the course of (likely repeated) infiltration of melts. Implicated melt compositions range from proto-kimberlitic (megacryst magma) through primitive OIB-like asthenospheric melts and alkali picrites to komatiitic (Gurney and Harte 1980; Nixon et al. 1981; Hervig et al. 1986; Smith 1988; Griffin et al. 1989b; Harte et al. 1993; Mahotkin et al. 2000).
2. A subset of peridotite xenoliths that are enriched in orthopyroxene from, e.g., the Kaapvaal and Siberian cratons (Boyd 1989; Boyd et al. 1997) is interpreted as evidence for Si-enrichment through melts (Rudnick et al. 1994; Kelemen et al. 1998). Based on the narrow, mantle-like $\delta^{18}O$ record of olivine from cratonic peridotites, including those with an opx-enriched signature, Si-enrichment through dacitic (trondhjemitic–tonalitic–granodioritic) slab melts (Rapp and Watson 1995) can be excluded, as it would inevitably lead to ^{18}O enriched signatures (Regier et al. 2018). Instead, Si-enrichment in cratonic peridotites may have occurred by melts generated through hydrous melting of peridotite (Mitchell and Grove 2015); reaction with basic melts, which initially dissolve clinopyroxene and, migrating further into the wall rock, precipitate orthopyroxene (Kelemen et al. 1992); or reaction with komatiite at high pressure (> 4 GPa; Tomlinson and Kamber 2021).
3. A comparative study of diamond suites from areas with normal (Finsch Mine) and anomalously low (Premier kimberlite at Cullinan Mine) seismic P-wave velocities in the diamond-stable lithospheric mantle beneath the Kaapvaal Craton allowed the identification of contrasting styles of metasomatic re-enrichment (Viljoen et al. 2014; see also Shirey et al. 2002). While harzburgitic diamond substrates at Finsch document low-temperature fluid style metasomatism, the peridotitic diamond sample at Premier shows a high proportion of the lherzolitic paragenesis among peridotitic diamonds, with evidence of high temperature melt metasomatism introducing Ca, Fe, Ti, Zr, Y and REE (Viljoen et al. 2014). The refertilization in major and trace elements of the peridotitic diamond substrates beneath Premier and the P-wave anomaly linked to the associated changes in mineralogy (conversion of harzburgite to lherzolite) is attributed to the formation of the 2 Ga Bushveld large igneous province (Shirey et al. 2002; Viljoen et al. 2014) and thus an example of extensive silicate melt metasomatism associated with a mantle plume. Another example of

intense modification of diamond substrates associated with plume magmatism is the 2.7 Ga Ventersdorp large igneous province and the inclusions in diamonds from the proximal Voorspoed Mine, which document the partial to complete conversion of depleted peridotite to websterite (Viljoen et al. 2018).

4. Over a wide range of pressures in the lithospheric and sublithospheric mantle, incipient melting of carbonated peridotites yields magnesio-carbonatites (e.g., Dalton and Presnall 1998). Their low density, high mobility, and high contents in incompatible trace elements make carbonate melts highly efficient agents of mantle metasomatism. An important feature of carbonate metasomatism is a minimal impact on the major element composition of affected substrates, typically with the exception of Ca only (Rudnick et al. 1993). Characteristic geochemical signatures of carbonatite metasomatism are high LREE/HREE, Nb/La, Ca/Al and Zr/Hf ratios and low Ti/Eu ratios (Rudnick et al. 1993; Yaxley 1993). Metasomatism through sodic magnesiocarbonatite, derived from melting of carbonated pargasite peridotite, was identified, e.g., in spinel peridotites from Mt Leura, Victoria, and may lead to conversion of spinel lherzolite to wehrlite at pressure < 2.1 GPa (Green and Wallace 1988). Sodic magnesio-carbonate metasomatism of peridotites is, however, limited to a narrow pressure range (2.1–3.1 GPa) bracketed by the breakdown of carbonate at lower pressures and the breakdown of pargasite at higher pressures.

In diamond stable lithospheric mantle, fO_2 conditions generally are on the reducing side of the EMOD buffer (see Stagno et al. 2013; Luth and Stachel 2014), limiting the *in situ* generation of carbonated melts to localized domains with elevated redox conditions, as observed for some samples from the Central Slave Craton (Creighton et al. 2010). In the absence of such carbonated domains, carbonate metasomatism of the deep lithospheric mantle must be caused by melts derived from below, as inferred, e.g., for the metasomatic modification of highly depleted peridotitic lithosphere beneath the Gregory Rift Valley in northern Tanzania (Rudnick et al. 1993). Asthenosphere-derived carbonatites may originate from upwelling metasomatized mantle that experiences redox melting via oxidation of diamond and reduction of Fe^{3+} when reaching depths < 250 km (Rohrbach and Schmidt 2011). In present day Earth, subducting oceanic crust only exceeds the anhydrous solidus of carbonated eclogite at depth > 400 km (i.e., ~ transition zone depth; Dasgupta et al. 2004; Thomson et al. 2016) but would have melted at increasingly shallower depth with the mantle potential temperature increasing towards the Archean. At some intermediate time, this may have allowed for carbonatite metasomatism of the lithospheric mantle directly from melting of carbonated eclogites and possibly sediments. Depending on the exact estimate for the temporal evolution of mantle potential temperature, Archean and Paleoproterozoic subduction zones may have been sufficiently hot to cause shallow carbonate melting and direct recycling back to the surface (Dasgupta and Hirschmann 2010), precluding subduction-driven mantle metasomatism through carbonated melts. Observational evidence to the contrary was, however, produced by Shu and Brey (2015), who employed subcalcic garnets in peridotite xenoliths and included in diamonds to study Archean metasomatism in the Kaapvaal lithospheric mantle. Based principally on Ti/Eu and Zr/Hf characteristics, they identified carbonate and carbonate–silicate (kimberlite) melts as the principal agents of metasomatism and associated diamond growth in harzburgitic substrates.

Ti/Eu and Zr/Hf systematics of metasomatic agents. The ratios of Ti/Eu and Zr/Hf of whole rocks, garnet and clinopyroxene are used to trace metasomatic interactions and to constrain the nature of metasomatic agents (Rudnick et al. 1993; Yaxley 1993; Shu and Brey 2015; Uenver-Thiele et al. 2017). Directly comparing the Ti/Eu and Zr/Hf systematics of garnets with those of potential metasomatic agents requires that garnet does not strongly fractionate these ratios during metasomatic equilibration. Experimentally determined partitioning data between garnet and dry basaltic melt (Johnson 1998), strongly hydrous

basanite (18–27 wt% H_2O; Green et al. 2000) and hydrous fluid (Stalder et al. 1998) show that garnet faithfully reflects the Zr/Hf ratio of the melt/fluid. The same applies to strongly subcalcic garnet (Ca# = 100Ca / (Ca + Mg + Fe) ≤ 5, approximately equivalent to CaO ≤ 2 wt%) in equilibrium with silico-carbonate ("kimberlite") melts, while more calcic lherzolitic garnets (average Ca# ~15) have D_{Zr}/D_{Hf} of ~ 0.6, i.e., Zr/Hf ratios 40% lower than the coexisting melt (Girnis et al. 2013). Garnet in equilibrium with carbonate melt at high pressure (6.6–8.6 GPa; Dasgupta et al. 2009) exhibits an offset to 25% lower ratios (D_{Zr}/D_{Hf} of ~ 0.75). With the exception of lherzolitic garnets in equilibrium with kimberlite melt, garnet Zr/Hf ratios thus are a good match for the fluid/melt they last equilibrated with. More limited partitioning data for Ti and Eu indicate that garnet in equilibrium with dry and hydrous (4.8 wt% H_2O) basalt will have approximately 30–40% lower Ti/Eu (Johnson 1998; Gaetani et al. 2003), while garnet in equilibrium with carbonatite has a 7 times higher ratio than the melt (Dasgupta et al. 2009). However, the extent of the offset in Ti/Eu of garnet relative to basaltic melts is not relevant on the very large scale of observed variations in Ti/Eu (Fig. 27). Also, considering the extremely low Ti/Eu of magnesio-carbonatites (average of 52; Chakhmouradian 2006; compared to, e.g., 7451 for N-MORB; Sun and McDonough 1989), the actual effect of preferential partitioning of Ti over Eu into garnet in equilibrium with carbonatites is very limited.

Strongly subchondritic Ti/Eu and superchondritic Zr/Hf (Rudnick et al. 1993; Yaxley 1993) of most of the studied Kaapvaal subcalcic garnets was used by Shu and Brey (2015) to establish mantle metasomatism through carbonate and silico-carbonate melts. Our database of xenolith-derived peridotitic garnets overall agrees with this finding, but suggests that HDFs should also be considered as a potential metasomatic agent for garnets with near-chondritic Zr/Hf (Fig. 27). For garnet inclusions in diamond with super-chondritic Zr/Hf (> 37), a number of samples have very low Ti/Eu (< 500) and closely match average compositions of magnesio-carbonatite while samples with more elevated Ti/Eu fall close to the primitive Group I and II kimberlite compositions (Fig. 27). Nearly half of the inclusions (55% of harzburgitic and 47% of lherzolitic garnets), however, have subchondritic Zr/Hf. Overall, HDFs in fibrous diamonds and the melts in equilibrium with MARID (mica–amphibole–rutile–ilmenite–diopside) and PIC (phlogopite–ilmenite–diopside) xenoliths from the Kaapvaal Craton (see caption of Fig. 27 for references), provide a better fit for the metasomatic agent required for the majority of inclusions, with some harzburgitic inclusions indicating even lower Zr/Hf in the metasomatic agent. Considering the principal types of REE_N patterns observed for peridotitic garnet inclusions, the median composition for harzburgitic garnets peaking at Nd (Zr/Hf = 30; Ti/Eu = 1297) closely matches the field for MARID and PIC melts, lherzolitic garnets peaking at Sm_N (median Zr/Hf = 53; Ti/Eu = 292) nearly overlap average magnesio-carbonatites, and lherzolitic garnets with normal REE_N (median Zr/Hf = 40; Ti/Eu = 5734) evolve towards primitive mantle (Zr/Hf = 37; Ti/Eu = 7825). These observations indicate that the carbonatitic metasomatism invoked for xenolith garnets (Shu and Brey 2015) likely affected some inclusion garnets, but is not the dominant metasomatic process reflected by inclusions. This interpretation is consistent with the observation that carbonate inclusions in smooth-faced monocrystalline diamonds are very rare; for the peridotitic suite, only one well established example is documented, consisting of a magnesite inclusion in a lherzolitic diamond from Namibia. As an alternative, equilibration with MARID-PIC melts (for inclusions with low Zr/Hf), HDFs or kimberlites (carbonate–silicate melts) provides better matches for a large number of inclusion garnets.

Considering the evolution of the entire garnet data set shown in Figure 27, the starting point are the harzburgite residues left behind by major Archean melt extraction events (see above). After exhaustion of clinopyroxene (D_{Zr}/D_{Hf} of clinopyroxene–melt is ~0.5–0.6; Johnson 1998; Norman et al. 2005), orthopyroxene controlled the continued decrease in the Zr/Hf ratio of the melting residues (D_{Zr}/D_{Hf} of orthopyroxene–melt is ~0.2–0.5; Ulmer 1989; Green et al. 2000). After elimination of cpx from the residues (D_{Ti}/D_{Eu} of clinopyroxene–melt is ~ 1; Johnson 1998; Norman et al. 2005), an increase in Ti/Eu ratio of the residues is

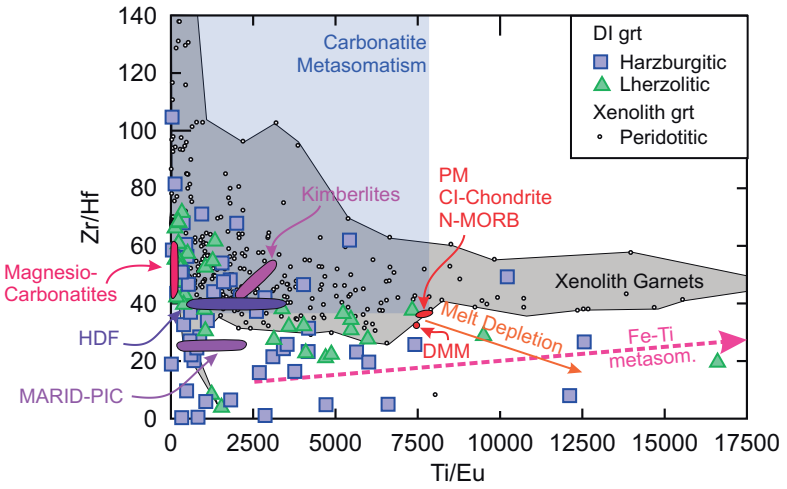

Figure 27. Zr/Hf versus Ti/Eu for harzburgitic and lherzolitic garnet inclusions in diamond. The **grey field** (with small dots indicating individual samples) outlines our database of garnets from cratonic garnet peridotite xenoliths. Two average compositions for magnesio-carbonatites worldwide (Chakhmouradian 2006; Chakhmouradian et al. 2009) are shown as a **red field**. Following Rudnick et al. (1993) and Yaxley (1993), carbonatite metasomatism is characterized by superchondritic Zr/Hf and subchondritic Ti/Eu, shown as a **pale blue field**. The **pink field** connects the primitive Group I (high Zr/Hf and Ti/Eu end) and Group II kimberlite compositions of Becker and Le Roex (2006). The **dark purple field** for high density fluids (HDFs) connects the two endmember trace element patterns ("planed" at the high Ti/Eu end and "ribbed" at the low Ti/Eu end) defined by Weiss et al. (2013). These two endmembers are not specific to particular major element compositions of HDFs, but the particular examples chosen by Weiss et al. (2013) are both hydrous silicic HDFs. The **light purple field** is for average melts in equilibrium with clinopyroxene from MARID (low Ti/Eu end) and PIC (high Ti/Eu end) xenoliths, calculated from clinopyroxene analyses of Fitzpayne et al. (2019) using $D_{cpx-melt}$ of Johnson (1998). The **small red oval** encompasses the compositions of primitive mantle, normal mid-ocean ridge basalt (both Sun and McDonough 1989) and CI-chondrite (McDonough and Sun 1995), the **small red dot** right below is the depleted MORB mantle (DMM) composition of Workman and Hart (2005). The **orange arrow** is an approximate trend for intense melt depletion leaving a spinel-harzburgite residue behind (after Shu and Brey 2015; see text for details). The **dashed pink arrow** points towards the composition of megacryst garnets (average composition for the Grib kimberlite, Arkhangelsk, with Zr/Hf of 39 and Ti/Eu of 28,060; Kargin et al. 2016), which likely precipitated from the metasomatic agent associated with Fe–Ti metasomatism (see text for details).

controlled by orthopyroxene (D_{Ti}/D_{Eu} of orthopyroxene–melt is ~3; Ulmer 1989; Green et al. 2000) and spinel (compatibility of Ti, at strict incompatibility of Eu, in Cr- and Fe^{3+}-rich spinels; Wijbrans et al. 2015). The approximate evolution of residues of large-scale Archean melt depletion is indicated as a solid arrow in Figure 27. The resulting high Ti/Eu and low Zr/Hf of the depleted protoliths of subcratonic lithospheric mantle were associated with very low concentrations of Ti, Eu, Zr and Hf, making these rocks highly susceptible to metasomatic overprint. This metasomatism involved a range of fluids/melts (see above) with variable Zr/Hf. High Eu (reflecting high LREE/HREE) and low Ti in the metasomatic agent(s) moved the affected diamond substrates to very low Ti/Eu.

Focusing only on inclusion garnets with Ti/Eu $\gtrsim$2500 and subchondritic Zr/Hf: if the observed spread from high Ti/Eu, akin to melt-depleted compositions, to ~2500 was due to metasomatic enrichment of Eu (trend of decreasing Ti/Eu), then a negative correlation of Ti/Eu with Eu content would be expected, but this is not the case (Fig. 28). Instead, there is a crude positive correlation of Ti/Eu with Ti content (Fig. 28), suggesting that the spread in Ti/Eu is largely a consequence of preferential re-enrichment in Ti that occurred as a second metasomatic event (dashed trend of increasing Ti/Eu in Fig. 27). Compared to the original

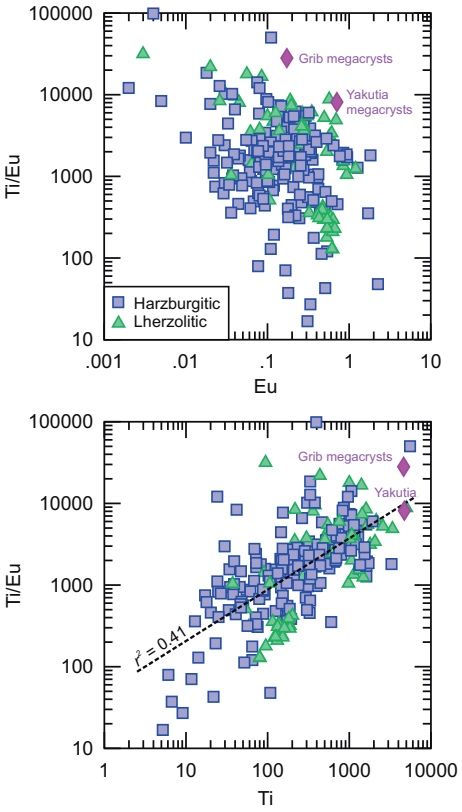

Figure 28. Ti/Eu versus Eu (**top**) and Ti content (**bottom**) in ppm in harzburgitic and lherzolitic garnet inclusions in diamond. The absence of a statistically significant negative correlation between Ti/Eu and Eu suggests that the spread in Ti/Eu is not principally due to variable metasomatic (LREE and) MREE enrichment. The presence of a crude positive correlation between Ti/Eu and Ti suggests that metasomatic enrichment in Ti (with little effect on Eu contents) is the principal factor in determining Ti/Eu ratios. Average garnet megacryst compositions for the Grib kimberlite, Arkhangelsk (n = 20; Kargin et al. 2016) and Yakutian kimberlites (n = 3; Kostrovitsky et al. 2013) are indicated as pink diamonds.

melt-depleted harzburgites, which also have high Ti/Eu (melt depletion trend in Fig. 27), the inclusion garnets with Ti/Eu > 2500 have higher Eu (metasomatic event 1, affecting all garnets inclusions) and higher Ti contents (metasomatic event 2, affecting only some garnets). Very high Ti/Eu ratios are documented as a consequence of melt metasomatism in garnet rim compositions from hot sheared peridotites, with Ti/Eu ratios of, e.g., 9800 from Lesotho (Smith et al. 1993) and 23,000 from Arkahangelsk (Kargin et al. 2017). They also characterize garnets precipitated from the megacrysts magma, with Ti/Eu of 4600–44,000 (Yakutia: Kostrovitsky et al. 2013; Arkahangelsk: Kargin et al. 2016, 2017). Thus, a possibly modified, generally mild form (cf. Figs. 7 and 13) of the Fe–Ti metasomatism documented in xenoliths (see above) and tentatively linked to the proto-kimberlite/megacryst magma (e.g., Kargin et al. 2016; Ashchepkov et al. 2017a; Shchukina et al. 2017) may have affected some diamond substrates. The inferred second stage re-enrichment in Ti appears to have had little effect on Zr/Hf ratios, implying moderate to low Zr/Hf and/or low Zr and Hf concentrations in the metasomatic melt (consistent with an absence of positive correlations of either Zr or Hf with Ti/Eu). With D_{Zr}/D_{Hf} of garnet–melt being in the range 0.6–1 (*see above*), the near-chondritic Zr/Hf ratio of megacrysts (34–44; Kargin et al. 2017) is approximately representative of their parental melt. Combined with its very high Ti/Eu ratio, the megacryst magma would consequently be consistent with the evolution seen in Figure 27 (dashed pink arrow labelled Fe-Ti metasomatism, pointing towards megacryst garnets).

Calculated melts in equilibrium with garnet inclusions. A different approach to constrain the nature of metasomatic agents is to calculate the composition of melts or fluids in equilibrium with garnet or clinopyroxene inclusions and to compare these calculated compositions to observed mantle melts or fluids (e.g., Shimizu 1975). For this approach to be valid in the context of diamond studies, the inclusion mineral and the metasomatic agent must have reached equilibrium. For syngenetic inclusions, which precipitate together with their diamond hosts from a metasomatic agent, this precondition is implicitly met. For preexisting minerals, equilibration is a diffusion-controlled process and for centimeter-sized crystals in coarse peridotites may take over a billion years at the temperatures of diamond stable lithospheric mantle. For protogenetic inclusions in diamond (see above), which are

typically recovered in the 0.1–0.2 mm range, diffusive equilibration during a fluid or melt infiltration event will, however, be rapid, e.g., ~20,000 years for REE in a 0.1 mm defect-free garnet residing at 1150 °C (Nestola et al. 2019b). Faster diffusion along dislocations could decrease the required time significantly. On that basis, we consider equilibrium between inclusion minerals and diamond-forming metasomatic fluids/melts highly likely even in the case of protogenetic inclusions.

A significant recent breakthrough for modelling the composition of metasomatic agents came from the experimental work of Kessel et al. (2015), who provided a large set (including the REE) of partition coefficients for both garnet and clinopyroxene with subsolidus HDFs (aqueous fluids with up to 36 wt% dissolved solids). For the calculation of model melts, we use the three principal garnet groups derived in Figure 18: harzburgitic garnets with REE_N peaking at Nd, lherzolitic garnets with sinusoidal patterns peaking at Sm, and lherzolitic garnets with normal REE_N patterns. For each of these garnet groups, we chose the 25th percentile, the median and the 75th percentile patterns to calculate the equilibrium compositions of HDF (6 GPa, 1000 °C; Kessel et al. 2015), hydrous melt (6 GPa, 1100 °C, melt with 39 wt% H_2O; Kessel et al. 2015) and "dry" melt (Johnson 1998). The suffix "dry" relates to the nominally dry Kilauea olivine tholeiite used in the experiments by Johnson (1998), but does not imply that the calculated melt compositions are only applicable to volatile-free systems. Because of the similarity in Zr/Hf and Ti/Eu of the median composition of lherzolitic garnets peaking at Sm and average magnesio-carbonatite (Fig. 27), for this garnet group we also use the partition coefficients for garnet-carbonatite of Dasgupta et al. (2009). The calculated equilibrium melts (Fig. 29) are then compared to (1) the spectrum of HDFs observed in diamonds, consisting of the typical "planed" and "ribbed" patterns of Weiss et al. (2013) and a potentially parental, saline HDF observed in a diamond from the Fox kimberlite (Weiss et al. 2015), (2) the primitive Group I and II kimberlite compositions of Becker and Le Roex (2006) and (3) in the case of the lherzolitic garnets peaking at Sm, the average magnesio-carbonatite composition of Chakhmouradian et al. (2009). The REE_N patterns for average MARID melt overlap the primary kimberlite compositions of Becker and Le Roex (2006), while the pattern for PIC melt shows the same slope but at about 1/3 of the REE concentrations (see caption of Fig. 27 for details on the calculation of MARID and PIC melt compositions). On the scale of Figure 29, the resulting offset, however, is so small that the kimberlite patterns may be viewed as representative for MARID and PIC melts as well.

For harzburgitic garnets peaking at Nd, all calculated HDF and melt REE_N patterns have very steep negative slopes (Fig. 29, top). The upward kink in the $HREE_N$ is interpreted to be imposed by the substrates rather than as a characteristic of the primary metasomatic medium (see above). As harzburgitic substrates generally reside at subsolidus conditions, only the calculated HDF pattern is relevant for comparison in this case (Fig. 29, top, right panel). The absolute trace element concentrations in HDFs observed in fibrous diamonds are mainly a reflection of inclusion density and hence were normalized to match the Dy content of the calculated HDF. The comparison reveals a modest fit, which is closest for the primitive saline pattern ("saline Fox"; Fig. 29, top). The $LREE_N$–$HREE_N$ fractionation in the calculated HDF covers almost three orders of magnitude, "ribbed" patterns span two orders of magnitude and "planed" patterns one order. Extrapolating the HREE slope (below the limit of quantification; Weiss et al. 2015) for the primitive saline pattern results in more similar overall $LREE_N$–$HREE_N$ fractionation, but differences to the calculated HDF are still prominent in the much steeper slope from Nd_N to Eu_N for the latter. This misfit in REE patterns between calculated HDF and primitive saline fluid is exacerbated when considering the experimental study of Rustioni et al. (2021), which showed that with increasing salinity the LREE/HREE ratio of garnet in equilibrium with fluid of a given REE content decreases strongly. For saline fluids, HDF compositions (Fig. 29) calculated using the partition coefficients of Kessel et al. (2015), therefore, underestimate the $LREE_N$–$HREE_N$ fractionation.

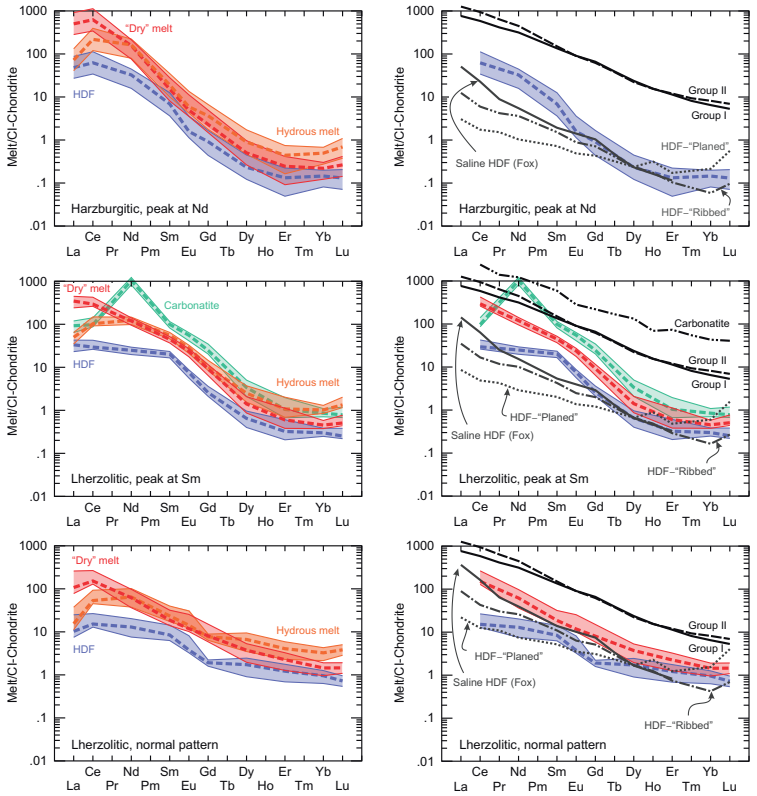

Figure 29. The **left panels** shows REE_N patterns of calculated HDFs and melts in equilibrium with peridotitic garnet inclusions in diamond that fall into the three principal groups of observed patterns: harzburgitic garnets peaking at Nd (**top**), lherzolitic garnets peaking at Sm (**middle**) and lherzolitic garnets with normal REE_N patterns (**bottom**). For all three garnet groups, the median compositions (**dashed lines**) and the interquartile range (25th and 75th percentile; **colored bands**) are used for the calculations. Hypothetical HDF and melt compositions were calculated from garnet compositions using three different sets of experimentally determined partition coefficients: for (1.) aqueous high-density-fluid (1000 °C, 6 GPa; **blue**) and (2.) hydrous melt (1100 °C, 6 GPa; **orange**) in equilibrium with metasomatized garnet lherzolite (Kessel et al. 2015) and (3) Kilauea olivine tholeiite in equilibrium with near-liquidus garnet and clinopyroxene ("dry" melt; 1430 °C and 3 GPa; Johnson 1998; **red**). In addition, for the group of lherzolitic garnets showing sinusoidal patterns peaking at Sm (**middle**), partition coefficients for carbonate melt in equilibrium with garnet lherzolite were used (1265–1470 °C and 6.6–8.6 GPa; Dasgupta et al. 2009; **green**). Kinks at Ce for the calculated melt/fluid compositions are interpreted as artifacts, related to generally low concentrations of La in inclusion garnets (affecting analytical precision) and difficulties in determining extremely small (10^{-2} to 10^{-3} range) partition coefficients from experimental charges with high accuracy. In the right panels, the calculated HDF and melt compositions are compared to primitive Group I and Group II kimberlite compositions (Becker and Le Roex 2006; **solid and dashed black lines**, respectively) and HDFs in fibrous diamonds with "planed" and "ribbed" traced element patterns (Weiss et al. 2013; **dotted and dotted-dashed grey lines**, respectively) and their potentially parental, saline fluid composition (Fox diamond E217; Weiss et al. 2015; **solid grey line**). Absolute trace element concentrations of fibrous diamonds are not only a function of the HDF inclusion composition but are strongly controlled by inclusion density. Consequently, for the comparison with calculated garnet fluids/melts, the "ribbed", "planed" and saline-Fox patterns were normalized to the Dy content of the median calculated HDF pattern. The average composition of magnesio-carbonatites worldwide is from Chakhmouradian et al. (2009). Since harzburgitic diamonds generally form at subsolidus temperatures, only the calculated HDF composition is used for the comparison in the top row. For lherzolitic garnets, both the calculated HDF and "dry" melt compositions are shown. The hydrous melt composition (see left panel) was only left out to avoid overcrowding. Because of likely poor precision, La in calculated HDF/melt is omitted for the comparisons with observed fluid/melt compositions.

For lherzolitic garnets peaking at Sm, the calculated HDF pattern shows a kink at Sm but otherwise is again most similar to the primitive saline HDF pattern (Fig. 29, middle), with the above caveat that the $LREE_N$–$HREE_N$ fractionation of the calculated HDF would increase if the effect of salinity was considered. The patterns for calculated silicate and carbonate melt compositions are even steeper than for the calculated HDF and hence do not match observed kimberlite and magnesio–carbonatite compositions. In comparison, the calculated HDF and melt compositions for lherzolitic garnets with normal REE_N patterns show much lower levels of $LREE_N$–$HREE_N$ fractionation. The calculated HDF and hydrous melt compositions (the latter shown only in the left panel of Fig. 29, bottom) are intermediate in slope between the observed "planed" and "ribbed" patterns, while the "dry" melt composition parallels primitive Group I and II kimberlites. The formation of lherzolitic diamonds generally above the wet lherzolite solidus makes the match with kimberlites particularly relevant.

An inherent problem of visual comparisons of calculated and observed fluid/melt trace element patterns is that REE concentrations in the various media cover almost five orders of magnitude. Consequently, as long as the sign of the slope is the same, very distinct patterns appear visually similar. To examine the differences in slope in the REE_N patterns of calculated and observed fluid and melt compositions in more detail, we use the chondrite-normalized ratio of Nd/Dy (Fig. 30). In addition, focusing exclusively on REE blurs the distinction between HDFs with "planed" and "ribbed" trace element patterns, for which a key distinguishing criterion is the presence ("ribbed") or absence ("planed") of a strong negative Nb anomaly (Weiss et al. 2013), expressed as a strongly elevated chondrite-normalized Ce/Nb ratio in Figure 30. Calculated HDF, hydrous melt and "dry" melt compositions all show similar Nd_N/Dy_N, decreasing strongly from equilibrium with garnets with sinusoidal REE_N peaking and Nd to those with normal patterns. Only for the melts in equilibrium with garnets with normal patterns are Nd_N/Dy_N ratios observed similar to HDFs and low volume mantle melts. Using partition coefficients for garnet-carbonatite (Dasgupta et al. 2009) leads to even more extreme LREE–MREE fractionation, with Nd_N/Dy_N ratios much higher than natural magnesio-carbonatites for all three garnet groups utilized for melt calculation. In terms of Ce_N/Nb_N ratio, only calculated carbonate melts in equilibrium with garnets with sinusoidal REE_N patterns peaking at Nd would show negative Nb anomalies (Ce_N/Nb_N of about 5). This excludes HDFs with "ribbed" trace element patterns as a principal diamond-forming metasomatic agent and instead highlights a similarity in the occurrence of mildly positive Nb anomalies ($Ce_N/Nb_N < 1$) for calculated HDF/melts with Group I kimberlites and with natural HDFs with "planed" trace element patterns.

Key observations and conclusions

Garnet, and for the lherzolitic paragenesis also clinopyroxene, are the principal carriers of incompatible trace elements among peridotitic inclusions in diamond. The REE_N patterns of garnet inclusions are typically sinusoidal, with harzburgitic garnet most commonly peaking at Nd and lherzolitic garnets at Sm. As another end-member type of REE_N patterns, some lherzolitic and very few harzburgitic garnets have normal patterns, characterized by flat $MREE_N$–$HREE_N$. This evolution from sinusoidal to normal garnet REE_N patterns is mirrored for clinopyroxene inclusions by a transition from patterns with a characteristic steep negative slope in the $LREE_N$ to humped patterns peaking at Nd_N.

Normalization to "primitive mantle" garnet/clinopyroxene documents a two-stage evolution of the protoliths (cf. Frey and Green 1974), starting with intense melt depletion causing overall REE depletion and steep positive $LREE_N/HREE_N$ slopes in the bulk rocks (preserved only in the HREE from Er to Lu). This depletion is typically followed by metasomatic re-enrichment through a medium with very high LREE and LREE/HREE and distinctly subchondritic HREE. Garnet with normal REE_N patterns and coexisting clinopyroxene with humped patterns indicate primitive mantle-like bulk rock REE concentrations and are a consequence of metasomatism through media with only moderately fractionated trace element contents. Whilst such near-

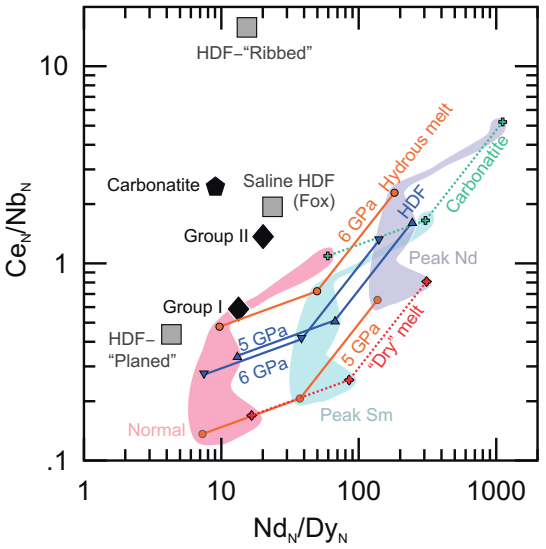

Figure 30. The chondrite normalized ratios of Ce/Nb and Nd/Dy are used to assess how well calculated melts for inclusion garnets representing the three principal groups of REE_N patterns match HDFs in fibrous diamonds and kimberlite and carbonatite melts. The three principal garnet patterns are (1) harzburgitic garnets peaking at Nd_N, (2) lherzolitic garnets peaking at Sm_N and (3) lherzolitic garnets with normal REE_N patterns. In all three cases the median compositions are used. Hypothetical melt compositions in equilibrium with the median garnet compositions were calculated using six different sets of experimentally determined partition coefficients: aqueous HDFs (1000 °C, pressures of 5 and 6 GPa; **blue**) and hydrous melts (1100 °C, pressures of 5 and 6 GPa; **orange**) in equilibrium with metasomatized garnet lherzolite (Kessel et al. 2015), Kilauea olivine tholeiite in equilibrium with near-liquidus garnet and clinopyroxene ("dry" melt; 1430 °C and 3 GPa; Johnson 1998; **red**) and carbonate melt in equilibrium with garnet lherzolite (1265–1470 °C and 6.6–8.6 GPa; Dasgupta et al. 2009; **green**). The calculated melt compositions are compared to primitive Group I and Group II kimberlite compositions (Becker and Le Roex 2006) and high-density-fluids in fibrous diamonds with "planed" and "ribbed" traced element patterns (Weiss et al. 2013) and their potentially parental saline fluid composition (Fox diamond E217; Weiss et al. 2015). The presence of a strong negative Nb anomaly for "ribbed" HDFs and the absence of such anomalies in "planed" HDFs is a key criterion for their distinction (Weiss et al. 2013). We use the Ce_N/Nb_N ratio as a measure for the presence and extent of negative ($Ce_N/Nb_N > 1$) and positive (< 1) Nb anomalies. The Nd_N/Dy_N ratio is a measure for the slope of REE_N patterns. Nd and Dy were chosen because of their comparatively high absolute abundances, with especially the HREE abundances in the analyzed fibrous diamonds being extremely low.

primitive REE_N patterns are rare among inclusions – about 5% of all garnet inclusions have normal REE_N—they strongly dominate among peridotite xenolith and xenocryst garnets. This is not only a function of reversed proportions of the harzburgitic and lherzolitic parageneses for inclusions (high ratio) and xenoliths (low ratio) but is also observed when looking at lherzolitic garnets only. Whether this observation reflects the well-established affinity of diamond to the most depleted peridotitic substrates (e.g., Gurney 1984), or an increasing metasomatic modification through time that inclusions were shielded from by their diamond hosts, or probably a combination of both, is not well constrained by currently existing data.

The nature of the metasomatic agents that re-enriched the diamond substrates and presumably also caused repeated episodes of diamond formation cannot be fully resolved. The HDF inclusions observed in coated and fibrous diamonds and sometimes detected in clear, smooth-faced monocrystalline diamonds are too "melt-like" in their trace element patterns to create the extreme LREE/HREE fractionation seen in the vast majority of garnet and clinopyroxene inclusions. Whether that reflects a temporal evolution, with Archean

diamond-forming HDFs showing overall stronger trace element fractionation, or if the HDFs precipitating either fibrous diamonds or diamond coats are more primitive members of a HDF fractionation series (e.g., through chromatographic column type fractionation; Navon and Stolper 1987; Bodinier et al. 1990) will have to be established through future research. Near-primitive trace element patterns are consistent with melt-like metasomatic agents (including the HDFs seen in fibrous diamonds) and, given the relationship between cratonic geotherms and the hydrous solidus of lherzolite, likely reflect infiltration of low volume hydrous melts, similar to primitive kimberlites. Conversely, the high temperatures required for hydrous melting of strongly depleted peridotites (harzburgites-dunites) shield such rocks against pervasive melt metasomatism, as such melts must freeze upon equilibration with their wall rocks.

ECLOGITIC–PYROXENITIC SUBSTRATES

Occurrence, mineralogy and classification of eclogite/pyroxenite inclusions and xenoliths

Occurrence. As broadly metabasaltic rocks sometimes containing coesite or diamond, eclogite occurs in dynamic settings where (ultra-)high-pressure metamorphism takes place. This encompasses deeply subducted and exhumed portions of oceanic crust consisting of pillow lavas, sheeted dikes and gabbros (e.g., White and Klein 2014), which are now sampled as lenses in orogens (e.g., Liou et al. 2004) and as xenoliths in kimberlites and related rocks (e.g., Jacob 2004). Diamond populations dominated by eclogitic inclusions are often associated with craton margins or cratonic lithosphere affected by later tectono-magmatism, suggestive of a subduction origin of the source rock (Sobolev 1985; Shirey et al. 2002; Stachel and Harris 2008). Some mantle xenolith suites are dominated by eclogite (e.g., at the Roberts Victor and Orapa mines in the Kaapvaal craton, and at Koidu in Sierra Leone in the West African craton; MacGregor and Carter 1970; Hills and Haggerty 1989). As the lithospheric mantle contains only a few percent (Schulze 1989), at most several 10s of percent (Garber et al. 2018) eclogite, this local dominance highlights preferential preservation of eclogite versus peridotite and/or non-representative sampling by kimberlite and lamproite magmas (e.g., Moss et al. 2018).

A proportion of garnet–clinopyroxene rocks in xenolith suites with jadeite-poor clinopyroxene classify as pyroxenite, although these are sometimes referred to as high-Mg or Group A eclogite (Coleman et al. 1965; Taylor and Neal 1989). While bimineralic pyroxenites grading into high-Mg eclogites form part of most cratonic xenolith suites (Aulbach et al. 2020a), orthopyroxene-bearing pyroxenites are more common in craton-margin and off-craton localities (Jacob 2004), where they record generally lower equilibration pressures than, and have an origin different from, eclogite (Schmädicke et al. 2011).

Mineralogy. Stachel and Harris (2008) found that garnet and clinopyroxene, the main rock-forming minerals in eclogite, comprised 56% and 39% of the total of inclusions in 1311 eclogitic diamonds; other common silicate and oxide inclusions being rutile (2.7%) and coesite/quartz (1.8%). In contrast, garnet, clinopyroxene, orthopyroxene, coesite and olivine constitute 38%, 37%, 21%, 3% and 1%, respectively of inclusions in 136 websteritic diamonds (Stachel and Harris 2008). Despite their accessory mineral status in common lithospheric mantle sources, sulfides are the most common inclusion in diamond (Harris and Gurney 1979; Haggerty 1986). However, they will not be further considered here, as their occurrence as an inclusion in diamond is considered as part of the diamond age-dating work and is reviewed in Smit et al. (2022).

Of 2451 xenoliths considered for comparison of mineralogy, commonly reported primary accessory and minor silicate and oxide minerals include diamond (n = 251), rutile (n = 83), kyanite (n = 67), graphite (n = 59; of these 10 also contain diamond), corundum (n = 25) and coesite/quartz (n = 11). Sulfides are common, though not necessarily reported as part of the

assemblage (pers. observation). Garnet clinopyroxenites (n = 334), which grade into websterite and olivine-poor lherzolite, more commonly contain orthopyroxene (n = 30 vs. 8 in eclogite xenoliths), but only 15 of 544 pyroxenite xenoliths (3%) are diamondiferous, compared to 12% of eclogite xenoliths. As the description of websteritic inclusion mineralogy provided in the previous paragraph is based on a different classification scheme than that applied to pyroxenite xenoliths (see Inclusion suites and parageneses), these findings are not entirely comparable.

The proportion of diamondiferous eclogite (12%) and pyroxenite samples (3%) may be high because such rocks are frequently specifically targeted for study. On the other hand, accessory minerals may be more common than they appear, because they need not be exposed at the section scale or may not have been reported, depending on the aims of the study. Whilst other minerals in the xenoliths, such as amphibole, plagioclase and phlogopite are likely to be of secondary, metasomatic origin, zircon, apatite and ilmenite could be primary, although more likely to be metasomatically introduced (Aulbach et al. 2020a, and references therein). In addition, Jacob (2004) notes the typical purity of minerals in mantle eclogite, which rarely contain inclusions, as opposed to their orogenic counterparts. Eclogites rich in CaO and Na_2O are particularly affected by texturally late alteration, resulting in the partial or complete replacement of primary jadeite-rich clinopyroxene by "spongy" diopside-rich clinopyroxene plus K-rich glass and other minerals (e.g., Snyder et al. 1997; Spetsius and Taylor 2002). This texturally late assemblage reflects the greater instability of jadeite-rich clinopyroxene in contact with an ultramafic carbonated agent such as kimberlite (e.g., Misra et al. 2004). Also, the presence of amphibole and phlogopite in the kelyphite rims of garnet and of K-rich glass in the spongy clinopyroxene suggests partial melting and kelyphite formation catalyzed by kimberlite-related fluids (Snyder et al. 1997; Spetsius and Taylor 2002).

Classification. Of the aforementioned 2451 xenoliths considered for mineralogy, only 946 have reported major element abundances for both garnet and clinopyroxene, allowing distinction of eclogites and pyroxenites. This yields 776 mantle eclogite samples (236 diamondiferous) and 170 pyroxenite samples (15 diamondiferous). Only a small proportion of diamondiferous samples have reported REE concentrations that further allow assignment to gabbroic, with positive Eu anomalies, vs. non-gabbroic sources (Table 3).

When inclusions are recast in the scheme applied to mantle xenoliths, clinopyroxene–garnet inclusion pairs comprise 235 eclogitic and 37 pyroxenitic diamonds. Of unpaired clinopyroxene, 481 are eclogitic (15 of 26 with REE data have a gabbroic signature) and 86 pyroxenitic (2 of 3 with REE data are gabbroic). Unpaired garnet can be assigned to high-Ca, high-Mg, low-Mg and gabbroic groups, bearing in mind that some high-Mg samples may actually derive from pyroxenite sources (~70% of pyroxenite xenoliths have high-Mg garnet) and some high-Ca samples without REE data may actually derive from gabbroic sources (67% of gabbroic xenoliths contain high-Ca garnet) (Table 3).

Ages of eclogite/pyroxenite xenoliths and inclusions

Obtaining accurate and precise formation ages from mantle eclogite and pyroxenite is challenging because bulk rocks are affected by kimberlite contamination, and because two-mineral isochrons yield kimberlite eruption or cooling ages. Also, zircon is rare in these rocks and can be of metasomatic origin (Jacob 2004; Aulbach et al. 2019a). Nevertheless, ages and the methods by which they were derived are summarized in Appendix Table 1. Worldwide, the oldest age arrays obtained from Pb–Pb, Sm–Nd and Re–Os geochronology on bulk rocks or mineral separates are often Mesoarchean to Neoarchean, (3.2 to 2.5 Ga) reflecting the suturing of continental nuclei and haphazard incorporation of intervening oceanic lithosphere to form larger cratonic entities. Exclusively Paleoproterozoic ages (2.5 to 1.6 Ga) have been obtained from eclogite and pyroxenite xenoliths in the northern and central Slave craton, which coincide with collision/accretion at the western craton margin, preceded by subduction of an intervening ocean floor.

Table 3. Number of eclogitic and pyroxenitic inclusions in diamond and of diamondiferous and barren xenoliths used in this study, and their classification.

Sample type/ classification	Total	High-Ca eclogite	High-Mg eclogite	Low-Mg eclogite	Gabbroic eclogite	Unclassified eclogite	Pyroxenite	Gabbroic pyroxenite	Unclassified pyroxenite
Inclusions in diamond									
Touching pairs*	23	0	0	0	3	12	1	0	7
% of classified		0	0	0	75		25	0	
Non-touching pairs*	249	4	5	4	10	197	3	1	25
% of classified		15	19	15	37		11	4	
Unpaired clinopyroxene**	567	11 non-gabbroic			15	466	1	2	83
% of classified		38			52		3	7	
Unpaired garnet***	906	20	10	7	71	798	?	?	?
% of classified		19	9	6	66				
Xenoliths									
Barren	695	86	110	50	294	0	102	53	0
% of classified		12	16	7	42	0	15	8	0
Diamondiferous*	251	1	7	6	56	166	1	0	14
% of classified		1	10	8	79		1	0	

Notes: Eclogite = Na/(Na+Ca) in clinopyroxene ≥ 0.2, pyroxenite < 0.2; gabbroic = whole-rock Eu/Eu* > 1.05; full classification is only possible when major and REE element data are available for both clinopyroxene and garnet, which is the case for all barren xenoliths chosen for this study. * A proportion of unclassified samples (no REE data) may be gabbroic. ** 11 eclogitic clinopyroxene inclusions with REE data are non-gabbroic, but cannot be classified as high-Ca, high-Mg or low-Mg in the absence of garnet. *** A proportion of garnet (in particular high-Mg) may be pyroxenitic, but cannot be attributed in the absence of clinopyroxene; a proportion of unclassified samples may be gabbroic (in particular high-Ca), but cannot be attributed without REE data.

Comparison between eclogitic/pyroxenitic inclusions in diamond and their barren and diamondiferous xenolithic counterparts

In the following, inclusions in diamond are compared with similar minerals in xenoliths, the latter distinguished according to whether they are reported as diamondiferous or barren. Median and average concentrations are typically very similar, especially for large numbers (100s) of samples in a given group. Differences are more apparent for pyroxenites, for which smaller numbers are available and which are a heterogeneous group with respect to their compositions and origins (Stachel and Harris 2008). Median compositions are used for comparison to safeguard against outliers, and median absolute deviations are reported as the corresponding uncertainty. Nevertheless, the relatively small number of inclusions (especially pyroxenitic) with trace-element or $\delta^{18}O$ data make comparisons and unambiguous interpretation tenuous. Also, minor elements, such Cr, Ni and K, are not consistently analysed and reported. Appendix Table 3 shows the statistical analysis for four eclogite and two pyroxenite classes. Minerals in diamond and similar ones in diamondiferous xenoliths are distinguished according to whether they are eclogitic or pyroxenitic and whether they are touching or non-touching, as the latter relationship affects calculated temperatures, and also some distribution coefficients. To simplify the following compositional comparison, touching and non-touching inclusions are considered together, and unpaired clinopyroxene, which allows classification into eclogite and pyroxenite, is subsumed with paired clinopyroxene. Finally, the gabbroic pyroxenite class shares the cumulate signature with gabbroic eclogites and the enriched signature with non-gabbroic pyroxenite xenoliths. For the sake of clarity, the gabbroic pyroxenite class is not described below or shown in most figures.

Mineral major and minor element compositions. Clinopyroxene in eclogitic diamond has a median Mg# of 76.5, a diopside content of 0.46 and a jadeite (Jd) component of 0.32 (Appendix Table 3). For clinopyroxene in diamondiferous eclogite these values are a higher Mg# (82.4) and a diopside content of (0.41) but similar Jd (0.35). In contrast, clinopyroxene in all classes of barren eclogite (gabbroic, high-Ca, high-Mg, low-Mg) have Mg# of 78.3–85.3, consistently higher diopside content (0.54–0.65) and mostly lower Jd, varying between 0.33 in gabbroic and 0.20 in high-Mg eclogites. Median K_2O contents of clinopyroxene in diamond (0.20 wt%) are more than twice as high as in diamondiferous eclogite (0.09 wt%) and 3–4 times as high as in barren eclogites (≤ 0.06 wt%). In a diagram of Jd vs. Mg#, (Fig. 31), clinopyroxene inclusions in eclogitic diamond span a large range, with diamondiferous eclogites shifted to higher Mg#, and barren eclogites to both higher Mg# and lower Jd. In pyroxenitic diamond, clinopyroxene has a median Mg# of 83.5 and a diopside content of 0.72, which is much lower than the Mg# (≥ 90.1) or diopside content (≥0.77) in clinopyroxene from diamondiferous or barren pyroxenite, but still higher than in eclogitic clinopyroxene. By definition, jadeite contents are lower in pyroxenitic than in eclogitic clinopyroxene, but Cr_2O_3 contents are higher (≥ 0.13 wt%), though overlapped by clinopyroxene in high-Mg eclogite with 0.14 wt%.

Garnet in eclogitic diamond has distinctly higher TiO_2 (0.61 wt%) and Na_2O contents (0.20 wt%) than garnet in diamondiferous eclogite (0.36 and 0.13 wt%, respectively) and various barren eclogite classes (≤ 0.27 and 0.09 wt%, respectively) (Appendix Table 3). Median Mg# of included garnet is 52.7. Garnet in diamondiferous eclogite has Mg# 61.7, which is very similar to that in gabbroic barren eclogite (62.2). All the three garnet groups referred to above have a Ca# (100Ca / (Ca + Mg + Fe^{total} + Mn)) of 24. Garnet in high-Mg barren eclogite has the highest Cr_2O_3 contents (0.13 wt%) and Mg# (68.6) and the lowest Ca# (11.2) of all eclogite classes, the nearest comparison being the unpaired high-Mg garnet in diamond (Cr_2O_3 0.17 wt%, Mg# 66.1, Ca# 11.1). Compared to paired inclusions, unpaired garnet specifically extends into the field of diamondiferous eclogites with high Mg#–Ca# typical of some gabbroic eclogites (Fig. 32a). Garnet inclusions in pyroxenitic diamond have again lower Mg# (63.2) and higher Ca# (14.3) than in diamondiferous pyroxenites (77.7 and

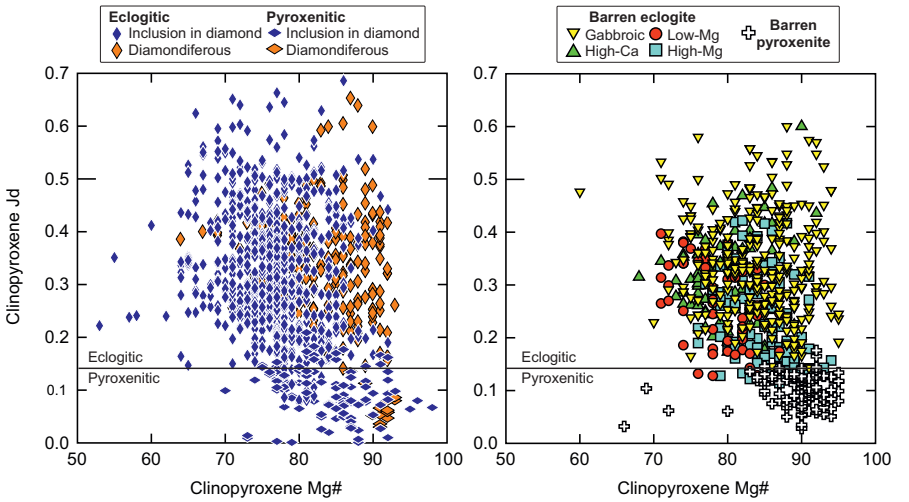

Figure 31. Jadeite content of clinopyroxene (Jd) as a function of Mg# (100Mg / (Mg + Fe^{total})). Eclogite and pyroxenite are roughly separated according to Jd (formally Na / (Na + Ca)), as indicated on **right**. Inclusions (paired and unpaired) and diamondiferous xenoliths on **left**, barren xenoliths on **right**.

10.2, respectively). Median Cr_2O_3 contents in pyroxenitic garnet (≥ 0.29 wt% for all classes) are higher than in eclogitic garnet (≤ 0.13 wt% for all classes), and many fall on a "lherzolite" trend of CaO vs. Cr_2O_3 that indicates buffering of CaO contents by orthopyroxene (Fig. 32b).

Ca# in garnet shows a broad positive correlation with Jd, where inclusions range to higher Jd at a given Ca# and are only weakly represented at Ca# ≳37 compared to diamondiferous eclogites (Fig. 33a). Combined, Na_2O in garnet and K_2O in clinopyroxene show a strongly diminished range both in diamondiferous and in barren eclogites/pyroxenites compared to inclusions (Fig. 33b).

Mineral trace element compositions. Trace elements for which at least tens of analyses for inclusions in diamond are available include Ni, Sr, Y, Zr, Nb, the REE and Hf (Appendix Table 3). For clinopyroxene, median Ni contents are lowest in inclusions (160 ppm, vs. 251 ppm in clinopyroxene from diamondiferous eclogite and 196–312 ppm from barren eclogite). Median Sr contents in inclusions (136 ppm) and in clinopyroxene from diamondiferous eclogite (142 ppm) are similar and intermediate between those from high-Ca eclogite (118 ppm) and gabbroic eclogite (162 ppm), whereas that in high-Mg and low-Mg eclogite is higher (186 and 193 ppm, respectively). Clinopyroxene in diamondiferous eclogite has low Y content (0.9 ppm), between that in gabbroic eclogite (0.6 ppm) and high-Ca eclogite (0.9 ppm), but inclusions have higher abundances (2.4 ppm). Median Zr contents of clinopyroxene in diamond (14.1 ppm) and diamondiferous xenoliths (10.5 ppm) are again similar to those in gabbroic and high-Ca eclogite (10.3 ppm and 16.4 ppm, respectively), being higher still in high-Mg and low-Mg eclogites. Conversely, by far the highest median Nb contents (0.25 ppm) are recorded for clinopyroxene in diamondiferous eclogites, followed by inclusions (0.10 ppm), whereas those in barren eclogites are lowest (≤ 0.08 ppm). The comparison for pyroxenite classes is hampered by the low number of trace-element analyses both for inclusions and for diamondiferous xenoliths (Appendix Table 3), and by the heterogeneous nature of their petrogenesis (Stachel and Harris 2008; Aulbach and Jacob 2016). Median concentrations of trace elements in clinopyroxene from pyroxenitic diamond are very different from those of their xenolithic counterpart, which are, in turn, more similar to those of high-Mg eclogite xenoliths (Appendix Table 3).

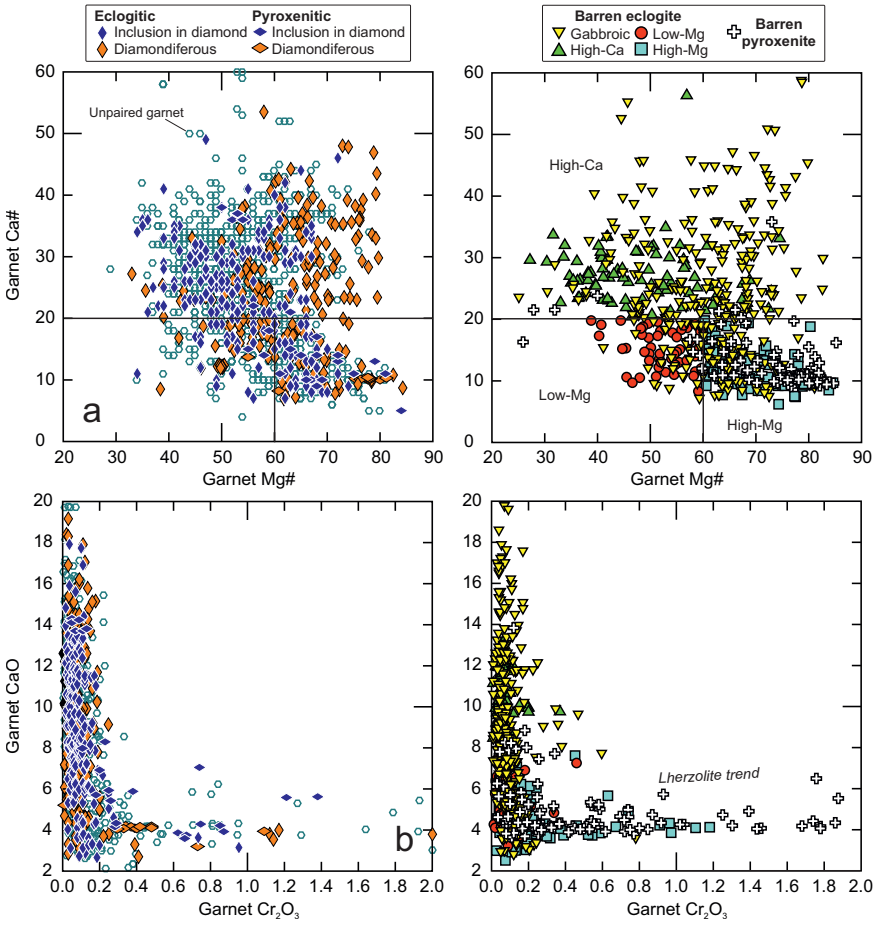

Figure 32. **a**. Ca# (100Ca / (Ca + Mg + Fe^{total} + Mn) as a function of Mg# in garnet. Garnet from non-gabbroic eclogite (whole-rock Eu/Eu* < 1.05; Eu/Eu* = chondrite-normalized Eu / $(Sm \times Gd)^{1/2}$; Rudnick and Fountain 1995) is classified into high-Mg, low-Mg and high-Ca varieties, as shown on the right. Garnet from gabbroic eclogite is typically high-Ca, but also occurs at lower Ca#. **b.** CaO (wt%) as a function of Cr_2O_3 (wt%). At $Cr_2O_3 \gtrsim 0.3$ wt%, garnet falls on a CaO–Cr_2O_3 trend typical of websterite and lherzolite, and indicative of buffering by orthopyroxene. Inclusions (paired and unpaired) and diamondiferous xenoliths are on the on **left**, barren xenoliths on the **right**.

Chondrite-normalized median REE patterns of clinopyroxene (Fig. 34a) show systematically decreasing abundances between Gd and Lu for all classes, except clinopyroxene in diamondiferous eclogite, which shows an upturn in Yb-Lu. The pattern of clinopyroxene in eclogitic diamond shows a hump in Nd_N, most similar to that in high-Ca eclogite, but differs from xenolithic clinopyroxene in having a less steep slope in the $MREE_N$–$HREE_N$ and higher concentrations of these elements. REE abundances in clinopyroxene from high-Mg and low-Mg eclogites are higher than for inclusions. Clinopyroxene in gabbroic eclogite shows a positive Eu anomaly (Eu/Eu* = 1.22), shared to a lesser extent by that in diamondiferous eclogite (1.19) and that in diamond (1.07). Individual REE_N patterns of clinopyroxene in pyroxenitic diamond are extremely heterogeneous, not only with respect to abundances, which vary by several orders of magnitude, but also to shape (not shown), which precludes calculation of a meaningful median composition. Individual inclusions have Eu/Eu* from 0.61 to 2.4, with a median of 1.07,

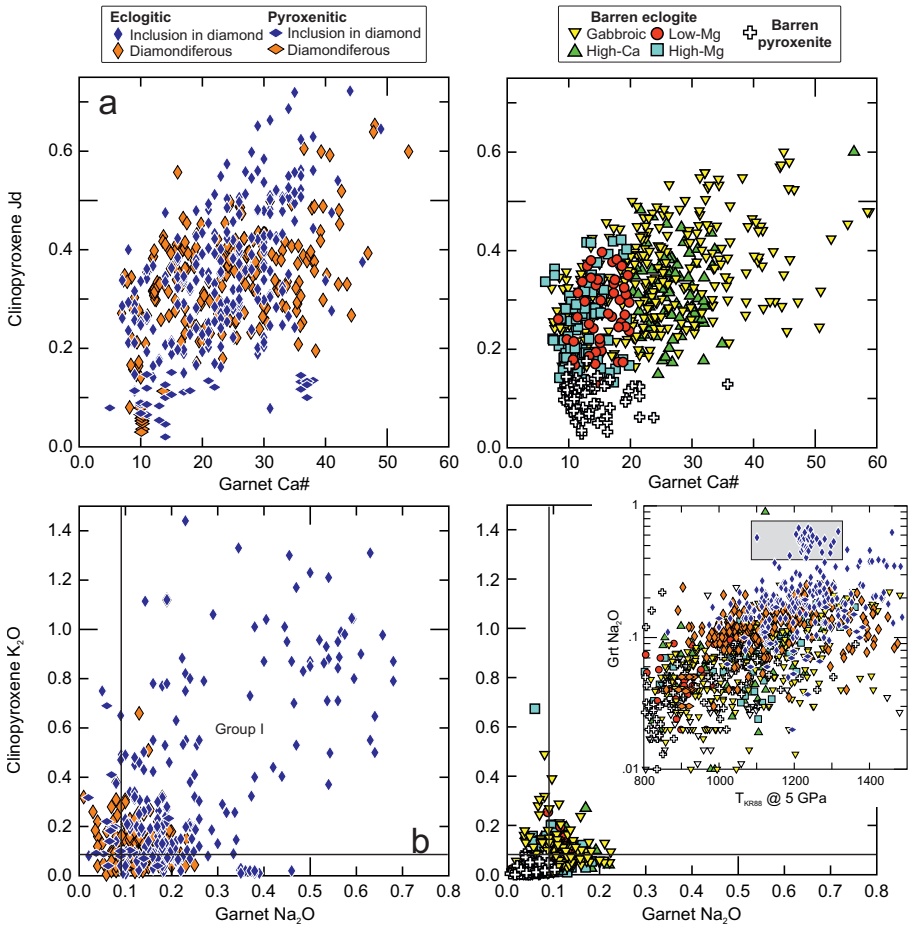

Figure 33. a. Jadeite content in clinopyroxene (Jd) as a function of Ca# (100Ca / (Ca + Mg + Fe^{total} + Mn)) in garnet. **b.** K_2O content (wt%) in clinopyroxene as a function of Na_2O content (wt%) in garnet. Samples with K_2O in clinopyroxene ≥ 0.08 wt% and Na_2O in garnet ≥ 0.09 wt%, with a higher likelihood of being diamondiferous, have been classified as Group I eclogites by McCandless and Gurney (1989); those in the lower left quadrant are Group II eclogites. **Inset in right panel** shows that Na_2O content in garnet increases with temperature, with a group offset to higher Na_2O. Inclusions and diamondiferous xenoliths on **left**, barren xenoliths on **right**.

i.e., slightly gabbroic. Clinopyroxene in the single diamondiferous pyroxenite with REE data, together with its barren counterpart, has the highest LREE abundances of all classes, but shows a stronger negative slope in the $MREE_N$–$HREE_N$, similar to that in gabbroic pyroxenite (Fig. 34a).

For garnet, median Ni and Sr contents are highest for inclusions in diamond (62 and 1.76 ppm, respectively), followed by that in diamondiferous eclogite (49 and 0.92 ppm, respectively) and barren eclogite classes (41–14 ppm and 0.62–0.26 ppm, respectively). Median Y contents of garnet in diamond (30 ppm), high-Ca eclogite (34 ppm) and low-Mg eclogite (36 ppm) are highest, whereas those of garnet in diamondiferous eclogite (19 ppm) are more similar to those of garnet in gabbroic eclogite (17 ppm). Median Zr contents are identical for garnet in diamond and in diamondiferous xenoliths (19 ppm), whereas those for garnet in high-Ca and low-Mg eclogite (11 ppm) and in gabbroic eclogite (9 ppm) are much lower. Median Nb contents vary widely, and are lowest for garnet in gabbroic eclogite (0.03 ppm), followed by

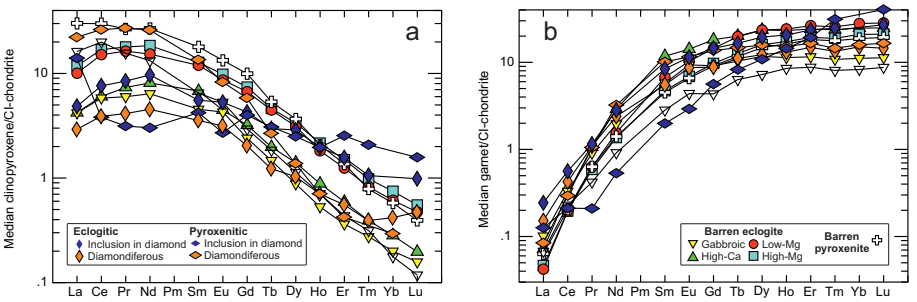

Figure 34. Chondrite-normalized REE patterns of **a.** clinopyroxene and **b.** garnet. Only median values per class are shown for clarity. CI-chondrite of Sun and McDonough (1989).

inclusions (0.06 ppm) and highest for garnet in diamondiferous eclogite (0.20 ppm), as applies to coexisting clinopyroxene.

Chondrite-normalized median REE patterns for garnet in the various eclogite classes are very similar at first glance, with low LREE, more or less strongly increasing abundances to Dy_N and then small or no increases to Lu_N (Fig. 34b). Garnet in diamond and in diamondiferous eclogite have the highest La and Ce abundances, but, in contrast to inclusions, garnet in diamondiferous eclogite shows a flatter $HREE_N$ pattern, similar to garnet in gabbroic eclogite. Contrary to clinopyroxene, REE_N patterns of individual garnet inclusions in pyroxenitic diamond are relatively coherent (not shown). The median REE_N pattern for garnet in pyroxenitic diamond shows a strong increase between Pr and Lu, and is very different from that of garnet in diamondiferous pyroxenite, which increases strongly between La and Sm and then flattens rather abruptly. This in turn differs from the REE_N pattern of garnet in barren pyroxenites, which does not attain as high LREE abundances.

Garnet oxygen isotopes For six paired eclogitic garnet inclusions the median $\delta^{18}O$ is +7.4‰, whereas in diamondiferous eclogite it is +6.1‰ and in barren xenoliths it is lower still, varying between +6.0‰ for garnet in low-Mg eclogite (n = 9) and +5.4‰ for that in high-Ca and gabbroic eclogite (both +5.4‰, n = 23 and 81, respectively). Unpaired high-Ca and low-Mg garnet inclusions, which are likely eclogitic, both have median $\delta^{18}O$ of +6.8‰ (n = 32 and 3, respectively), whereas for high-Mg garnet $\delta^{18}O$ is +6.6‰ (n = 9). The variability of $\delta^{18}O$ is high (> 6‰ for garnets in eclogite xenoliths with Mg# < 50 but diminishes to < 3‰ at Mg# > 75, especially in barren pyroxenite xenoliths (Fig. 35). Inclusions show a crude negative correlation of $\delta^{18}O$ vs. Mg# (r^2 = 0.2, n = 50) and are barely represented in the field of sub-mantle $\delta^{18}O$ at low Mg#, where a group of garnets from barren high-Ca and gabbroic eclogite xenoliths plots (Fig. 35). The latter are exclusively from the Roberts Victor eclogite. No $\delta^{18}O$ data are available for clinopyroxene inclusions in the database, or for garnet in pyroxenitic diamond or diamondiferous pyroxenite. Garnet in barren pyroxenite has $\delta^{18}O$ of +5.5‰.

Temperature estimates. For all samples, temperatures are calculated with the Mg–Fe exchange thermometer of Krogh (1988; T_{KR88}), either at a pre-set pressure of 5 GPa using total Fe contents, in keeping with Stachel and Luth (2015), or solved iteratively with regional model conductive geotherms from Hasterok and Chapman (2011; hereafter HC11). The geotherm for non-touching inclusions corresponds to a surface heat flow of 38 mW/m^2, chosen to yield median pressures identical to those obtained for touching inclusions (see below). Samples yielding temperatures < 800 °C are not displayed or counted because temperatures may be underestimated at T < 900 °C (Krogh 1988) and because there is overlap with lower crustal xenoliths, e.g., in the Kaapvaal craton (Pearson et al. 1995). Temperatures > 1500 °C are inferred to reflect disequilibrium, although the cut-off may actually be lower depending on lithosphere thickness.

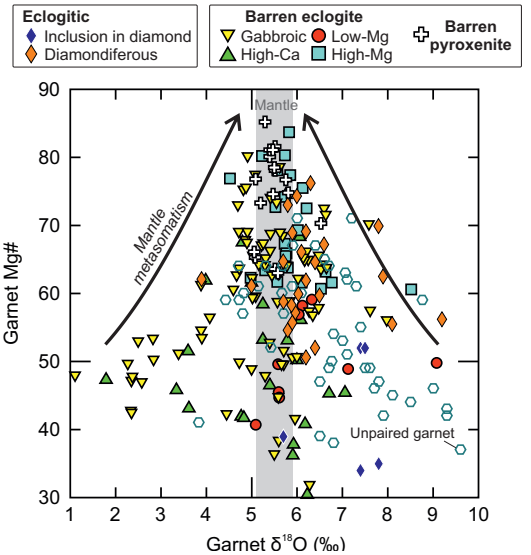

Figure 35. Mg# (100Mg / (Mg + Fe^{total})) in garnet as a function of $\delta^{18}O$ (‰ deviation of $^{18}O/^{16}O$ from the VSMOW standard). **Arrows** qualitatively indicate how the range of $\delta^{18}O$ at the highest Mg# in barren eclogites narrows towards typical mantle values (5.1–5.9‰; Mattey et al. 1994) in response to mantle metasomatism (Aulbach et al. 2020a).

Non-touching and touching eclogitic inclusions record median temperatures of 1225 and 1132 °C, respectively, reduced to 1207 and 1099 °C, respectively when the inclusions in Argyle diamonds, which are derived from an atypical high-temperature environment, are not considered (cf. Stachel and Harris 2008). These values compare with 1134 °C for diamondiferous eclogites (Appendix Table 3). Barren eclogites yield lower median temperatures, between 1087 °C for high-Mg eclogites and 962 °C for low-Mg eclogites. Non-touching and touching pyroxenitic inclusions give 1198 and 1065 °C, respectively, whereas temperature estimates for diamondiferous and barren pyroxenites are much lower, 920 and 974 °C, respectively. Temperature distributions are displayed in Figure 36a.

Trace element distribution. The distribution of trace elements between garnet and clinopyroxene in mantle eclogite and pyroxenite xenoliths has been shown to variably depend on garnet Ca#, jadeite (Jd) in clinopyroxene, and temperature and pressure (O'Reilly and Griffin 1995; Harte and Kirkley 1997). Mantle metasomatism of eclogite tends to lower Ca# and jadeite content, with preferred trace element partitioning into clinopyroxene, which can lead to the paradoxical observation that garnet from metasomatized eclogite has abundances of some incompatible elements similar to or even lower than garnet in unmetasomatized specimens (Aulbach et al. 2020a).

Garnet Ca# and jadeite content in clinopyroxene from diamond and diamondiferous eclogite show a broad positive covariation (r^2 = 0.25, n = 515). This is also recognizable in barren eclogite (r^2 = 0.34, n = 694), albeit at a lower jadeite intercept value, reflecting a higher proportion of pyroxenite (Fig. 33a). Thus, Ca# in garnet and Jd in clinopyroxene, which do not co-vary significantly with temperature, are coupled. With the exception of one outlier, inclusions, diamondiferous xenoliths and barren xenoliths show a negative correlation of log D_{Sr} (the distribution coefficient D of Sr between clinopyroxene and garnet) with garnet Ca# (r^2 = 0.64, n = 24; r^2 = 0.29, n = 78 and r^2 = 0.38, n = 635, respectively). These trends are

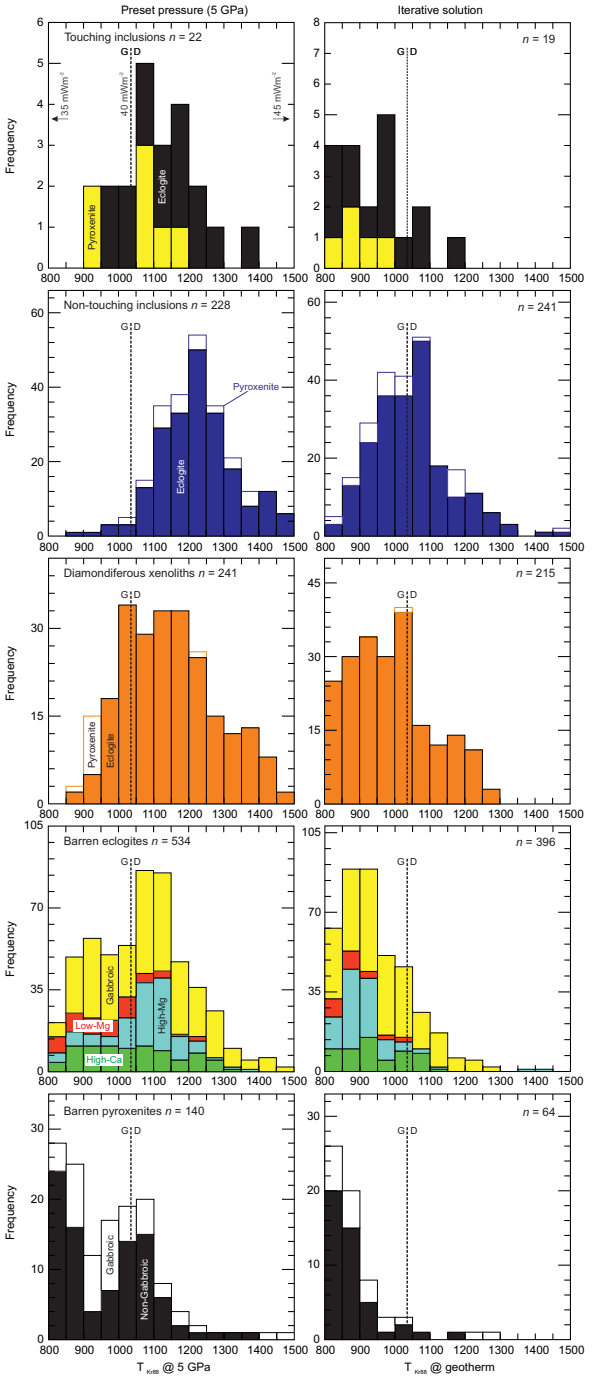

Figure 36. Distribution of estimated temperatures, based on **a.** T_{KR88} at 5 GPa, and **b.** T_{KR88} solved iteratively with peridotite-derived regional conductive geotherms parameterized from Hasterok and Chapman (2011), for touching and non-touching inclusions and diamondiferous and barren xenoliths. The temperature where diamond becomes stable along conductive geotherms corresponding to surface heat flows of 35, 40 and 45 mW/m^2 (Hasterok and Chapman 2011) is indicated in the **top left panel**, and for the 40 mW/m^2 instance, as a **dashed line** in both panels.

offset to increasingly higher log D_{Sr} at a given garnet Ca# for diamondiferous and barren xenoliths (Fig. 37a). This variation is also true for the more incompatible trace element Ce (excluding four outliers), where inclusions have $r^2 = 0.35$ ($n = 31$), diamondiferous xenoliths have $r^2 = 0.44$ ($n = 71$) and barren xenoliths have $r^2 = 0.59$ ($n = 674$) (Fig. 37b). This trace-element relationship similarly applies to Zr and Nb (not shown), except that there is greater overlap between inclusions in diamond and barren eclogites. The distribution of Y, which is compatible in bulk eclogite (see, e.g., distribution coefficients for garnet and clinopyroxene in equilibrium with tonalite melt in Barth et al. 2002), is strongly negatively correlated with Ca# ($r^2 = 0.64$, $n = 783$), but there are no distinct trends for diamondiferous and barren samples (not shown). Both log D_{Sr} and log D_{Ce} show marked negative correlation with $T_{KR88(5\ GPa)}$ ($r^2 = 0.43$, $n = 747$ and $r^2 = 0.31$, $n = 752$, respectively), whereas log D_Y shows no correlation. As trace element data are available for only one touching inclusion, the effect of cooling and re-equilibration on trace element distribution cannot be assessed.

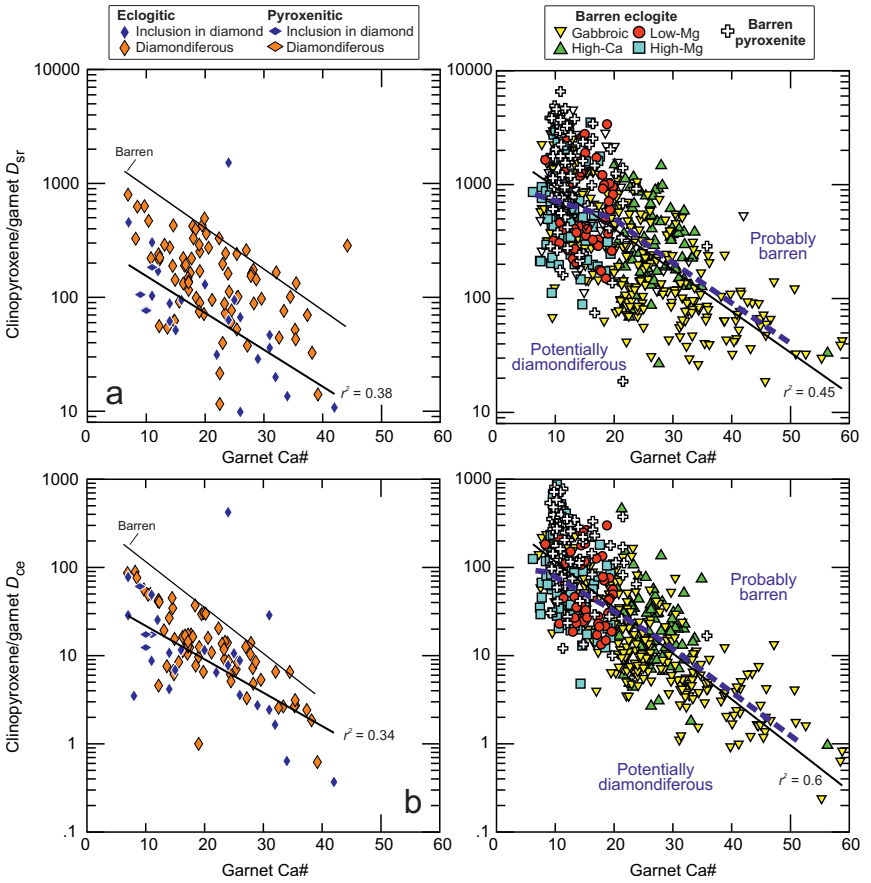

Figure 37. Log distribution of **a.** D_{Sr} and **b.** D_{Ce} between clinopyroxene and garnet as a function of garnet Ca# (100Ca / (Ca + Mg + Fe^{total} + Mn)). Separate regressions for inclusions and barren xenoliths are indicated. **Thick stippled line** separates the field encompassing inclusions and diamondiferous xenoliths from the field where almost exclusively barren xenoliths occur. Inclusions and diamondiferous xenoliths on **left**, barren xenoliths on **right**.

Reconstructed whole rocks. Following Aulbach and Jacob (2016), whole rocks are reconstructed from 55 wt% garnet and 45 wt% clinopyroxene, bearing in mind that HFSE abundances are minima when rutile is not considered. The presence of minor kyanite and/or orthopyroxene can further adversely affect accuracy of whole rock estimates, which is the case for only < 3% kyanite-bearing and < 2% orthopyroxene-bearing xenoliths, coesite being reported for even fewer xenoliths in this study. The above mineral modes correspond to the median modes determined for large eclogite xenoliths reported in Agashev et al. (2018), with a standard deviation of 5%. While bulk major-element compositional variations are largely accommodated by both garnet and clinopyroxene compositions (Aulbach and Jacob 2016), a single mode is unlikely to be representative of the true variation, and, in particular, pyroxenites may have higher clinopyroxene/garnet ratios. Typical uncertainties in major-element contents of reconstructed bulk rocks for a 10% modal uncertainty are displayed in Figure 38.

From the compilations in Figure 38, median whole-rock FeO contents for inclusions (11.8 wt%) are higher than for diamondiferous eclogites (9.8 wt%), and most similar to barren high-Ca eclogites (12.4 wt%), whereas those in high-Mg and gabbroic eclogites are much lower (9.7 and 9.4 wt%) (Appendix Table 3). Conversely, whole-rock MgO contents for inclusions (10.1 wt%) are lower than those for diamondiferous eclogites (11.5 wt%), and are lowest for barren high-Ca eclogites (9.6 wt%) and, by definition, highest for high-Mg eclogites (14.8 wt%). Also by definition, CaO contents are highest in high-Ca eclogites (12.5 wt%), whereas diamondiferous eclogites have 11.6 wt% and inclusions have 10.8 wt%. For other oxides not shown in Figure 38, the whole-rock Al_2O_3 contents of inclusions (16.3 wt%) and diamondiferous eclogites (16.5 wt%) are most similar to gabbroic eclogites (16.3 wt%), and higher than in other barren eclogites, the lowest values being observed in high-Mg eclogites (14.7 wt%). Similar variations are mirrored by Na_2O contents: 2.5 wt% for inclusions and diamondiferous eclogites, 2.3 wt% for gabbroic and high-Ca eclogites, and only 1.6 wt% for high-Mg eclogites. Whole-rock Cr_2O_3 contents are lowest for high-Ca eclogites (0.05 wt%) and inclusions (0.06 wt%), and highest for high-Mg eclogites (0.14 wt%).

Whole rock reconstruction for pyroxenitic inclusions shows FeO contents (11.1 wt%) that are higher than for diamondiferous pyroxenites (7.0 wt%) or barren pyroxenites (7.3 wt%), as applies to eclogites. Conversely, MgO contents are lowest for inclusions (15.9 wt%) and highest for diamondiferous pyroxenites (18.6 wt%), whereas CaO (11.6–11.7 wt%) and Cr_2O_3 contents (0.28–0.30 wt%) are indistinguishable and Al_2O_3 contents similar (13.4 wt% for inclusions, 13.9 wt% for diamondiferous and barren pyroxenites). Moreover, Na_2O contents are higher for inclusions (0.90 wt%) than for diamondiferous pyroxenites (0.65 wt%), but similar to barren pyroxenites (0.92 wt%). The major-element relationships of Figure 38 illustrate the offset of xenolith chemistry towards overall lower FeO and higher MgO, Cr_2O_3 and CaO contents compared to inclusions.

Chondrite-normalized median REE patterns for bulk rocks reconstructed from inclusions (Fig. 39) show strong LREE depletion, similar to reconstructed diamondiferous, high-Ca and gabbroic eclogite. The REE pattern flattens out for gabbroic eclogite and, at twice higher abundances, high-Ca eclogite. In contrast, both diamond and diamondiferous eclogite show a continuous increase towards the HREE. Low-Mg and high-Mg eclogites are characterized by much higher LREE abundances and slightly increasing abundances in the HREE. Positive Eu anomalies are common to whole rocks reconstructed from inclusions (1.05), for diamondiferous eclogites (1.16) and, by definition, for gabbroic eclogites (1.21). The other eclogite classes have lower median Eu/Eu* (0.96–0.98). Reconstruction of pyroxenites from inclusions is hampered by the small number of samples and their wide compositional variation, as described for individual minerals. The single diamondiferous pyroxenite has a REE_N pattern similar to its barren non-gabbroic counterpart (Fig. 39). Barren gabbroic pyroxenite shares positive Eu/Eu* and low HREE with barren eclogite, but is LREE-enriched.

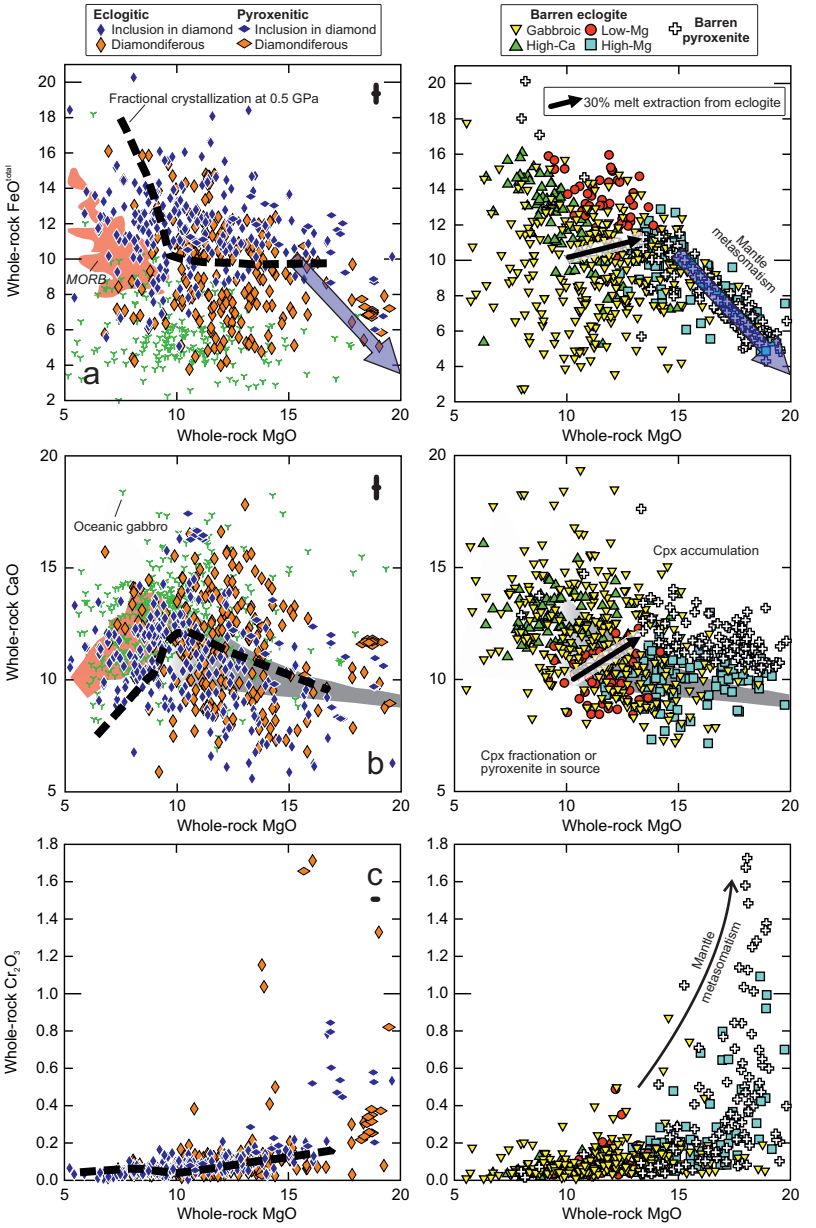

Figure 38. a. FeO, **b.** CaO and **c.** Cr_2O_3 as a function of MgO (all wt%) in whole rocks reconstructed from 55% garnet and 45% clinopyroxene, with typical uncertainties for a 10% modal variation from Aulbach et al. (2020a; indicated in top right of each graph in the left panel). "Mantle metasomatism" trend in a. reflects addition of high-temperature pyroxene from carbonated, ultramafic melt (Aulbach et al. 2020a). **Orange field in the left panels** encompasses MORBs (crystallising at ~0.05 GPa) from Jenner and O'Neill (2012), **green symbols** show gabbros (Eu/Eu* > 1.05) from PetDB (www.earthchem.org/petdb), and the **thick stippled line** is for fractional crystallization of picrite at a pressure of 0.5 GPa from Aulbach and Jacob (2016). The **grey field in b.** shows expected compositions for differentiating primitive mantle-derived melts, with higher and lower CaO suggestive of clinopyroxene accumulation and fractionation, respectively (Herzberg and Asimow 2008). **Right panels for a. and b.** show **arrows** corresponding to the quantitative compositional change after 30% melt extraction from eclogite, as calculated from experimental melting residues (see Aulbach and Jacob 2016). Inclusions and diamondiferous xenoliths on left, barren xenoliths on right. High Cr_2O_3. **c.** is associated with intense mantle metasomatism, where almost exclusively barren xenoliths occur.

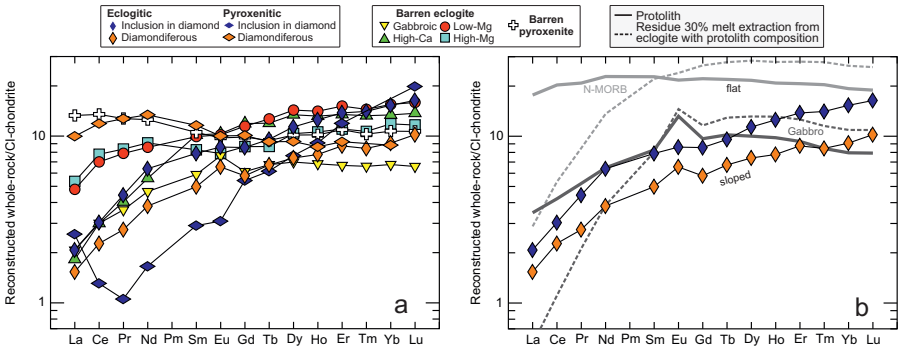

Figure 39. a. Chondrite-normalized REE patterns of whole rocks reconstructed from inclusions and xenoliths. Median values per class are shown for clarity. Only a single pyroxenite inclusion pair has reported Tm and Yb, which causes a spurious spike in the median pattern and is therefore not considered. **b.** Patterns of inclusions and diamondiferous eclogites, with positive slopes throughout the REE. Shown for comparison, NMORB (Gale et al. 2013) and average gabbro (Benoit et al. 1996), and hypothetical eclogites with NMORB and gabbro composition that lost 30% partial melt (from Aulbach et al. 2020b; **dashed lines**), with flat MREE–HREE patterns. CI-Chondrite of Sun and McDonough (1989).

Thermobarometry for eclogitic/pyroxenitic inclusions, and kinetically inhibited element redistribution

Some thoughts on inclusion thermobarometry. Accurate barometry for eclogitic and pyroxenitic garnet–clinopyroxene pairs remains elusive (cf., Nimis 2022), although some formulations have been proposed (e.g., Beyer et al. 2015; Ashchepkov et al. 2017b). In most instances, the thermal gradient of the regional lithospheric mantle has been independently determined from peridotitic minerals or assemblages, so that pressures can be estimated by solving T_{KR88} iteratively with the appropriate gradient, assuming equilibration to the conductive geotherm (e.g., Aulbach et al. 2020a). Because in xenoliths, minerals used for geothermobarometry remain in contact and equilibrate to ambient mantle temperatures until entrainment, they reflect the thermal state of the lithosphere at the time of kimberlite emplacement. The same should apply to touching garnet–clinopyroxene pairs included in diamond. Thus, for xenoliths and touching inclusions, T_{KR88} is solved iteratively with geothermal gradients parameterized from Hasterok and Chapman (2011; HC11), corresponding to surface heat flows of 38–35 mW/m^2. These model geotherms either correspond to those directly determined based on peridotitic assemblages or clinopyroxene relative to HC11 geotherms, as is the case for Koidu, West Africa. In other instances, they were roughly translated from the older Pollack and Chapman (1977) family of geotherms as quoted in older literature (Appendix Table 1). Application of iterative solutions moves a fraction of xenoliths to temperatures < 800 °C, and results in pressures > 8 GPa (> 250 km) for high-temperature samples equilibrated to cool geotherms (35 mW/m^2). Keeping all solutions, this results in average pressures of 4.9 ± 1.5 GPa and temperatures of 950 ± 110 °C for the small number of touching eclogitic inclusions (n = 15). These values compare relatively well with 5.2 ± 1.2 and 970 ± 130 °C for 228 diamondiferous eclogites (37 mW/m^2). With touching pyroxenite inclusions (n = 8) average pressures and temperatures vary between 3.8 ± 0.5 GPa and 860 ± 80 °C (38 mW/m^2), whilst 14 diamondiferous pyroxenites yield 4.1 ± 0.7 and 740 ± 100 °C (36 mW/m^2). Of the latter, ten are from the northern Slave craton where the lithosphere is characterized by a cold geotherm (Grütter 2009).

The appropriate choice of a geotherm for non-touching inclusions, which last equilibrated at the time of encapsulation, is less certain. As outlined above, eclogitic diamond formation commenced around 3 Ga, when lithospheric conductive gradients would have been higher. One could assume that the lithosphere experienced only cooling, and that touching and non-

touching inclusions formed over the same pressure range. The conductive geotherm for iterative calculations is then chosen such that the median pressure for non-touching inclusion pairs equals that of touching inclusions. According to Hasterok and Chapman (2011), this situation occurs when the geotherm corresponds to a surface heat flow of 38 mW/m^2, and 220 non-touching eclogitic inclusions give values of 4.9 ± 0.8 GPa and 1040 ± 130 °C. The resultant cooling by only some 100 °C is consistent with stabilization of cool continental lithosphere by the Mesoarchean, before substantial eclogitic diamond formation. In addition, pressure–temperature conditions for non-touching inclusions can be underestimated if they experienced decompression due to extension, as suggested for the Kimberley area in the Kaapvaal craton (Phillips et al. 2004; Stachel and Luth 2015) and the western Zimbabwe craton margin (Aulbach et al. 2017). A comparison of Figure 36a and 36b shows a marked difference in the determined temperatures using pre-set and iteratively determined estimates.

Age constraints indicate that at least some eclogitic diamond suites (Slave, Kaapvaal) formed in close temporal relationship to major subduction events (for details on suggested diamond forming processes during subduction, see further below). If so, they could have followed ancient subduction geotherms, different from those in the coeval continental lithosphere or modern subduction zones. These thermobaric gradients must have been lower than those obtained for exhumed ≥ 2 Ga metamorphic rocks (> 375 °C/GPa; Brown and Johnson 2018), in order to allow a pressure–temperature path consistent with diamond stability. A possible Archean slab gradient is roughly reconstructed in Figure 40a, based on following observations: Orogenic eclogite with an oceanic crustal protolith from the Archean Belomorian Belt indicates peak conditions of 1.85 GPa and 710 °C (Li et al. 2015). Elastic geobarometry on quartz inclusions in garnet from mantle eclogite at Mir (Siberian craton) yielded a pressure of 3 GPa at 850 °C, and was interpreted as reflecting entrapment during prograde metamorphism corresponding to a surface heat flow of 40–50 mW/m^2 (Alvaro et al. 2020). This may be linked to Archean subduction, as eclogite xenoliths from the Siberian craton have yielded Mesoarchean ages (Appendix Table 1). Combined with the pressure–temperature estimates for non-touching inclusions, these provide a predictive pressure–temperature path for subducting Archean oceanic crust (Fig. 40a).

In contrast to the low temperatures obtained from iterative solutions on non-touching inclusions (average 1040 ± 120 °C), constraints from the aggregation of N impurities in eclogitic diamonds, which is a function of N concentration, temperature and age, indicate average mantle residence temperatures of 1140 ± 50 °C for a 3 Ga eclogitic diamond age (Stachel and Harris 2008). As N-based temperatures reflect time-integrated thermal states, they may include transient heating events associated with melt migration. Moreover, not all eclogitic diamonds formed during relatively cold subduction, but may instead be associated with (renewed) growth during later melt metasomatism (Stachel and Luth 2015), as supported by multiple Proterozoic eclogitic diamond formation events based on inclusion dating (Wiggers de Vries et al. 2013; Gress et al. 2021), and by ca. 1.6 Ga eclogitic diamonds from Argyle recording atypically high temperatures (Stachel and Harris 2008).

Inhibited minor element redistribution in touching inclusions. As described above, the distribution of some minor and trace elements between clinopyroxene and garnet is temperature-dependent. Thus, touching inclusions and their xenolithic counterparts should show similar systematics, whereas non-touching inclusions might differ due to higher equilibration temperatures. Specifically, the distribution coefficient of both Na_2O and TiO_2 between clinopyroxene and garnet decreases with increasing temperature, as higher concentrations of these elements are accommodated in garnet (Aulbach 2020). If this should be the case, then D_{Na_2O,TiO_2} for clinopyroxene–garnet would be expected to be higher for touching inclusions than for non-touching inclusions. However, when D_{Na_2O} is considered as a function of T_{KR88} calculated at 5GPa, it becomes evident that several touching inclusions

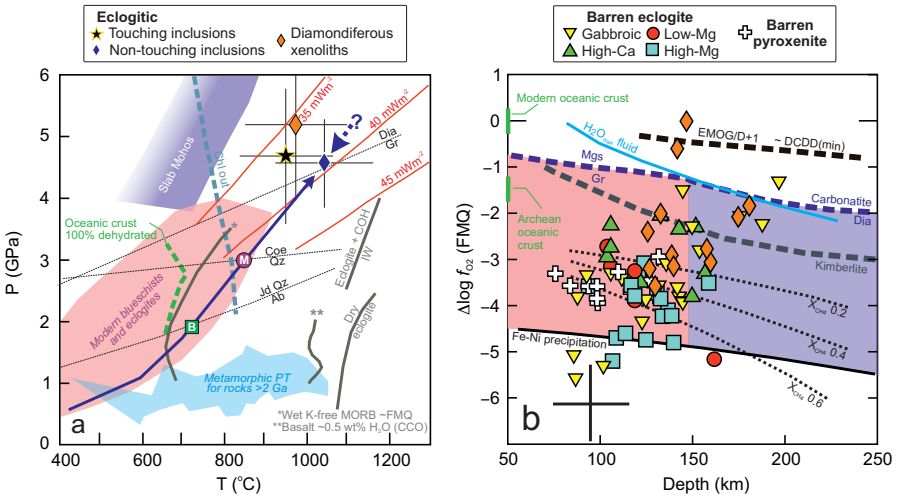

Figure 40. a. Pressure (GPa)–temperature (°C) diagram showing average values and 1σ error bars for iterative solutions for touching and non–touching inclusions and diamondiferous xenoliths. The geotherm for non–touching inclusions was chosen such that they give an average pressure similar to touching inclusions although this may yield underestimated pressure–temperature conditions if the latter experienced decompression in addition to cooling (indicated by **dashed arrow with "?"**). Also shown are: solidi (solid grey lines) for dry, nearly–dry or wet eclogite at various oxygen buffering equilibria (CCO carbon–carbon monoxide, FMQ fayalite–magnetite–quartz, IW iron–wüstite) from Schmidt and Poli (2014), Litasov et al. (2014) and Ziaja et al. (2014); a **curve** depicting 100% dehydration of oceanic crust (Laurie et al. 2013); oceanic and continental high–pressure fields for rocks in modern subduction zones (Penniston–Dorland et al. 2015); and the peak pressure–temperature conditions of metamorphic rocks older than 2 Ga from Brown and Johnson (2018). Shown in addition is a peak pressure–temperature for Neoarchaean orogenic eclogites ("B" – Belomorian Belt, Russia) from Li et al. (2015) and the pressure–temperature of entrapment of quartz inclusions in garnet from a presumably Archaean eclogite xenolith from Mir ("M" – Siberian craton) from Alvaro et al. (2020); these points define a suggested subduction path for Archaean oceanic crust, shown by the **thick dark blue arrow**. Model conductive geotherms corresponding to surface heat flows of 35, 40 and 45 mW/m^2 from Hasterok and Chapman (2011), the diamond–graphite boundary from Day (2012), and the coesite–quartz boundary and albite–jadeite–quartz reaction after Brown and Johnson (2018). The chlorite–out curve and pressure–temperature conditions for warm slab Mohos (**purple field**) allowing deserpentinization within the diamond stability field are from Syracuse et al. (2010). **b.** Oxygen fugacity estimates (fO_2) based on the eclogite oxybarometer of Stagno et al. (2015) for mantle eclogite and pyroxenite xenoliths relative to the fayalite–magnetite–quartz buffer (expressed as $\Delta\log fO_2$ (FMQ)) as a function of depth (samples in Aulbach et al. 2019b and references therein, plus those from Burness et al. 2020 and Mikhailenko et al. 2020). Data for diamondiferous eclogites are from a single study (Mikhailenko et al. 2020) and may not be representative. Estimates for modern and Archaean oceanic crust are from Aulbach et al. (2019b). Shown for comparison are the fO_2-dependent fraction of CH_4 in CHO fluids, and conditions with maximum H2O in the fluid (from Luth and Stachel 2014), the stability of carbonatite, carbonated silicate melt with 10 mol% CO_2 (~kimberlite) vs. diamond and graphite (from Stagno et al. 2013), and the minimum fO_2 for the reaction dolomite + coesite = diopside + diamond (DCDD), which lies at least one log unit above the reaction enstatite + magnesite = olivine + graphite/diamond (EMOG/D; Luth 1993; Stachel and Luth 2015), all applicable for a 40 mW/m^2 geotherm as calculated by the cited authors.

in eclogitic and pyroxenitic diamonds have low *D* values at a given temperature (Fig. 41a). These low *D* values are more similar to those of (higher-temperature) non-touching inclusions than to (similar-temperature) diamondiferous xenoliths, which suggests that at least minor element redistribution for inclusions is inefficient. Figure 41b shows that a similar situation applies for TiO_2. The decreasing TiO_2 solubility in both garnet and clinopyroxene with decreasing temperature leads to exsolution of rutile, with the implication that this mineral is more likely to be observed in lower-temperature specimens, and that TiO_2 concentrations

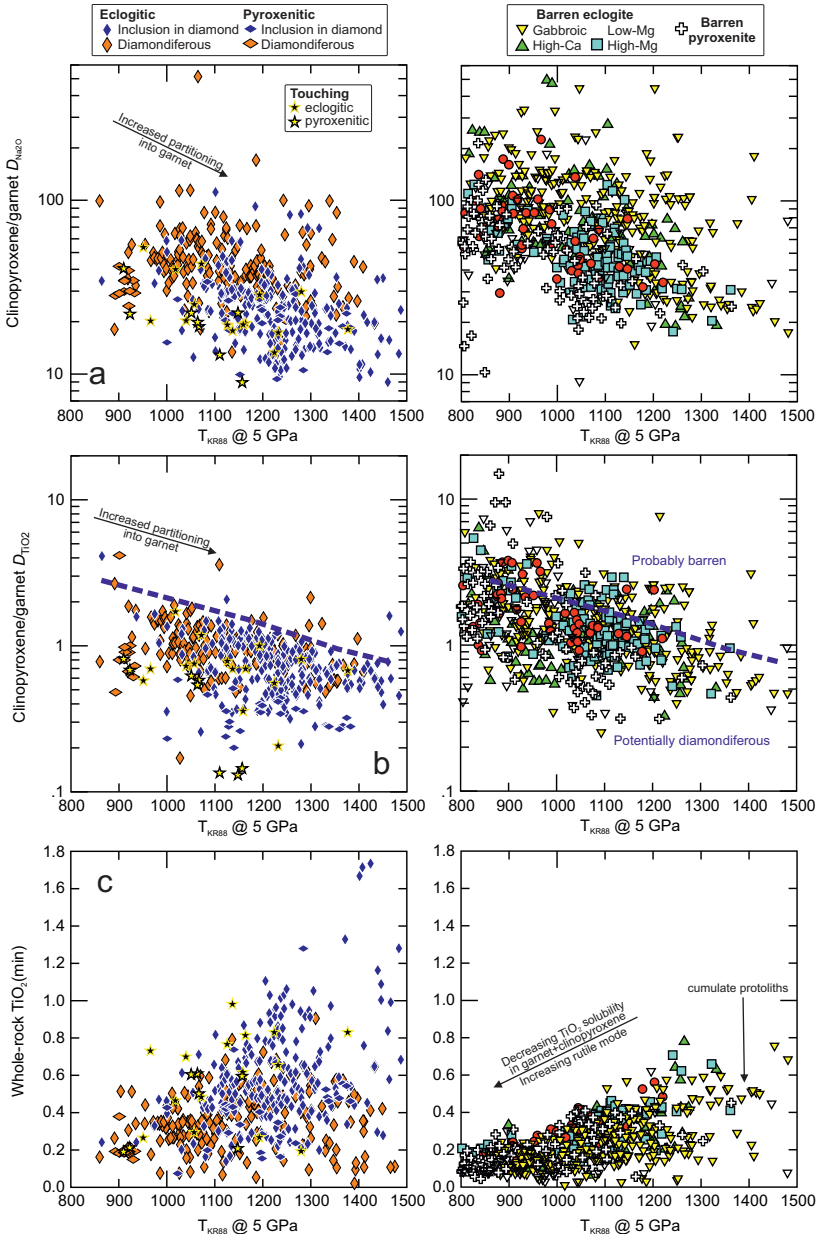

Figure 41. Log distribution of **a.** D_{Na_2O} and **b.** D_{TiO_2} between clinopyroxene and garnet as a function of T_{KR88} at 5 GPa. High temperatures (pressures along conductive geotherms) lead to increased partitioning of Na_2O and TiO_2 into garnet. High D values at a given temperature may be associated with barren xenoliths, whereas those with low D values may be diamondiferous (indicated by **blue stippled line**). **c.** Minimum TiO_2 content (wt%; reconstructed without rutile) as a function of T_{KR88} at 5 GPa, illustrating that inclusions have higher average TiO_2 contents consistent with higher temperatures compared to xenoliths, which favors TiO_2 uptake in both garnet and clinopyroxene, whereas free rutile is required to accommodate bulk rock TiO_2 contents at low temperatures (Aulbach 2020). Many touching inclusions have high TiO_2 at their estimated temperatures, presumably because they have not purged excess TiO_2 from their lattice, whereas continued Mg–Fe exchange allowed them to equilibrate to lower average temperatures than isolated inclusions. The **vertical arrow in right panel** illustrates the effects of accumulation in low-pressure protoliths, leading to low bulk TiO_2 contents in particular in gabbroic eclogites. Inclusions and diamondiferous xenoliths on **left**, barren xenoliths on **right**.

in bulk rocks are increasingly underestimated when only garnet and clinopyroxene are considered (Aulbach 2020). Minimum (rutile-free) bulk-rock TiO_2 contents reconstructed from non-touching inclusions as a function of T_{KR88} loosely follow the xenolith trend, but with higher average contents consistent with higher entrapment temperatures and rutile solubility (Fig. 41c). However, there is also an off-set to higher TiO_2 at a given temperature compared to xenoliths, which may reflect the inability of included garnet to purge the excess TiO_2 from its lattice, first via nucleation of lamellae and then by recrystallization and formation of discrete rutile grains. One may speculate that this is due to the dryness of the inclusions where structural hydrogen, once lost to the inclusion–diamond interface (Nimis et al. 2016), is not replenished in contrast to matrix minerals. Conversely, the similar temperature estimates for touching inclusions and diamondiferous eclogites suggest that the redistribution of MgO and FeO, on which T_{KR88} is based, is more efficient.

Source rocks of eclogitic and pyroxenitic diamond

Source rocks of eclogitic diamond. Inclusions in diamonds are expected to reflect the mineralogy and composition of their various substrates (Boyd and Gurney 1986; Meyer 1987), in this case mantle eclogite. With respect to major elements, eclogitic inclusions cover nearly the entire range displayed by xenoliths, but are more common at bulk-rock MgO < 13 wt%. They seemingly overlap mostly with high-Ca and gabbroic eclogites (Fig. 38). Mantle eclogites with positive Eu anomalies (gabbroic class) and low total REE abundances (ΣREE) derive from sources that experienced plagioclase–olivine accumulation, partially followed by reaction with melt, which explains the wide range of compositions in this group (Aulbach and Jacob 2016). The fractionated melts develop negative Eu anomalies. Broadly, high-Ca and some high-Mg eclogites have more- and less-differentiated basaltic protoliths, respectively, whereas low-Mg eclogites may require Fe-rich protoliths. Inclusions follow the expected systematics of low-pressure cumulates vs. differentiated melts with respect to Eu/Eu* and ΣHREE (Fig. 42a; only HREE are summed to exclude effects of LREE loss via melt depletion and gain via metasomatism). Also, 65% of unpaired garnet and 58% of unpaired clinopyroxene inclusions have Eu/Eu* > 1.05. The proportion of gabbroic xenoliths (i.e., showing positive Eu anomalies) amongst diamondiferous xenoliths with reported REE contents is much higher at 80%. These numbers agree well with estimates that some 70% of modern oceanic crust is constituted by a gabbroic layer, the remainder being pillows, flows and sheeted dike complexes where magma freezes in layers and conduits (White and Klein 2014). Conversely, as noted for cratonic eclogite (Aulbach and Arndt 2019a), a mantle cumulate origin is precluded because eclogitic inclusions do not show the predicted positive correlation of Y with MgO, but weak negative correlation instead ($r^2 = 0.25$, $n = 21$; Fig. 42b).

Following the low-pressure igneous stage at spreading ridges, low- and high-temperature seawater alteration produces minerals with higher and lower $\delta^{18}O$, respectively, compared to the mantle (Muehlenbachs and Clayton 1972a,b). These signatures are still recognizable in many mantle eclogites (Jacob 2004), and in garnet inclusions (Fig. 35). Due to the cross-over of alteration signatures and the oxygen isotope mantle range at intermediate temperature conditions of crustal alteration, or just a lack of alteration, mantle-like $\delta^{18}O$ is not proof against low-pressure protoliths (Smart et al. 2012). Subsequent subduction and metamorphism of oceanic crust causes dehydration and loss of a LREE-enriched silicic partial melt in some, though not all eclogites (Schulze et al. 2003), especially in warm slabs. Eclogitic diamond sources now residing at temperatures ≳ 800 °C would have crossed the solidus of wet metabasalt (Schmidt and Poli 2014), which is supported by the pressure–temperature paths of exhumed ancient orogenic eclogites (Fig. 40a). Experimental phase relationships further indicate that this entails loss of SiO_2 and Na_2O, accompanied by an increase in MgO, FeO and CaO, while the presence of substantial amounts of garnet in the residue leads to compatible behaviour of

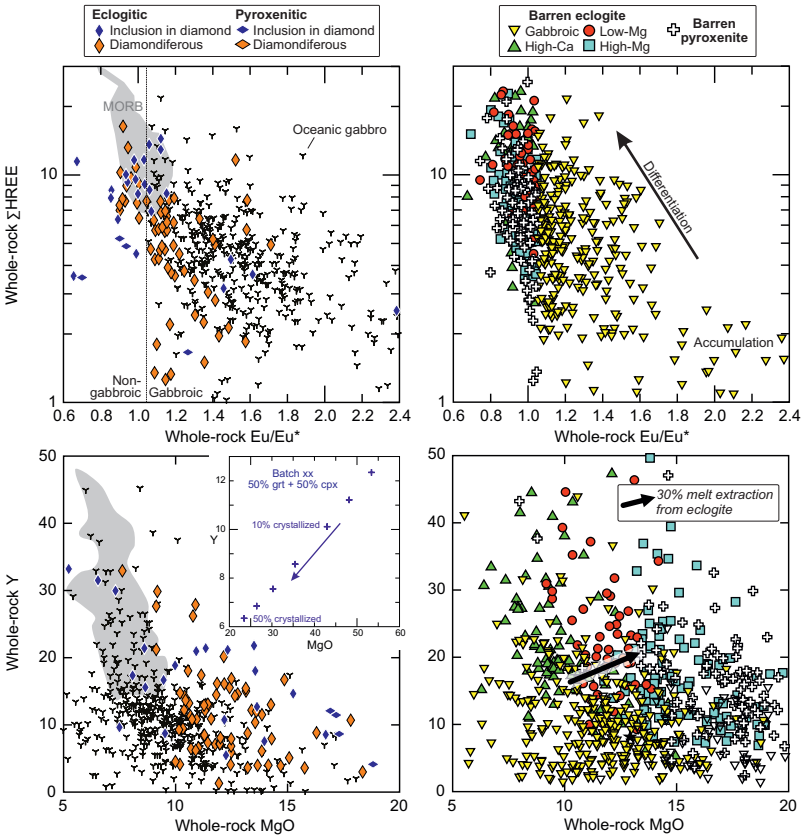

Figure 42. a. ΣHREE (ppm, summed from Tb to Lu) as a function of Eu/Eu* (chondrite-normalized Eu / (Sm × Gd)$^{1/2}$; CI-chondrite of Sun and McDonough 1989) in reconstructed bulk rocks, illustrating the effects of low-pressure olivine + plagioclase accumulation and evolution of residual melts. Shown for comparison is the field for MORB (Jenner and O'Neill 2012) and gabbros (PetDB database). **b.** Y (ppm) as a function of MgO (wt%) in reconstructed bulk rocks, illustrating that mantle eclogites and inclusions do not follow the trend (**inset in left panel**) expected for high-pressure crystallization ("xx") of picritic melts (calculated trend from Aulbach and Arndt 2019b). **Arrow in right panel** shows quantitatively the compositional change associated with extraction of 30% melt from eclogite. Inclusions and diamondiferous xenoliths on **left**, barren xenoliths on **right**.

the HREE and Y, and incompatible behaviour of the LREE during melting (Aulbach and Jacob 2016). Indeed, high MgO, low SiO_2 and Na_2O as well as low LREE/HREE in both inclusions and mantle eclogites have been interpreted as signatures of melt loss from eclogite (e.g., Ireland et al. 1994; Jacob 2004; Stachel et al. 2004), although low SiO_2 and LREE/HREE can also be a primary signature of oceanic crustal cumulates (Aulbach and Jacob 2016). The strong LREE-depletion in high-Ca and gabbroic eclogite xenoliths (Fig. 39) may causally reflect their higher original Na_2O content, because the jadeite component in clinopyroxene, together with quartz/coesite and H_2O, participate in melt production (Laurie and Stevens 2012). A higher initial Na level will ultimately cause higher levels of depletion after melt loss. Again, the majority of bulk rocks reconstructed from inclusions have LREE-depleted REE_N patterns most similar to gabbroic and high-Ca eclogites, but with some important differences (Fig. 39) that provide insights into diamond formation processes discussed below.

Depending on the fertility after initial dehydration melting at low pressure and on the redox state of the eclogite and infiltrating fluid, oceanic crust may experience second-stage partial melting during fluid ingress (Fig. 40a). Diamondiferous eclogites and inclusions do not extend to the extremely melt-depleted compositions (very low Ce/Yb_{NMORB}) observed in some barren eclogites, perhaps due to the failure of diamond to crystallize from fluids in such depleted rocks. Otherwise, as noted above, the proportion of inclusions (~60%) and diamondiferous eclogites (80%) with gabbroic protoliths is similar to that in modern oceanic crust, indicating that diamond formation occurs in all portions of the oceanic crust, with a preference for intrusive sections indicated by diamondiferous eclogites. Given mechanisms for eclogitic diamond formation discussed below, this need not, however, reflect the extent to which C is originally distributed in these rocks. Curiously, few inclusions have strongly gabbroic signatures (low whole-rock Y or HREE abundances, strong positive Eu anomalies, Fig. 42), possibly indicating that deep crustal cumulate sections are less propitious substrates for the formation of inclusion-bearing diamonds.

Source rocks of pyroxenitic/websteritic diamond. For inclusions in diamond, the websteritic paragenesis is compositionally less well defined than the eclogitic one, which probably reflects multiple formation mechanisms (Stachel and Harris 2008). Similarly, pyroxenite xenoliths, which include rocks referred to as "high-Mg eclogites" in the literature, have multiple suggested origins (Aulbach and Jacob 2016). Bimineralic pyroxenite xenoliths grading into orthopyroxene-bearing websterites and, for inclusions in diamond, the websteritic inclusion suite from Venetia have been interpreted as the products of the interaction of slab-derived silicic melt with peridotite (Aulbach et al. 2002, 2007; Smit et al. 2014b), based on the similarity to experiments where peridotite was hybridized with eclogite-derived melts (Yaxley and Green 1998). On the other hand, a large proportion of bimineralic pyroxenite grading into high-Mg eclogites (20–40% of most eclogite-bearing xenolith suites) shows evidence for an origin via metasomatic interaction of mantle eclogite with a small-volume carbonated ultramafic melt similar to kimberlite (Aulbach et al. 2020a). Some pyroxenitic inclusions share major element features with the metasomatized group. This includes high MgO and low FeO (Fig. 38a), high CaO (Fig. 38b) and high Cr_2O_3 at high MgO (Fig. 38c), all of which have been interpreted as reflecting addition of a high-temperature pyroxene from the metasomatic melt (Aulbach et al. 2020a). A single diamondiferous pyroxenite with trace element data (from the Siberian craton) has a pattern similar to median barren pyroxenite (Fig. 39). Diamond in pyroxenite xenoliths from the northern Slave craton, where kimberlite-like metasomatism has been recognized, may have a similar origin (Smart et al. 2009). However, the few inclusions in pyroxenitic diamonds with REE data have spoon-shaped patterns with steep positive slopes in the $MREE_N$–$HREE_N$ that cross-cut those of pyroxenite xenoliths (Fig. 39). Similarly high resultant La_N/Pr_N and Lu_N/Gd_N are seen in only a few pyroxenite xenoliths. Finally, some pyroxenitic inclusions have lower MgO contents combined with relatively high FeO (Fig. 38a), and low ΣHREE contents (Fig. 42b), perhaps reflecting a deep crustal cumulate protolith, with insufficient Na_2O to metamorphose into eclogite with Jd-rich clinopyroxene.

The dearth of trace-element data makes it difficult to confidently distinguish between different scenarios for the origin of pyroxenitic diamond source rocks. As applies to high-Mg eclogite, an origin of pyroxenitic inclusions as direct mantle cumulates is precluded by the lack of the predicted element relationships proposed for precipitation of substantial amounts of garnet (e.g., correlated Y-MgO; Fig. 42b). The small proportion of pyroxenitic diamond (15%, of all pyroxenitic–eclogitic inclusions, based on paired and isolated clinopyroxene) suggests that this rock type is a subordinate diamond source. Note that Stachel and Harris (2008), based on different classification criteria (elevated Mg# and Cr_2O_3, low Ca content in garnet, presence of orthopyroxene), obtain a relative abundance for websteritic inclusions (amongst lithospheric diamonds) of only 2.3%, as opposed to 5.3% in this study.

Diamond formation mechanisms in eclogitic/pyroxenitic source rocks

Diamond formation from saline fluids. A group of eclogitic inclusions has very high Na_2O in garnet and K_2O in clinopyroxene, occupying a field where diamondiferous or barren eclogite does not occur (Fig. 33b). Garnets with Na_2O content > 0.4 wt% are off-set from trends of increasing Na concentrations with increasing temperature (inset in Fig. 33b), and therefore reflect a bulk compositional effect, as previously noted by Grütter and Quadling (1999). The same interpretation applies for K-rich clinopyroxenes, and therefore, these inclusion compositions reflect Na–K-rich bulk rocks. They are not associated with any major or trace element signature except low Cr_2O_3 and high Sr contents, although not enough trace-element data are available to further establish the nature of the metasomatic agent. This may point to diamond precipitation from saline high-density fluids, which are observed in (though not limited to) eclogitic diamond (Izraeli et al. 2001, 2004), and may be ultimately linked to subducted slabs based on observational data (Weiss et al. 2014, 2015, 2022), modelling (Sverjensky and Huang 2015) and experiments (Shatskiy et al. 2019). Omphacite occurring with saline high-density fluid in the same eclogitic diamond has elevated Na_2O (6.7 wt%) and K_2O (0.6 wt%; Weiss and Goldstein 2018). Any medium involved in the formation of diamond cannot be dissociated from the substrate in which the diamond forms (i.e., mineral inclusions and eclogite have the same composition at the locus of encapsulation in diamond). Therefore, the exclusive occurrence of high Na_2O in garnet and high K_2O in clinopyroxene inclusions in diamonds (Fig. 33b), whereas eclogite xenoliths lack these signatures in their garnet or clinopyroxene, indicates that such compositions do not survive during subsequent mantle eclogite evolution. This suggests efficient removal of this signature from the substrate during subsequent interaction with Na_2O- and K_2O undersaturated fluids or melts. If this interpretation is correct, 14% of eclogitic diamond (containing garnets with Na_2O content > 0.4 wt%) may have formed from saline high-density fluids.

Diamond formation from small-volume melts or COH fluids. Mantle eclogites are dominantly LREE-depleted, indicative of partial melt loss without subsequent re-enrichment. This is gauged by normalization to a putative low-pressure protolith with flat REE_N patterns, such as NMORB, and equally applicable to oceanic crust formed from a higher melt fraction, such as picrite. A sizable proportion of bulk high-Mg eclogites and pyroxenites (37%) show LREE-enrichment (Nd/Yb_{NMORB} or La/Sm_{NMORB} > 1), accompanied by a lowering of Jd (Fig. 43) and also of Ca# in garnet, which are both hallmarks of metasomatism by kimberlite-like melt (Aulbach et al. 2020a). As the lowering of garnet Ca# is accompanied by decreased partitioning of many incompatible elements into garnet, this leads to weak signatures of metasomatism based on trace elements in garnet alone (Aulbach et al. 2020a). From an fO_2 perspective, carbonated silicate melts, such as kimberlite, are stable to lower fO_2 than pure carbonatite (Fig. 40b), allowing for coexistence of melts with dilute carbonate content and diamond over a large fO_2 range (Stagno et al. 2015; Mikhailenko et al. 2020). The ability of kimberlite-like melt to be stable with eclogite to lower fO_2 than with peridotite implies carbon mobility over a wider range of conditions, and may thus help explain the overabundance of eclogitic relative to peridotitic diamonds (Stagno et al. 2015). In addition, small-volume melts (like kimberlite) or fluids imparting LREE-enrichment are important drivers of diamond formation in peridotite source rocks (Stachel et al. 2004; Stachel and Luth 2015; this work). However, less than a quarter of eclogitic-pyroxenitic bulk rocks reconstructed from inclusions (23%) show LREE-enrichment and associated high $LREE_N/HREE_N$ (Fig. 43), the hallmark of mantle metasomatism by diamond-forming CHO-fluids and small-volume melts in peridotite. Thus, although the trace-element database for eclogitic/pyroxenitic inclusions in diamond is limited, it appears that diamond formation in the eclogite system is not dominantly linked to a typical mantle metasomatic signature.

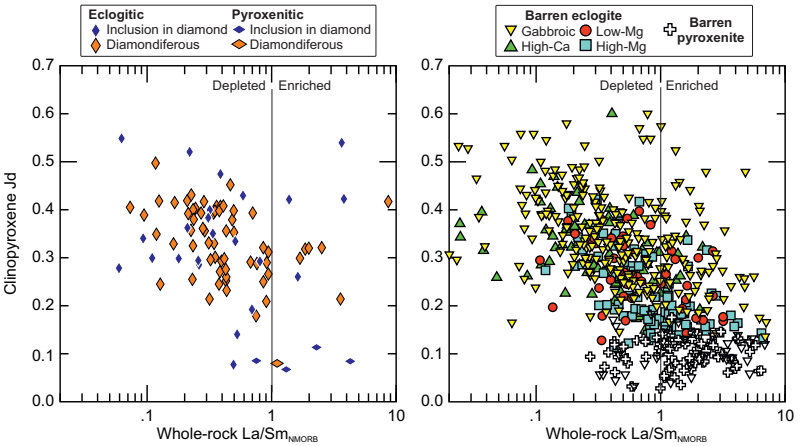

Figure 43. Jadeite content in clinopyroxene as a function of NMORB-normalized La/Sm of reconstructed whole rocks, illustrating enrichment and depletion. NMORB of Gale et al. (2013). Inclusions and diamondiferous xenoliths on **left**, barren xenoliths on **right.**

Diamond formation during subduction. Age distributions (Smit et al. 2022) suggest formation of the first eclogitic diamond populations in or associated with Archean (Kalahari Craton) and Paleoproterozoic (Slave craton) subduction zones, perhaps linked to the onset of plate tectonics at ~ 3 Ga (Shirey and Richardson 2011). This initial formation was followed by renewed growth or formation of eclogitic diamond during Proterozoic tectonothermal events, up to at least the Mesozoic (Timmerman et al. 2017). The coincidence of eclogite xenolith ages with eclogitic diamond ages and with craton amalgamation in the Kaapvaal craton (ca. 3.0–2.9 Ga) and with collision at the craton margin in the Slave craton (ca. 1.9 Ga) is most readily explained by interaction of oceanic crust with C-bearing fluids liberated in subduction zones. The median composition of diamondiferous eclogites is most similar to that of barren gabbroic eclogites with respect to strong positive Eu anomalies and LREE depletion (Fig. 39). The median composition of whole rocks reconstructed from eclogitic inclusions does not have as strong a gabbroic character and is more similar to barren high-Ca eclogite. The $MREE_N$–$HREE_N$ patterns of bulk rocks reconstructed from both eclogitic and pyroxenitic inclusions show marked positive slopes that cut across the flatter pattern of high-Ca eclogite (Fig. 39), resulting in high NMORB-normalized Yb/Gd. This slope is unlike that of potential protoliths and can also not be achieved by extraction of partial melt (modelled compositions in Fig. 39b). Similar patterns have been ascribed to disequilibrium processes involving large fluid volumes, such as those encountered in subduction zones (Aulbach et al. 2020b). In particular, serpentinite has been implicated as a major fluid source in subducting slabs (Rüpke et al. 2004), and disequilibrium REE_N patterns with LREE–MREE depletion and HREE enrichment have been observed in orogenic eclogites affected by fluids derived from deserpentization (Beinlich et al. 2010). In this scenario, the low LREE contents of diamondiferous eclogites and inclusions need not be (solely) due to melt extraction, but can result from auto-metasomatism (i.e., fluid indigenous to the slab), whereby the compatible HREE partition into garnet, and the incompatible LREE are removed with the fluid (Aulbach et al. 2020b).

The viability of a scenario of diamond formation via interaction of slab-derived fluids with oceanic crust is supported by thermal modelling, which indicates that carbon and volatiles in subducting slabs can escape shallow decarbonation and dehydration (Shirey et al. 2021). It can be assessed by considering phase relations of oceanic slabs and the stability of diamond

vs. other carbon minerals as a function of pressure, temperature and oxygen fugacity. Oceanic crust dehydrates, accompanied by loss of a small amount of melt, at forearc depth (Spandler and Pirard 2013), where diamond is not stable (Fig. 40a). The small melt fraction explains the persistence of coesite (which participates in the melting reaction) in some mantle eclogites (Schulze et al. 2003). In contrast, pulsed dehydration of deep crust and oceanic mantle, which follows cooler subduction geotherms than slab tops (John et al. 2012; Laurie and Stevens 2012; Spandler and Pirard 2013), could flush oceanic crust within the diamond stability field. If ancient oceanic crust followed a cool subduction path, aided by the proximity of early-cooled cratonic lithosphere (Eaton and Perry 2013), it could enter the diamond stability field at pressures < 4 GPa (Fig. 40a). Whether the high-pressure interaction of eclogite with fluids causes partial melting, as suggested by Stachel and Luth (2015), depends on the refractoriness of the oceanic crust after initial dehydration melting and the redox state of the fluid, which determine the eclogite solidus.

Carbonate, disordered carbonaceous matter, and CaO, are efficiently mobilized in crustal COH fluids (Frezzotti et al. 2011; Menzel et al. 2020; Vitale Brovarone et al. 2020). These materials may be one factor contributing to a preponderance of Ca-rich compositions amongst inclusions and diamondiferous eclogites. As graphite and dolomite are observed in eclogite-hosted veins (Li et al. 2020; Zhu et al. 2020), and microdiamond occurs in fluid inclusions in oceanic subduction zones (Frezzotti et al. 2014), clearly subduction-related fluids can mobilize and supersaturate in carbon or carbonate. Almost all mantle eclogites have fO_2 where simple CHO fluids are near the H_2O-maximum or on the reduced side, increasingly rich in CH_4 (Fig. 40b). However, fluids at high pressures are more complex, containing dissolved solids (Kessel et al. 2005) and possibly a multitude of additional hydrocarbon species (Huang et al. 2017). Since massive fluid flow is invoked in the subduction model, diamondiferous eclogites may represent a fluid-buffered system, in which reducing fluids would impose their fO_2 on eclogite. This lends support to models of diamond formation via oxygen-conserving reactions in CHO fluids (Stachel and Luth 2015), occurring during interaction of deep deserpentinization fluids with overlying oceanic crust. At the relatively low, subsolidus temperatures in a subducting slab, oxygen-conserving diamond formation from fluids may also be achieved due to a drop in pH (Sverjensky and Huang 2015).

The small number of eclogite xenoliths reflecting fO_2 conditions above the H_2O-maximum (Fig. 40b) suggests that the stability of diamond in eclogite to 1 log unit higher fO_2 values compared to peridotite (Luth 1993) plays a subordinate role in explaining the relative overabundance of eclogitic diamonds relative to the small volume of eclogite in the lithospheric mantle. Deserpentization fluids have been inferred to be both oxidising (Debret and Sverjensky 2017) and reducing (Piccoli et al. 2019). Thus, percolation of more oxidized, CO_2-rich fluid into originally reduced eclogite would allow for diamond formation via reduction of CO_2. But the mixing of such fluids with different redox character alone would be a highly effective process. At the water maximum, only about 2% of other species (CO_2, CH_4) are permitted, and if, as an example, fluid 1 contains 4% CO_2 and fluid 2 contains 4% CH_4, they will precipitate 50% of their carbon as diamond upon mixing in an oxygen preserving reaction (Deines 1980; Luth and Stachel 2014). A CH_4-dominated fluid at lower fO_2 interacting with initially more oxidized eclogite at mantle depth might precipitate diamond coupled to reduction of Fe^{3+} in eclogite. Both interpretations are consistent with an evaluation of diamond formation mechanisms in eclogite calling for isochemical diamond precipitation from CH_4-dominated fluids or oxidation of methane on infiltration of eclogite (Smit et al. 2019b). In summary, the preponderance of diamonds forming in eclogitic over peridotitic substrates may reflect that serpentinized harzburgite can carry far more water than the crust, and, as it dewaters at greater depth than the oceanic crust, those fluids leave to form diamond in the overlying crustal portion of the slab now sampled as eclogites.

Evolution of the mantle eclogite reservoir and consequences for diamond preservation

A composite present-day mantle eclogite/pyroxenite reservoir. Inclusions in eclogitic/pyroxenitic diamonds represent the most pristine record of the mantle eclogite reservoir at the time of encapsulation, with the caveat that the diamond-forming process itself may have introduced some modification (e.g., Ca–HREE enrichment during disequilibrium interaction with dehydration fluids in subduction zones). Inclusions do not reflect the kimberlite-related late (pre-eruption) metasomatism typically affecting the mantle lithosphere (and xenoliths during transport), unless their diamond host only formed during this process, as discussed for fibrous diamonds (Boyd et al. 1987; Gurney et al. 2010). Conversely, mantle xenoliths reflect the state of the eclogite/pyroxenite source at the time of typically much later kimberlite magmatism. In order to facilitate a comparison between inclusions, diamondiferous eclogites/pyroxenites and their barren counterparts, we calculate the composition of a composite present-day mantle eclogite/pyroxenite source, taking median compositions for each of the six classes weighted by their proportion. Pyroxenite xenoliths are included in the composite as many have geochemical signatures indicative of interaction of carbonated ultramafic melt with mantle eclogite (Aulbach et al. 2020a), and they therefore constitute an integral part of the evolution of the mantle eclogite source. Median compositions of the composite eclogite, diamondiferous eclogite and bulk rocks reconstructed from eclogitic inclusions are given in Table 4.

Mantle eclogite evolution. The mantle eclogite reservoir is affected by mantle metasomatism, as also recognized in its peridotitic counterpart (e.g., Dawson 1984). It encompasses stealth effects (addition of minerals forming part of the primary mineral assemblage), modal effects (addition of clearly metasomatic minerals such as phlogopite) and cryptic effects (changes to the trace element composition such as LREE-enrichment) (Harte 1983; O'Reilly and Griffin 2013). Metasomatic effects on mantle eclogite include a reduction of the jadeite component in clinopyroxene and grossular component in garnet, a decrease in bulk-rock FeO and Al_2O_3 contents and increase in MgO, Cr_2O_3, ± SiO_2, as well as LREE-enrichment accompanied by higher Sr, Pb, Th, U, ± Zr, ± Nb, and lower Li, Cu, ± Zn (Aulbach et al. 2020a). Strong metasomatism was suggested to be accompanied by a muting of typically crustal signatures, such as non-mantle $\delta^{18}O$ and the size of Eu anomalies. Rare studies on eclogite xenoliths with inclusion-bearing diamonds have shown that the inclusions retain evidence for partial melting, while the host eclogite has been subsequently enriched in MgO, Cr_2O_3 and incompatible elements, and depleted in Na_2O and CaO by a kimberlite-like metasomatic agent (Ireland et al. 1994; Smart et al. 2012). A comparison of composite mantle eclogite with bulk rocks reconstructed from eclogitic inclusions shows that the mantle eclogite reservoir has gained 0.52 wt% CaO (+5% relative), 3.0 wt% MgO (+29%) and 0.06 wt% Cr_2O_3 (+87%), and lost 0.91 wt% Al_2O_3 (–6%), 2.2 wt% FeO (–18%), 0.58 wt% Na_2O (–24%), and 0.04 wt% K_2O (–56%). These changes are ascribed to the effects of mantle metasomatism over time. Lower minimum TiO_2 content (–0.35 wt%, –63%) in the mantle eclogite reservoir is linked to lower average temperatures (1050 °C at 5 GPa vs. 1220 °C for inclusions), and corresponding lower TiO_2 solubility in garnet, clinopyroxene and consequently reconstructed bulk rock, and higher inferred rutile modes (Aulbach 2020). With respect to trace elements, evolution of the mantle eclogite reservoir comprises an increase in Sr (+43%) and LREE abundances (e.g., +140% for La), and a dilution of Y (–22%) and HREE abundances (e.g., –42% for Lu), whereby Sm is least affected (–2%), and Zr and Hf also change little (–2%) (Table 4). These systematics are consistent with interaction with a small-volume melt that is LREE-enriched and HREE-depleted relative to bulk eclogite, such as kimberlite. The similar relative abundance of garnet with positive Eu anomalies (Eu/Eu* > 1.05) amongst inclusions (65%) and barren eclogites and pyroxenites (66%) suggests that the metasomatic evolution does not lead to significant muting of this crustal signature in garnet, whereas it is muted in clinopyroxene. Like TiO_2, lower Nb abundances in the xenoliths (–46%) are not (solely) related to metasomatism, but reflect the increased presence of accessory rutile, which strongly partitions Nb and Ta, at lower average temperatures (Aulbach 2020).

Diamond-destructive effect of mantle metasomatism. Diamondiferous xenoliths are expected to have experienced the metasomatic evolution recorded by the barren eclogite reservoir, with the important exception that they do not capture mantle processes that were diamond-destructive. A direct comparison with inclusions must consider that diamondiferous eclogites have a much stronger gabbroic signature (bulk-rock Eu/Eu*=1.16) than eclogitic inclusions (1.05). This difference may at least in part explain 1.7% higher bulk Al_2O_3, 7% higher CaO contents, nearly 20% lower FeO, and lower REE abundances (Table 4; Figs. 38a,b, 39b) in diamondiferous xenoliths. The increase in bulk MgO and Cr_2O_3 is not as marked as for barren xenoliths (+14% vs. +29% for Mg, and +10% vs. +87% for Cr), and there is no dilution of bulk Na_2O content in contrast to barren xenoliths (Table 4). Similarly, in diamondiferous xenoliths, Sr is less enriched (+12%) than in barren xenoliths (+43%), and the strong positive slope in the REE is retained (i.e., high Yb/Gd_{NMORB}). These systematics are taken to indicate that strong mantle metasomatism, with greater enrichment in MgO, Cr_2O_3 and some incompatible elements leads to diamond destruction, via dissolution into C-undersaturated melts. The intermediate TiO_2 content in diamondiferous eclogite (0.36 wt%; a minimum estimate as rutile is not considered) is consistent with its intermediate median temperature (1130 °C at 5 GPa). In contrast, for unclear reasons, median Nb abundances are highest in diamondiferous eclogites (0.24 ppm).

The higher median temperatures (pressures along conductive geotherms) recorded in diamondiferous compared to barren eclogites suggest that the low-pressure population was thinned out by diamond-destructive mantle metasomatism that particularly affects the mid-lithosphere, close to the lower stability limit of diamond (Aulbach et al. 2020a). The low Na_2O contents in garnet from barren eclogite and pyroxenite xenoliths therefore reflect the superposition of two effects: Firstly, the effect of lower average temperatures, and pressures along conductive geotherms, where diamond is not stable, and secondly, the effect of diamond-destructive mantle metasomatism, during which Na_2O is diluted (Aulbach et al. 2020a). Diamond destruction during pyroxenitization, with a marked lowering of bulk Na_2O and Jd component associated with strong metasomatism by kimberlite-like melt, may also explain why diamondiferous pyroxenite xenoliths make up only 6% of all diamondiferous xenoliths. Indeed, the diamond-destructive effect of kimberlite melt at mantle depth has been experimentally demonstrated (Fedortchouk et al. 2017; 2019). Thus, the enrichment in LREE over MREE (La/Sm) in almost a quarter of bulk eclogites and pyroxenites reconstructed from inclusions is probably not linked to such mantle metasomatism, except in a few localities (e.g., northern Slave craton; Smart et al. 2009), suggesting a delicate balance between diamond saturation vs. resorption in kimberlite-like melts, which is also documented by the inferred precipitation of fibrous diamond from kimberlites (Boyd et al. 1987; Gurney et al. 2010).

Compositional indicators for diamondiferous vs. barren sources. When both clinopyroxene and garnet are available for study, log D_{Ce} for clinopyroxene–garnet at a given garnet Ca# may be useful to predict the presence of diamond in eclogite, whereby the combination of low garnet Ca# and high log D_{Ce} reflects the small-volume melt metasomatism dominating in barren eclogites and pyroxenites (Fig. 37b).

The following relationship can be formulated for the recognition of diamondiferous eclogite substrates:

$$\log D_{Ce} < -5.06 \times Ca\#_{garnet}/100 + 2.54$$

This equation predicts that 50% of diamond-free eclogite and pyroxenite may actually contain diamond. It accurately determines the presence of diamond in 97% of diamondiferous xenoliths and in 94% of the eclogitic inclusions. Based on garnet only, the density of inclusions and diamondiferous xenoliths is smaller at garnet MgO content > 16 wt%, as only 11% of diamond-associated garnets have this feature, compared to 31% of barren xenoliths,

Table 4. Temperatures and salient compositional characteristics of calculated bulk eclogite compositions, reconstructed from inclusions (DI) and diamondiferous and barren xenoliths.

Sample type	TKR885 °C	$TiO_2$1 wt%	Al_2O_3 wt%	Cr_2O_3 wt%	FeO^{total} wt%	MgO wt%	CaO wt%	Na_2O wt%	K_2O wt%	Sr ppm	Y ppm
Eclogitic DI median	1221	0.55	16.3	0.07	11.8	10.1	10.8	2.5	0.07	53	17
Diamondiferous eclogite median	1134	0.36	16.5	0.07	9.8	11.5	11.6	2.5	0.09	59	11
% change vs. DI		–34	2	10	–17	14	7	1	33	12	–36
Composite eclogite median[6]	1046	0.20	15.3	0.12	9.7	13.1	11.4	1.9	0.03	76	13
% change vs. DI		–63	–6	87	–18	29	5	–24	–56	43	–22

Sample type	Zr_{min} ppm[1]	Nb_{min}[1] ppm	La ppm	Sm ppm	Lu ppm	Hf_{min}[1] ppm	Nd/Yb[2] NMORB	Yb/Gd[2] NMORB	Eu/Eu*[3]	ΣHREE[4]
Eclogitic DI median	16	0.08	0.49	1.2	0.41	0.55	0.29	1.69	1.05	8.6
Diamondiferous eclogite median	19	0.24	0.36	0.8	0.26	0.50	0.36	1.51	1.16	5.7
% change vs. DI	17	192	–26	–37	–38	–8	24	–11	10	–34
Composite eclogite median[6]	16	0.06	1.17	1.2	0.24	0.54	0.70	1.25	1.09	6.5
% change vs. DI	–2	–32	139	–2	–42	–2	139	–26	4	–25

Notes:

[1]Concentrations in the bulk rock are minima because rutile, which dominates the Nb-Ta budget and concentrates Zr, was not considered in bulk rock reconstruction. The deficit is higher for lower-temperature samples than for higher-temperature samples.

[2] Normalized to NMORB of Gale et al. (2013).

[3]Defined as chondrite-normalized Eu / $(Sm \times Gd)^{1/2} > 1.05$ (Rudnick and Fountain 1995); chondrite of Sun and McDonough (1989).

[4]Sum of HREE abundances from Tb to Lu.

[5]Temperature using the thermometer of Krogh (1988) and calculated at a pre-set pressure of 5 GPa.

[6]Reconstructed from median compositions of barren eclogite and pyroxenite classes reported in Appendix 2, weighted by their relative abundances as per Table 3.

typically high-Mg eclogites and pyroxenites (Fig. 44a). Finally, not only elevated Na_2O (here > 0.04 wt%) in garnet can be indicative of a diamondiferous eclogite source (Robinson et al. 1984; McCandless and Gurney 1989), but also elevated TiO_2 contents (> 0.1 wt%). Despite unquestionable bulk compositional effects (Grütter and Quadling 1999), both of these minor elements increase in concentration in garnet with increasing temperature (pressure along conductive geotherms), therefore representing graphite- vs. diamond-stable conditions. More than 66% of diamond-free eclogite and pyroxenite xenoliths and 98% of inclusions plus diamondiferous xenoliths are correctly assigned by this combined criterion (Fig. 44b). The number of inclusions and diamondiferous xenoliths increases at values of $Na_2O \geq 0.07$ wt% in garnet (Gurney 1984) and $TiO_2 \geq 0.2$ wt% in garnet, matched by 37% of barren xenoliths, and 89% of inclusions plus diamondiferous xenoliths.

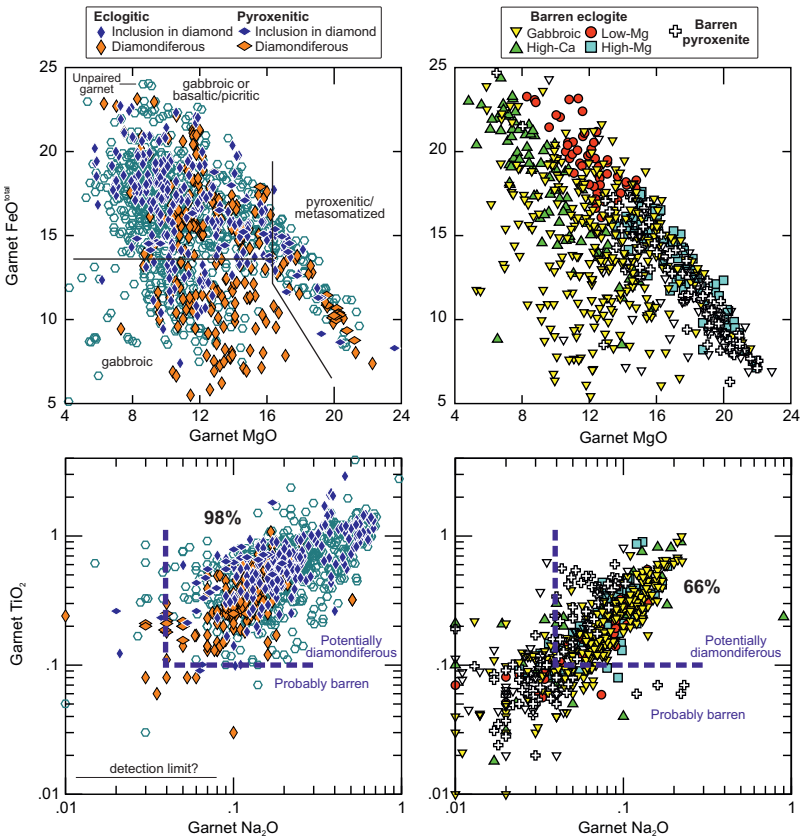

Figure 44. a. FeO (wt%) as a function of MgO (wt%) in garnet. Fields on left roughly separate garnet derived from pyroxenites or metasomatized eclogites from garnet derived from gabbroic eclogite and that derived from either gabbroic or non-gabbroic eclogite. **b.** TiO_2 (wt%) as a function of Na_2O (wt%) in garnet. 98% of inclusions and diamondiferous xenoliths occur at high abundances of these minor elements in a field occupied by 66% of barren xenoliths. Inclusions and diamondiferous xenoliths on **left**, barren xenoliths on **right**.

Key observations and conclusions

Eclogitic inclusions in lithospheric diamond have major and trace element systematics broadly similar to those of mantle eclogites, which originated as variably differentiated oceanic crust. Direct formation of eclogite from magma at mantle pressures is not supported.

Non-mantle $\delta^{18}O$ compositions in some inclusions and xenoliths point to a variably seawater-altered oceanic crust (AOC) protolith, which lost a small volume partial melt during subsequent dehydration melting in the course of subduction, causing some LREE-depletion. Known oxygen fugacity values of mantle eclogite are mostly below the FMQ buffer. Thus, the stability of diamond in eclogite to higher fO_2 than in peridotite plays a subordinate role in explaining the overabundance of eclogitic diamonds relative to the abundance of eclogite in the mantle lithosphere. Less than a quarter of inclusions (23%) and even fewer diamondiferous xenoliths (11%) show the LREE-enrichment that ensues from kimberlite–eclogite or CHO–fluid–eclogite interaction. Thus, eclogitic diamond formation is not dominantly linked to a typical mantle metasomatic signature, which in eclogite appears to be responsible for diamond destruction rather than growth. Therefore, the stability of diamond together with carbonated silicate melt at fO_2 conditions much lower than is the case for pure carbonatite, also is not important in explaining eclogitic diamond formation. Inclusions and diamondiferous xenoliths are depleted in $MREE_N$ relative to $HREE_N$, which is not seen in barren xenoliths and possible crustal protoliths. This depletion is interpreted as a disequilibrium feature caused by interaction with large fluid volumes during subduction-related dehydration of underlying oceanic mantle. If so, oxygen fugacity values indicate that diamond may have formed either by reduction of CO_2 in relatively oxidized fluids, or during mixing of CHO fluids falling on either side of the water maximum, a feature observed during deserpentinization. The subduction environment, with the availability of large redox contrasts and large volumes of mobile fluids, may be favourable for the disproportionately higher amount of eclogitic than peridotitic diamond growth. Whether the carbon involved in this growth is derived directly from the dehydration of serpentinized peridotite or picked up by the dehydration fluid as it migrates through the oceanic crust may be resolved using multiple stable isotopes (e.g., C–N isotopes of diamond and O–S isotopes of inclusions compared to various portions of oceanic lithosphere). While elevated MgO and Cr_2O_3 contents in garnet and high D_{Ce} between clinopyroxene–garnet at a given Ca# are associated with barren eclogites, high combined TiO_2 and Na_2O in garnet are indicative of high-temperature (pressure along conductive geotherm) sources that were little affected by mantle metasomatism and have high diamond potential.

ACKNOWLEDGEMENTS

Kelsey Graversen (University of Alberta) is thanked for her tremendous help in adding full references (DOIs) and in error checking the inclusion-in-diamond database. Amber Yu (University of Alberta) upgraded the xenolith database into a truly useful tool and assembled an additional database for trace elements in xenolith minerals. Fanus Viljoen (University of Johannesburg), Steve Richardson (University of Cape Town), as formal reviewers, and Steve Shirey (Carnegie Institution), as our editor, significantly improved the manuscript. Herman Grütter (SRK Consulting) is thanked for valuable comments on an early version of the manuscript. Saebyul Choe of The American Museum of Natural History kindly shipped crush and a fragment of the primitive J4 xenolith to us. Andrew Locock and Yan Luo (both University of Alberta) are thanked for their help in analysing J4 mineral separates with EPMA and sector field ICPMS, respectively. T.S. acknowledges long-term support for his diamond research program through the Discovery and the Collaborative Research Development (CRD) grant programs of the Natural Sciences and Engineering Research Council of Canada (NSERC), and additional grants from the Canada Research Chairs program and the Canada Foundation for Innovation (CFI). S.A. thanks the German Research Foundation for their continued support, currently via grant DFG AU356/11. Diamond research would not happen without the continued generous support of major (principally De Beers and Rio Tinto) and many junior companies active in diamond exploration and mining. We sincerely thank all the enthusiastic geologists, engineers and diamond sorters in these companies who helped us with samples, gave of their expertise and occasionally organized some financial support.

REFERENCES

Ackerson MR, Watson EB, Tailby ND, Spear FS (2017) Experimental investigation into the substitution mechanisms and solubility of Ti in garnet. Am Mineral 102:158–172

Agashev AM, Pokhilenko LN, Pokhilenko NP, Shchukina EV (2018) Geochemistry of eclogite xenoliths from the Udachnaya kimberlite pipe: Section of ancient oceanic crust sampled. Lithos 314:187–200

Alvaro M, Mazzucchelli ML, Angel RJ, Murri M, Campomenosi N, Scambelluri M, Nestola F, Korsakov A, Tomilenko AA, Marone F, Morana M (2020) Fossil subduction recorded by quartz from the coesite stability field. Geology 48:24–28

Angel RJ, Alvaro M, Nestola F (2022) Crystallographic methods for non-destructive characterization of mineral inclusions in diamonds. Rev Mineral Geochem 88:257–306

Ashchepkov IV, Ntaflos T, Spetsius ZV, Salikhov RF, Downes H (2017a) Interaction between protokimberlite melts and mantle lithosphere: Evidence from mantle xenoliths from the Dalnyaya kimberlite pipe, Yakutia (Russia). Geosci Front 8:693–710

Ashchepkov IV, Ntaflos T, Logvinova AM, Spetsius ZV, Downes H, Vladykin NV (2017b) Monomineral universal clinopyroxene and garnet barometers for peridotitic, eclogitic and basaltic systems. Geosci Front 8:775–795

Aulbach S (2012) Craton nucleation and formation of thick lithospheric roots. Lithos 149:16–30

Aulbach S (2020) Temperature-dependent rutile solubility in garnet and clinopyroxene from mantle eclogite: Implications for continental crust formation and V-based oxybarometry. J Petrol 61:egaa065

Aulbach S, Jacob DE (2016) Major- and trace-elements in cratonic mantle eclogites and pyroxenites reveal heterogeneous sources and metamorphic processing of low-pressure protoliths. Lithos 262:586–605

Aulbach S, Arndt NT (2019a) Eclogites as palaeodynamic archives: Evidence for warm (not hot) and depleted (but heterogeneous) Archaean ambient mantle. Earth Planet Sci Lett 505:162–172

Aulbach S, Arndt NT (2019b) Origin of high-Mg bimineralic eclogite xenoliths in kimberlite—reply to comment from Claude Herzberg. Earth Planet Sci Lett 510:234–237

Aulbach S, Stachel T, Viljoen KS, Brey GP, Harris JW (2002) Eclogitic and websteritic diamond sources beneath the Limpopo Belt - is slab-melting the link? Contrib Mineral Petrol 143:56–70

Aulbach S, Pearson NJ, O'Reilly SY, Doyle BJ (2007) Origins of xenolithic eclogites and pyroxenites from the central Slave craton, Canada. J Petrol 48:1843–1873

Aulbach S, Shirey SB, Stachel T, Creighton S, Muehlenbachs K, Harris JW (2009) Diamond formation episodes at the southern margin of the Kaapvaal Craton: Re-Os systematics of sulfide inclusions from the Jagersfontein Mine. Contrib Mineral Petrol 157:525–540

Aulbach S, Jacob DE, Cartigny P, Stern RA, Simonetti SS, Wörner G, Viljoen KS (2017) Eclogite xenoliths from Orapa: Ocean crust recycling, mantle metasomatism and carbon cycling at the western Zimbabwe craton margin. Geochim Cosmochim Acta 213:574–592

Aulbach S, Creaser RA, Stachel T, Heaman LM, Chinn IL, Kong J (2018) Diamond ages from Victor (Superior Craton): Intra-mantle cycling of volatiles (C, N, S) during supercontinent reorganisation. Earth Planet Sci Lett 490:77–87

Aulbach S, Heaman LM, Jacob DE, Viljoen KS (2019a) Ages and sources of mantle eclogites: ID-TIMS and in situ MC-ICPMS Pb-Sr isotope systematics of clinopyroxene. Chem Geol 503:15–28

Aulbach S, Woodland AB, Stern RA, Vasilyev P, Heaman LM, Viljoen KS (2019b) Evidence for a dominantly reducing Archaean ambient mantle from two redox proxies, and low oxygen fugacity of deeply subducted oceanic crust. Sci Rep 9:20190

Aulbach S, Viljoen KS, Gerdes A (2020a) Diamondiferous and barren eclogites and pyroxenites from the western Kaapvaal craton record subduction processes and mantle metasomatism, respectively. Lithos 368:105588

Aulbach S, Massuyeau M, Garber JM, Gerdes A, Heaman LM, Viljoen KS (2020b) Ultramafic carbonated melt- and auto-metasomatism in mantle eclogites: Compositional effects and geophysical consequences. Geochem Geophys Geosyst 21:e2019GC008774

Ayers JC, Dittmer SK, Layne GD (1997) Partitioning of elements between peridotite and H_2O at 2.0–3.0 GPa and 900–1100°C, and application to models of subduction zone processes. Earth Planet Sci Lett 150:381–398

Bailey DK (1982) Mantle metasomatism—continuing chemical change within the Earth. Nature 296:525–530

Banas A, Stachel T, Muehlenbachs K, McCandless TE (2007) Diamonds from the Buffalo Head Hills, Alberta: Formation in a non-conventional setting. Lithos 93:199–213

Barth MG, Foley SF, Horn I (2002) Partial melting in Archean subduction zones: constraints from experimentally determined trace element partition coefficients between eclogitic minerals and tonalitic melts under upper mantle conditions. Precambrian Res 113:323–340

Bauer M (1904) Precious Stones. Translated from German with Additions by L. J. Spencer. Charles Griffin & Company, London

Beard BL, Fraracci KN, Taylor LA, Snyder GA, Clayton RA, Mayeda TK, Sobolev NV (1996) Petrography and geochemistry of eclogites from the Mir kimberlite, Yakutia, Russia. Contrib Mineral Petrol 125:293–310

Becker M, Le Roex AP (2006) Geochemistry of South African on- and off-craton, Group I and Group II kimberlites: Petrogenesis and source region evolution. J Petrol 47:673–703

Beinlich A, Klemd R, John T, Gao J (2010) Trace-element mobilization during Ca-metasomatism along a major fluid conduit: Eclogitization of blueschist as a consequence of fluid–rock interaction. Geochim Cosmochim Acta 74:1892–1922
Benoit M, Polvé M, Ceuleneer G (1996) Trace element and isotopic characterization of mafic cumulates in a fossil mantle diapir (Oman ophiolite). Chem Geol 134:199–214
Bernstein S, Kelemen PB, Hanghoj K (2007) Consistent olivine Mg# in cratonic mantle reflects Archean mantle melting to the exhaustion of orthopyroxene. Geology 35:459–462
Beyer C, Frost DJ, Miyajima N (2015) Experimental calibration of a garnet–clinopyroxene geobarometer for mantle eclogites. Contrib Mineral Petrol 169:18
Bishop FC, Smith JV, Dawson JB (1976) Na, P, Ti and coordination of Si in garnet from peridotite and eclogite xenoliths. Nature 260:696–697
Bodinier JL, Vasseur G, Vernières J, Dupuy C, Fabriès J (1990) Mechanisms of mantle metasomatism: Geochemical evidence from the Lherz orogenic peridotite. J Petrol 31:597–628
Boutan ME (1886) Le diamant. *In*: Frémy's Encyclopédie Chimique. Paris
Boyd FR (1989) Compositional distinction between oceanic and cratonic lithosphere. Earth Planet Sci Lett 96:15–26
Boyd FR, Gurney JJ (1986) Diamonds and the African lithosphere. Science 232:472–477
Boyd SR, Mattey DP, Pillinger CT, Milledge HJ, Mendelssohn M, Seal M (1987) Multiple growth events during diamond genesis: an integrated study of carbon and nitrogen isotopes and nitrogen aggregation state in coated stones. Earth Planet Sci Lett 86:341–353
Boyd FR, Pokhilenko NP, Pearson DG, Mertzman SA, Sobolev NV, Finger LW (1997) Composition of the Siberian cratonic mantle: evidence from Udachnaya peridotite xenoliths. Contrib Mineral Petrol 128:228–246
Branchetti M, Zepper JCO, Peters STJ, Koornneef JM, Davies GR (2021) Multi-stage garnet formation and destruction in Kimberley harzburgitic xenoliths, South Africa. Lithos 390–391:106119
Brewster D (1861) On the pressure cavities in topaz, beryl and diamond and their bearing on geological theories. Trans R Soc Edinburgh 23:39–44
Brey GP, Köhler T (1990) Geothermobarometry in four-phase lherzolites II. New thermobarometers, and practical assessment of existing thermobarometers. J Petrol 31:1353–1378
Brey GP, Shu Q (2018) The birth, growth and ageing of the Kaapvaal subcratonic mantle. Mineral Petrol 112:23–41
Brey G, Brice WR, Ellis DJ, Green DH, Harris KL, Ryabchikov ID (1983) Pyroxene-carbonate reactions in the upper mantle. Earth Planet Sci Lett 62:63–74
Brown M, Johnson T (2018) Secular change in metamorphism and the onset of global plate tectonics. Am Mineral 103:181–196
Bulanova GP (1995) The formation of diamond. J Geochem Explor 53:1–23
Burgess R, Turner G, Laurenzi M, Harris JW (1989) $^{40}Ar/^{39}Ar$ laser probe dating of individual clinopyroxene inclusions in Premier eclogitic diamonds. Earth Planet Sci Lett 94:22–28
Burgess SR, Harte B (1999) Tracing lithospheric evolution trough the analysis of heterogeneous G9/G10 garnets in peridotite xenoliths, I: Major element chemistry. *In*: The JB Dawson Volume, Proceedings of the VIIth International Kimberlite Conference. Vol 45. Gurney JJ, Gurney JL, Pascoe MD, Richardson SH (eds) Red Roof Design, Cape Town, p 66–80
Burness S, Smart KA, Tappe S, Stevens G, Woodland AB, Cano E (2020) Sulphur-rich mantle metasomatism of Kaapvaal craton eclogites and its role in redox-controlled platinum group element mobility. Chem Geol 542:119476
Bussweiler Y, Pearson DG, Stachel T, Kjarsgaard BA (2018) Cr-rich megacrysts of clinopyroxene and garnet from Lac de Gras kimberlites, Slave Craton, Canada—implications for the origin of clinopyroxene and garnet in cratonic lherzolites. Mineral Petrol 112:583–596
Bussweiler Y, Giuliani A, Greig A, Kjarsgaard BA, Petts D, Jackson SE, Barrett N, Luo Y, Pearson DG (2019) Trace element analysis of high-Mg olivine by LA-ICP-MS – Characterization of natural olivine standards for matrix-matched calibration and application to mantle peridotites. Chem Geol 524:136–157
Cameron M, Papike JJ (1981) Structural and chemical variations in pyroxenes. Am Mineral 66:1–50
Canil D (2004) Mildly incompatible elements in peridotites and the origins of mantle lithosphere. Lithos 77:375–393
Cardoso P (1980) A study of mantle inclusions in the Koffiefontein Kimberlite pipe, South Africa. MSc thesis University of Cape Town
Carswell DA, Gibb FGF (1987) Evaluation of mineral thermometers and barometers applicable to garnet herzolite assemblages. Contrib Mineral Petrol 95:499–511
Chakhmouradian AR (2006) High-field-strength elements in carbonatitic rocks: Geochemistry, crystal chemistry and significance for constraining the sources of carbonatites. Chem Geol 235:138–160
Chakhmouradian AR, Boehm CO, Demeny A, Reguir EP, Hegner E, Creaser RA, Halden NM, Yang P (2009) "Kimberlite" from Wekusko Lake, Manitoba: Actually a diamond-indicator-bearing dolomite carbonatite. Lithos 112:347–357
Chaussidon M, Albarede F, Sheppard SMF (1987) Sulfur isotope heterogeneity in the mantle from ion microprobe measurements of sulfide inclusions in diamonds. Nature 330:242–244
Clark JR, Papike JJ (1968) Crystal-chemical characterization of omphacites. Am Mineral 53:840–868

Coleman RG, Lee DE, Beatty LB, Brannock WW (1965) Eclogites and eclogites: their differences and similarities. Geol Soc Amer Bull 76:483–508
Creighton S, Stachel T, Eichenberg D, Luth RW (2010) Oxidation state of the lithospheric mantle beneath Diavik diamond mine, central Slave craton, NWT, Canada. Contrib Mineral Petrol 159:645–657
Czas J, Pearson DG, Stachel T, Kjarsgaard BA, Read GH (2020) A Palaeoproterozoic diamond-bearing lithospheric mantle root beneath the Archean Sask Craton, Canada. Lithos 356–357:105301
Dalton JA, Presnall DC (1998) Carbonatitic melts along the solidus of model lherzolite in the system CaO–MgO–Al_2O_3–SiO_2–CO_2 from 3 to 7 GPa. Contrib Mineral Petrol 131:123–135
Dasgupta R, Hirschmann MM (2010) The deep carbon cycle and melting in Earth's interior. Earth Planet Sci Lett 298:1–13
Dasgupta R, Hirschmann MM, Withers AC (2004) Deep global cycling of carbon constrained by the solidus of anhydrous, carbonated eclogite under upper mantle conditions. Earth Planet Sci Lett 227:73–85
Dasgupta R, Hirschmann MM, McDonough WF, Spiegelman M, Withers AC (2009) Trace element partitioning between garnet lherzolite and carbonatite at 6.6 and 8.6 GPa with applications to the geochemistry of the mantle and of mantle-derived melts. Chem Geol 262:57–77
Davies GR, van den Heuvel Q, Matveev S, Drury MR, Chinn IL, Gress MU (2018) A combined cathodoluminescence and electron backscatter diffraction examination of the growth relationships between Jwaneng diamonds and their eclogitic inclusions. Mineral Petrol 112:231–242
Davis GL (1977) The ages and uranium contents of zircons from kimberlites and associated rocks. Carnegie Inst Wash Yearb 76:631–654
Dawson JB (1984) Contrasting types of upper mantle metasomatism. *In*: Kimberlites II. The Mantle and Crust–Mantle Relationships. Kornprobst J (ed) Elsevier, Amsterdam, p 289–294
Day HW (2012) A revised diamond-graphite transition curve. Am Mineral 97:52–62
de Beer ES (ed) (1955) The diary of John Evelyn, Vol. 2: Kalendarium, 1620–1649. Oxford Universirty Press, Oxford
De Hoog JCM, Gall L, Cornell DH (2010) Trace-element geochemistry of mantle olivine and application to mantle petrogenesis and geothermobarometry. Chem Geol 270:196–215
De Hoog JCM, Stachel T, Harris JW (2019) Trace-element geochemistry of diamond-hosted olivine inclusions from the Akwatia Mine, West African Craton: implications for diamond paragenesis and geothermobarometry. Contrib Mineral Petrol 174:100
Debret B, Sverjensky DA (2017) Highly oxidising fluids generated during serpentinite breakdown in subduction zones. Sci Rep 7:10351
Deines P (1980) The carbon isotopic composition of diamonds: relationship to diamond shape, color, occurrence and vapor composition. Geochim Cosmochim Acta 44:943–961
Deines P, Harris JW, Gurney JJ (1993) Depth-related carbon isotope and nitrogen concentration variability in the mantle below the Orapa kimberlite, Botswana, Africa. Geochim Cosmochim Acta 57:2781–2796
Doroshev AM, Brey GP, Girnis AV, Turkin AI, Kogarko LN (1997) Pyrope–knorringite garnets in the Earth's mantle: Experiments in the MgO–Al_2O_3–SiO_2–Cr_2O_3 system. Russ Geol Geophys 38:559–586
Droop GTR (1987) A general equation for estimating Fe^{3+} concentrations in ferromagnesian silicates and oxides from microprobe analyses, using stoichiometric criteria. Geol Mag 51:431–435
Eaton DW, Perry HKC (2013) Ephemeral isopycnicity of cratonic mantle keels. Nat Geosci 6:967–970
Eaton DW, Darbyshire F, Evans RL, Grütter H, Jones AG, Yuan X (2009) The elusive lithosphere–asthenosphere boundary (LAB) beneath cratons. Lithos 109:1–22
Eggler DH, Baker DR (1982) Reduced volatiles in the system C–O–H: Implications for mantle melting, fluid formation and diamond genesis. *In*: High pressure research in geophysics. Akimoto S, Manghnani MH, (eds). Center for Acad Publ, Tokyo, p 237–250
Eldridge CS, Compston W, Williams IS, Harris JW, Bristow JW (1991) Isotope evidence for the involvement of recycled sediments in diamond formation. Nature 353:649–653
Eppler WF (1961) Inclusions in diamond. J Gemmol 8:1–13
Farquhar J, Wing BA, McKeegan KD, Harris JW, Cartigny P, Thiemens MH (2002) Mass-independent sulfur of inclusions in diamond and sulfur recycling on early Earth. Science 298:2369–2372
Ferrando S, Castelli D, Frezzotti ML (2017) Fluid properties control degassing or storage of abiogenic CH_4 during slab exhumation: the fluid inclusion record from the Western Alps. American Geophysical Union, Fall Meeting 2017, abstract #V41A-04
Fedortchouk Y, Chinn IL, Kopylova MG (2017) Three styles of diamond resorption in a single kimberlite: Effects of volcanic degassing and assimilation. Geology 45:871–874
Fedortchouk Y, Liebske C, McCammon C (2019) Diamond destruction and growth during mantle metasomatism: An experimental study of diamond resorption features. Earth Planet Sci Lett 506:493–506
Frezzotti ML, Selverstone J, Sharp ZD, Compagnoni R (2011) Carbonate dissolution during subduction revealed by diamond-bearing rocks from the Alps. Nat Geosci 4:703–706
Frezzotti M-L, Huizenga J-M, Compagnoni R, Selverstone J (2014) Diamond formation by carbon saturation in C-O-H fluids during cold subduction of oceanic lithosphere. Geochim Cosmochim Acta 143:68–86
Fipke CE, Gurney JJ, Moore RO (1995) Diamond exploration techniques emphasising indicator mineral geochemistry and Canadian examples. Geol Surv Canada Bull 423:24–36

Fitzpayne A, Giuliani A, Maas R, Hergt J, Janney P, Phillips D (2019) Progressive metasomatism of the mantle by kimberlite melts: Sr–Nd–Hf–Pb isotope compositions of MARID and PIC minerals. Earth Planet Sci Lett 509:15–26

Frey FA, Green DH (1974) The mineralogy, geochemistry and origin of lherzolite inclusions in Victorian basanites. Geochim Cosmochim Acta 38:1023–1059

Frost DJ, McCammon CA (2008) The redox state of Earth's mantle. Annu Rev Earth Planet Sci 36:389–420

Futergendler SI (1960) X-ray study of solid inclusions in Ural and Yakutia diamonds. Mat Vses Nauchi Issled Geol Inst 40:83–87 (in Russian)

Futergendler SI, Frank-Kamenetsky VA (1961) Oriented inclusions of olivine, garnet and chrome-spinel in diamonds. Zapisky Vses Mineral Obsh 90:230–236 (in Russian)

Gaetani GA, Kent AJR, Grove TL, Hutcheon ID, Stolper EM (2003) Mineral/melt partitioning of trace elements during hydrous peridotite partial melting. Contrib Mineral Petrol 145:391–405

Gale A, Dalton CA, Langmuir CH, Su Y, Schilling J-G (2013) The mean composition of ocean ridge basalts. Geochem Geophys Geosyst 14:489–518

Garber JM, Maurya S, Hernandez JA, Duncan MS, Zeng L, Zhang HL, Faul U, McCammon C, Montagner JP, Moresi L, Romanowicz BA (2018) Multidisciplinary constraints on the abundance of diamond and eclogite in the cratonic lithosphere. Geochem Geophys Geosyst 19:2062–2086

Giardini AA, Melton CE (1975) Nature of cloud-like inclusions in two Arkansas diamonds. Am Mineral 60:931–933

Girnis AV, Brey GP (1999) Garnet–spinel–olivine–orthopyroxene equilibria in the FeO–MgO–Al_2O_3–SiO_2–Cr_2O_3 systems; II, Thermodynamic analysis. Eur J Mineral 11:619–636

Girnis AV, Stachel T, Brey GP, Harris JW, Phillips D (1999) Internally consistent geothermobarometers for garnet harzburgites: model refinement and application. *In*: The J.B. Dawson Volume, Proceedings of the VIIth International Kimberlite Conference. Gurney JJ, Gurney JL, Pascoe MD, Richardson SH (eds) Red Roof Design, Cape Town, 247–254

Girnis AV, Bulatov VK, Brey GP, Gerdes A, Höfer HE (2013) Trace element partitioning between mantle minerals and silico-carbonate melts at 6–12 GPa and applications to mantle metasomatism and kimberlite genesis. Lithos 160–161:183–200

Glinnemann J, Kusaka K, Harris JW (2003) Oriented graphite single-crystal inclusions in diamond. Z Kristallogr 218:733–739

Göppert HR (1864) Ueber Einschlüsse im Diamant. Die Erben Loosjes, Haarlem

Green TH (1994) Experimental studies of trace-element partitioning applicable to igneous petrogenesis—Sedona 16 years later. Chem Geol 117:1–36

Green DH, Wallace ME (1988) Mantle metasomatism by ephemeral carbonatite melts. Nature 336:459–462

Green TH, Blundy JD, Adam J, Yaxley GM (2000) SIMS determination of trace element partition coefficients between garnet, clinopyroxene and hydrous basaltic liquids at 2–7.5 GPa and 1080–1200°C. Lithos 53:165–187

Grégoire M, Bell DR, Le Roex AP (2003) Garnet lherzolites from the Kaapvaal Craton (South Africa): Trace element evidence for a metasomatic history. J Petrol 44:629–657

Gress MU, Pearson DG, Chinn I, Thomassot E, Davies GR (2021) Mesozoic to Paleoproterozoic diamond growth beneath Botswana recorded by Re Os ages from individual eclogitic and websteritic inclusions. Lithos 388–389:106058

Griffin WL, Ryan CG (1995) Trace-elements in indicator minerals - Area selection and target evaluation in diamond exploration. J Geochem Explor 53:311–337

Griffin WL, Jaques AL, Sie SH, Ryan CG, Cousens DR, Suter GF (1988) Conditions of diamond growth—A proton microprobe study of inclusions in west Australian diamonds. Contrib Mineral Petrol 99:143–158

Griffin WL, Cousens DR, Ryan CG, Sie SH, Suter GF (1989a) Ni in chrome pyrope garnets: a new geothermometer. Contrib Mineral Petrol 103:199–202

Griffin WL, Smith D, Boyd FR, Cousens DR, Ryan CG, Sie SH, Suter GF (1989b) Trace-element zoning in garnets from sheared mantle xenoliths. Geochim Cosmochim Acta 53:561–567

Griffin WL, O'Reilly SY, Ryan CG (1999a) The composition and origin of subcontinental lithospheric mantle. *In*: Mantle Petrology: Field Observations and High Pressure Experimentation: A tribute to Francis R (Joe) Boyd. Vol Special Publication No. 6. Fei Y, Bertka CM, Mysen BO, (eds). The Geochemical Society, Houston, p 13–45

Griffin WL, Doyle BJ, Ryan CG, Pearson NJ, O'Reilly SY, Davies R, Kivi K, VanAchterbergh E, Natapov LM (1999b) Layered mantle lithosphere in the Lac de Gras area, Slave Craton: Composition, structure and origin. J Petrol 40:705–727

Grütter HS (2006) Cr-pyrope and chromite inside and outside diamond: - a tribute to the work of Jeff Harris. Abstract, Goldschmdt Conference 2006, Geochim Cosmochim Acta 70:A219-A219

Grütter HS (2009) Pyroxene xenocryst geotherms: Techniques and application. Lithos 112:1167–1178

Grütter HS, Quadling KE (1999) Can sodium in garnet be used to monitor eclogitic diamond potential? *In*: The JB Dawson Volume, Proceedings of the VIIth International Kimberlite Conference. Gurney JJ, Gurney JL, Pascoe MD, Richardson SH, (eds). Reed Roof Design, Cape Town, p 314–319

Grütter HS, Menzies AH (2017) Discrete Ti-Al±Ca metasomatism at ~53 kbar in chromite–garnet peridotites from Newlands kimberlite, South Africa. 11th International Kimberlite Conference: Extended Abstracts

Grütter HS, Apter DB, Kong J (1999) Crust-mantle coupling: evidence from mantle-derived xenocrystic garnets. *In*: The JB Dawson Volume, Proceedings of the VIIth International Kimberlite Conference. Gurney JJ, Gurney JL, Pascoe MD, Richardson SH (eds) Red Roof Design, Cape Town, p 307–313

Grütter HS, Gurney JJ, Menzies AH, Winter F (2004) An updated classification scheme for mantle-derived garnet, for use by diamond explorers. Lithos 77:841–857

Grütter HS, Latti D, Menzies A (2006) Cr-saturation arrays in concentrate garnet compositions from kimberlite and their use in mantle barometry. J Petrol 47:801–820

Gübelin E (1952) Inclusions in diamonds. J Gemmol 3:174–187

Gurney JJ (1984) A correlation between garnets and diamonds in kimberlites. *In*: Kimberlite Occurrence and Origin: A Basis for Conceptual Models in Exploration. Vol 8. Glover JE, Harris PG, (eds). Publs Geol. Dept. & Univ. Extension, Univ. West. Aust., Perth, p 143–166

Gurney JJ (1989) Diamonds. *In*: Kimberlites and Related Rocks GSA Spec Publ 14. Vol Vol 2. Ross J, *et al.* (eds). Blackwell, Carlton, p 935–965

Gurney JJ, Harte B (1980) Chemical variations in upper mantle nodules from Southern African kimberlites. Philos Trans R Soc London Ser A 297:273–293

Gurney JJ, Switzer GS (1973) The discovery of garnets closely related to diamonds in the Finsch pipe, South Africa. Contrib Mineral Petrol 39:103–116

Gurney JJ, Harris JW, Rickard RS (1984) Minerals associated with diamonds from the Roberts Victor Mine. *In*: Kimberlites II: the mantle and crust-mantle relationships. Kornprobst J (ed) Elsevier, Amsterdam, p 25–32

Gurney JJ, Helmstaedt HH, Richardson SH, Shirey SB (2010) Diamonds through time. Econ Geol 105:689–712

Haggerty SE (1986) Diamond genesis in a multiply-constrained model. Nature 320:34–37

Hardman MF, Pearson DG, Stachel T, Sweeney RJ (2018) Statistical approaches to the discrimination of crust- and mantle-derived low-Cr garnet—Major-element-based methods and their application in diamond exploration. J Geochem Explor 186:24–35

Harris JW (1968a) The recognition of diamond inclusions. Part 1: Syngenetic mineral inclusions. Ind Diam Rev 28:402–410

Harris JW (1968b) The recognition of diamond inclusions. Part 2: Epigenetic mineral inclusions. Ind Diam Rev 28:558–561

Harris JW, Gurney JJ (1979) Inclusions in diamond. *In*: The Properties of Diamond. Field JE (ed) Academic Press, London, p 555–591

Harris JW, Smit KV, Fedortchouk Y, Moore M (2022) Morphology of monocrystalline diamond and its inclusions. Rev Mineral Geochem 88:119–166

Harte B (1983) Mantle peridotites and processes - the kimberlite sample. *In*: Continental basalts and mantle xenoliths. Hawkesworth CJ, Norry MJ (eds) Shiva Publishing Ltd, Nantwich, p 46–91

Harte B (1987) Metasomatic events recorded in mantle xenoliths: an overview. *In*: Mantle Xenoliths. Nixon PH (ed) John Wiley & Sons Ltd., Chichester, p 625–640

Harte B, Kirkley MB (1997) Partitioning of trace elements between clinopyroxene and garnet: Data from mantle eclogites. Chem Geol 136:1–24

Harte B, Hunter RH, Kinny PD (1993) Melt geometry, movement and crystallization, in relation to mantle dykes, veins and metasomatism. Philos Trans R Soc London Ser A342:1–21

Hasterok D, Chapman DS (2011) Heat production and geotherms for the continental lithosphere. Earth Planet Sci Lett 307:59–70

Helmstaedt HH, Schulze DJ (1989) Southern African kimberlites and their mantle sample: implications for Archean tectonics and lithosphere evolution. *In*: Kimberlites and Related Rocks GSA Spec Publ 14. Vol. 1. Ross J, *et al.* (eds). Blackwell, Carlton, p 358–368

Helmstaedt HH, Gurney JJ, Richardson SH (2010) Ages of cratonic diamond and lithosphere evolution: constraints on Precambrian tectonics and diamond exploration. Can Mineral 48:1385–1408

Hervig RL, Smith JV, Dawson JB (1986) Lherzolite xenoliths in kimberlites and basalts: petrogenetic and crystallochemical significance of some minor and trace elements in olivine, pyroxenes, garnet and spinel. Trans R Soc Edinburgh: Earth Sci 77:181–201

Herzberg C (2004) Geodynamic information in peridotite petrology. J Petrol 45:2507–2530

Herzberg C, Asimow PD (2008) Petrology of some oceanic island basalts: PRIMELT2.XLS software for primary magma calculation. Geochem Geophys Geosyst 9:Q09001

Herzberg C, Rudnick R (2012) Formation of cratonic lithosphere: An integrated thermal and petrological model. Lithos 149:4–15

Hills DV, Haggerty SE (1989) Petrochemistry of eclogites from the Koidu kimberlite complex, Sierra-Leone. Contrib Mineral Petrol 103:397–422

Howell D, Stachel T, Stern RA, Pearson DG, Nestola F, Hardman MF, Harris JW, Jaques AL, Shirey SB, Cartigny P, Smit KV (2020) Deep carbon through time: Earth's diamond record and its implications for carbon cycling and fluid speciation in the mantle. Geochim Cosmochim Acta 275:99–122

Huang F, Daniel I, Cardon H, Montagnac G, Sverjensky DA (2017) Immiscible hydrocarbon fluids in the deep carbon cycle. Nat Commun 8:15798

Huang Y, Nakatani T, Nakamura M, McCammon C (2019) Saline aqueous fluid circulation in mantle wedge inferred from olivine wetting properties. Nat Commun 10:5557

Hunt L, Stachel T, Morton R, Grütter H, Creaser RA (2009) The Carolina kimberlite, Brazil—Insights into an unconventional diamond deposit. Lithos 112:843–851
Ionov DA, Blichert-Toft J, Weis D (2005) Hf isotope compositions and HREE variations in off-craton garnet and spinel peridotite xenoliths from central Asia. Geochim Cosmochim Acta 69:2399–2418
Ireland TR, Rudnick RL, Spetsius Z (1994) Trace-elements in diamond inclusions from eclogites reveal link to Archean granites. Earth Planet Sci Lett 128:199–213
Izraeli ES, Harris JW, Navon O (2001) Brine inclusions in diamonds: a new upper mantle fluid. Earth Planet Sci Lett 187:323–332
Izraeli ES, Harris JW, Navon O (2004) Fluid and mineral inclusions in cloudy diamonds from Koffiefontein, South Africa. Geochim Cosmochim Acta 68:2561–2575
Jablon BM, Navon O (2016) Most diamonds were created equal. Earth Planet Sci Lett 443:41–47
Jacob DE (2004) Nature and origin of eclogite xenoliths from kimberlites. Lithos 77:295–316
Jaques AL, Green DH (1980) Anhydrous melting of peridotite at 0–15 kb pressure and the genesis of tholeiitic basalts. Contrib Mineral Petrol 73:287–310
Jaques AL, Hall AE, Sheraton JW, Smith CB, Sun S-S, Drew RM, Foudoulis C, Ellingsen K (1989) Composition of crystalline inclusions and C-isotopic composition of Argyle and Ellendale diamonds. *In*: Kimberlites and related rocks. GSA Spec Publ 14. Vol 2. Ross J, *et al.* (eds). Blackwell, Carlton, p 966–989
Jenner FE, O'Neill HS (2012) Analysis of 60 elements in 616 ocean floor basaltic glasses. Geochem Geophys Geosyst 13:Q02005
John T, Gussone N, Podladchikov YY, Bebout GE, Dohmen R, Halama R, Klemd R, Magna T, Seitz HM (2012) Volcanic arcs fed by rapid pulsed fluid flow through subducting slabs. Nat Geosci 5:489–492
Johnson KTM (1998) Experimental determination of partition coefficients for rare earth and high-field-strength elements between clinopyroxene, garnet, and basaltic melt at high pressures. Contrib Mineral Petrol 133:60–68
Jordan TH (1978) Composition and development of the continental tectosphere. Nature 274:544–548
Kargin AV, Sazonova LV, Nosova AA, Tretyachenko VV (2016) Composition of garnet and clinopyroxene in peridotite xenoliths from the Grib kimberlite pipe, Arkhangelsk diamond province, Russia: Evidence for mantle metasomatism associated with kimberlite melts. Lithos 262:442–455
Kargin AV, Sazonova LV, Nosova AA, Pervov VA, Minevrina EV, Khvostikov VA, Burmii ZP (2017) Sheared peridotite xenolith from the V. Grib kimberlite pipe, Arkhangelsk Diamond Province, Russia: Texture, composition, and origin. Geosci Front 8:653–669
Kelemen PB, Dick HJB, Quick JE (1992) Formation of harzburgite by pervasive melt/rock reaction in the upper mantle. Nature 358:635–641
Kelemen PB, Hart SR, Bernstein S (1998) Silica enrichment in the continental upper mantle via melt/rock reaction. Earth Planet Sci Lett 164:387–406
Kessel R, Ulmer P, Pettke T, Schmidt MW, Thompson AB (2005) The water-basalt system at 4 to 6 GPa: Phase relations and second critical endpoint in a K-free eclogite at 700 to 1400 °C. Earth Planet Sci Lett 237:873–892
Kessel R, Pettke T, Fumagalli P (2015) Melting of metasomatized peridotite at 4–6 GPa and up to 1200 °C: an experimental approach. Contrib Mineral Petrol 169:1–19
Kesson SE, Ringwood AE (1989) Slab-mantle interactions. 2. The formation of diamonds. Chem Geol 78:97–118
Klein-BenDavid O, Izraeli ES, Hauri E, Navon O (2007) Fluid inclusions in diamonds from the Diavik mine, Canada and the evolution of diamond-forming fluids. Geochim Cosmochim Acta 71:723–744
Klein-BenDavid O, Pettke T, Kessel R (2011) Chromium mobility in hydrous fluids at upper mantle conditions. Lithos 125:122–130
Klemme S (2004) The influence of Cr on the garnet–spinel transition in the Earth's mantle: experiments in the system $MgO–Cr_2O_3–SiO_2$ and thermodynamic modelling. Lithos 77:639–646
Koornneef JM, Davies GR, Döpp SP, Vukmanovic Z, Nikogosian IK, Mason PRD (2009) Nature and timing of multiple metasomatic events in the sub-cratonic lithosphere beneath Labait, Tanzania. Lithos 112:896–912
Koornneef JM, Gress MU, Chinn IL, Jelsma HA, Harris JW, Davies GR (2017) Archaean and Proterozoic diamond growth from contrasting styles of large-scale magmatism. Nat Commun 8:648
Korenaga J (2008) Urey ratio and the structure and evolution of Earth's mantle. Rev Geophys 46:2007RG000241
Kostrovitsky SI, Solov'eva LV, Yakovlev DA, Suvorova LF, Sandimirova GP, Travin AV, Yudin DS (2013) Kimberlites and megacrystic suite: Isotope-geochemical studies. Petrology 21:127–144
Kramers JD (1979) Lead, uranium, strontium, potassium and rubidium in inclusion-bearing diamonds and mantle-derived xenoliths from southern Africa. Earth Planet Sci Lett 42:58–70
Krogh EJ (1988) The garnet–clinopyroxene Fe–Mg geothermometer—A reinterpretation of existing experimental data. Contrib Mineral Petrol 99:44–48
Kushiro I (1994) Recent experimental studies on partial melting of mantle peridotites at high pressures using diamond aggregates. J Geol Soc Jpn 100:103–110
Labrosse S, Jaupart C (2007) Thermal evolution of the Earth: Secular changes and fluctuations of plate characteristics. Earth Planet Sci Lett 260:465–481
Laurie A, Stevens G (2012) Water-present eclogite melting to produce Earth's early felsic crust. Chem Geol 314:83–95
Laurie A, Stevens G, van Hunen J (2013) The end of continental growth by TTG magmatism. Terra Nova 25:130–136

Lewis HC, Bonney TG (1897) Papers and notes on the genesis and matrix of the diamond. Longmans, Green and Co., London
Li JP, O'Neill HSC, Seifert F (1995) Subsolidus phase-relations in the system MgO–SiO_2–Cr–O in equilibrium with metallic Cr, and their significance for the petrochemistry of chromium. J Petrol 36:107-132
Li XL, Zhang LF, Wei CJ, Slabunov AI (2015) Metamorphic *PT* path and zircon U–Pb dating of Archean eclogite association in Gridino complex, Belomorian province, Russia. Precambrian Res 268:74–96
Li J-L, Schwarzenbach EM, John T, Ague JJ, Huang F, Gao J, Klemd R, Whitehouse MJ, Wang X-S (2020) Uncovering and quantifying the subduction zone sulfur cycle from the slab perspective. Nature Commun 11:514
Liou JG, Tsujimori T, Zhang RY, Katayama I, Maruyama S (2004) Global UHP metamorphism and continental subduction/collision: The Himalayan model. Int Geol Rev 46:1–27
Litasov KD, Shatskiy A, Ohtani E (2014) Melting and subsolidus phase relations in peridotite and eclogite systems with reduced C–O–H fluid at 3–16 GPa. Earth Planet Sci Lett 391:87–99
Liu J, Pearson DG, Wang LH, Mather KA, Kjarsgaard BA, Schaeffer AJ, Irvine GJ, Kopylova MG, Armstrong JP (2021) Plume-driven recratonization of deep continental lithospheric mantle. Nature 592:732–736
Luth RW (1993) Diamonds, eclogites, and the oxidation-state of the Earth's mantle. Science 261:66–68
Luth RW, Stachel T (2014) The buffering capacity of lithospheric mantle: implications for diamond formation. Contrib Mineral Petrol 168:1–12
Luth RW, Palyanov YN, Bureau H (2022) Experimental petrology applied to natural diamond growth. Rev Mineral Geochem 88:755–808
MacGregor ID, Carter JL (1970) The chemistry of clinopyroxenes and garnets of eclogite and peridotite xenoliths from the Roberts Victor mine, South Africa. Phys Earth Planet Sci 3:391–397
MacGregor ID, Manton WI (1986) Roberts Victor eclogites—Ancient oceanic crust. J Geophys Res 91:14063–14079
Mahotkin IL, Gibson SA, Thompson RN, Zhuravlev DZ, Zherdev PU (2000) Late Devonian diamondiferous kimberlite and alkaline picrite (proto-kimberlite?) magmatism in the Arkhangelsk region, NW Russia. J Petrol 41:201–227
Malinovsky IY, Doroshev AM (1975) Effect of temperature and pressure on the composition of Cr-bearing phases of the garnet + enstatite + spinel + forsterite associations. Experimental research on mineralogy. Bull Inst Geol Geophys, Novosibirsk, p 121–125 (in Russian)
Matjuschkin V, Woodland AB, Yaxley GM (2019) Methane-bearing fluids in the upper mantle: an experimental approach. Contrib Mineral Petrol 174:1
Mattey D, Lowry D, Macpherson C (1994) Oxygen-isotope composition of mantle peridotite. Earth Planet Sci Lett 128:231–241
McCandless TE, Gurney JJ (1989) Sodium in garnet and potassium in clinopyroxene: Criteria for classifying mantle eclogites. *In*: Kimberlites and Related Rocks, Vol 2 Their Mantle/Crust Setting, Diamonds and Diamond Exploration. Vol 14. Ross J, Jacques AL, Ferguson J, Green DH, O'Reilly SY, Danchin RV, Janse AJA (eds) Geological Society of Australia Special Publication No. 14. Blackwell Scientific, Carlton, p 827–832
McDonough WF, Rudnick RL (1998) Mineralogy and composition of the upper mantle. Rev Mineral 37:139–164
McDonough WF, Sun S-S (1995) The composition of the Earth. Chem Geol 120:223–253
Meen JK, Eggler DH, Ayers JC (1989) Experimental evidence for very low solubility of rare-earth elements in CO_2-rich fluids at mantle conditions. Nature 340:301–303
Menzel MD, Garrido CJ, López Sánchez-Vizcaíno V (2020) Fluid-mediated carbon release from serpentinite-hosted carbonates during dehydration of antigorite–serpentinite in subduction zones. Earth Planet Sci Lett 531:115964
Meyer HOA (1968) Chrome pyrope: an inclusion in natural diamond. Science 160:1446–1447
Meyer HOA (1987) Inclusions in diamond. *In*: Mantle xenoliths. Nixon PH, (ed) John Wiley & Sons Ltd., Chichester, p 501–522
Meyer HOA, Boyd FR (1972) Composition and origin of crystalline inclusions in natural diamonds. Geochim Cosmochim Acta 36:1255–1273
Mibe K, Fujii T, Yasuda A (1998) Connectivity of aqueous fluid in the Earth's upper mantle. Geophys Res Lett 25:1233–1236
Mikhailenko D, Stagno V, Korsakov AV, Andreozzi GB, Marras G, Cerantola V, Malygina EV (2020) Redox state determination of eclogite xenoliths from Udachnaya kimberlite pipe (Siberian craton), with some implications for the graphite/diamond formation. Contrib Mineral Petrol 175:107
Misra KC, Anand M, Taylor LA, Sobolev NV (2004) Multi-stage metasomatism of diamondiferous eclogite xenoliths from the Udachnaya kimberlite pipe, Yakutia, Siberia. Contrib Mineral Petrol 146:696–714
Mitchell AL, Grove TL (2015) Melting the hydrous, subarc mantle: the origin of primitive andesites. Contrib Mineral Petrol 170:13
Mitchell RS, Giardini AA (1953) Oriented olivine inclusions in diamond. Am Mineral 38:136–138
Moss SW, Kobussen A, Powell W, Pollock K (2018) Kimberlite emplacement and mantle sampling through time at A154N kimberlite volcano, Diavik Diamond Mine: lessons from the deep. Mineral Petrol 112:397–410
Muehlenbachs K, Clayton RN (1972a) Oxygen isotope studies of fresh and weathered submarine basalts. Can J Earth Sci 9:172–184
Muehlenbachs K, Clayton RN (1972b) Oxygen isotope geochemistry of submarine greenstones. Can J Earth Sci 9:471–478

Navon O, Stolper E (1987) Geochemical consequences of melt percolation: The upper mantle as a chromatographic column. J Geol 95:285–307
Nestola F, Nimis P, Angel RJ, Milani S, Bruno M, Prencipe M, Harris JW (2014) Olivine with diamond-imposed morphology included in diamonds. Syngenesis or protogenesis? Int Geol Rev 56:1658–1667
Nestola F, Jung H, Taylor LA (2017) Mineral inclusions in diamonds may be synchronous but not syngenetic. Nat Commun 8:14168–14168
Nestola F, Jacob DE, Pamato MG, Pasqualetto L, Oliveira B, Greene S, Perritt S, Chinn I, Milani S, Kueter N, Sgreva N (2019a) Protogenetic garnet inclusions and the age of diamonds. Geology 47:431–434
Nestola F, Zaffiro G, Mazzucchelli ML, Nimis P, Andreozzi GB, Periotto B, Princivalle F, Lenaz D, Secco L, Pasqualetto L, Logvinova AM (2019b) Diamond-inclusion system recording old deep lithosphere conditions at Udachnaya (Siberia). Sci Rep 9:12586
Nickel KG, Green DH (1985) Empirical geothermobarometry for garnet peridotites and implications for the nature of the lithosphere, kimberlites and diamonds. Earth Planet Sci Lett 73:158–170
Nimis P (2022) Pressure and temperature data for diamonds. Rev Mineral Geochem 88:533–566
Nimis P, Alvaro M, Nestola F, Angel RJ, Marquardt K, Rustioni G, Harris JW, Marone F (2016) First evidence of hydrous silicic fluid films around solid inclusions in gem-quality diamonds. Lithos 260:384–389
Nixon PH, Rogers NW, Gibson IL, Grey A (1981) Depleted and fertile mantle xenoliths from southern African kimberlites. Annu Rev Earth Planet Sci 9:285–309
Norman M, Garcia MO, Pietruszka AJ (2005) Trace-element distribution coefficients for pyroxenes, plagioclase, and olivine in evolved tholeiites from the 1955 eruption of Kilauea Volcano, Hawai'i, and petrogenesis of differentiated rift-zone lavas. Am Mineral 90:888–899
O'Hara MJ, Saunders M, Mercy ELP (1975) Garnet peridotite, possible ultrabasic magmas and eclogite: interpretation of upper mantle processes in kimberlite. Phys Chem Earth 9:681–713
O'Neill HSC, Wall VJ (1987) The olivine-orthopyroxene-spinel oxygen-geobarometer, the nickel precipitation curve and the oxygen fugacity of the earth's upper mantle. J Petrol 28:1169–1191
O'Reilly SY, Griffin WL (1995) Trace-element partitioning between garnet and clinopyroxene in mantle-derived pyroxenites and eclogites—*P–T–X* controls. Chem Geol 121:105–130
O'Reilly SY, Griffin WL (2013) Mantle metasomatism. *In*: Metasomatism and the Chemical Transformation of Rock. Harlov DE, Austrheim H (eds) Springer Verlag, Berlin Heidelberg, p 471–533
Orlov YL (1959) Oriented olivine inclusions in diamond. Tr Mineral Muz, Akad Nauk SSSR 10:103–120 (in Russian)
Orlov YL (1977) The mineralogy of the diamond. John Wiley & Sons, New York
Pamato MG, Novella D, Jacob DE, Oliveira B, Pearson DG, Greene S, Afonso JC, Favero M, Stachel T, Alvaro M, Nestola F (2021) Protogenetic sulfide inclusions in diamonds date the diamond formation event using Re–Os isotopes. Geology 49:941–945
Pearson DG, Wittig N (2008) Formation of Archaean continental lithosphere and its diamonds: the root of the problem. J Geol Soc 165:895–914
Pearson DG, Wittig N (2014) The formation and evolution of cratonic mantle lithosphere—Evidence from mantle xenoliths. *In*: Treatise on Geochemistry (Second Edition). Turekian HDHK, (ed) Elsevier, Oxford, p 255–292
Pearson NJ, O'Reilly SY, Griffin WL (1995) The crust–mantle boundary beneath cratons and craton margins: A transect across the south-west margin of the Kaapvaal craton. Lithos 36:257–287
Pearson DG, Shirey SB, Harris JW, Carlson RW (1998) Sulphide inclusions in diamonds from the Koffiefontein kimberlite, S Africa: constraints on diamond ages and mantle Re–Os systematics. Earth Planet Sci Lett 160:311–326
Pearson DG, Canil D, Shirey SB (2004) Mantle samples included in volcanic rocks: xenoliths and diamonds. *In*: Treatise on Geochemistry Volume 2: The Mantle and Core. Carlson RW, (ed) Elsevier-Pergamon, Oxford, p 171–275
Pearson DG, Scott JM, Liu J, Schaeffer A, Wang LH, van Hunen J, Szilas K, Chacko T, Kelemen PB (2021) Deep continental roots and cratons. Nature 596:199–210
Penniston-Dorland SC, Kohn MJ, Manning CE (2015) The global range of subduction zone thermal structures from exhumed blueschists and eclogites: Rocks are hotter than models. Earth Planet Sci Lett 428:243–254
Perchuk AL, Gerya TV, Zakharov VS, Griffin WL (2020) Building cratonic keels in Precambrian plate tectonics. Nature 586:395–401
Phillips D, Harris JW, Viljoen KS (2004) Mineral chemistry and thermobarometry of inclusions from De Beers Pool diamonds, Kimberley, South Africa. Lithos 77:155–179
Phillips D, Harris JW, de Wit MCJ, Matchan EL (2018) Provenance history of detrital diamond deposits, west coast of Namaqualand, South Africa. Mineral Petrol 112:259–273
Philpotts JA, Schnetzler CC, Thomas HH (1972) Petrogenetic implications of some new geochemical data on eclogitic and ultrabasic inclusions. Geochim Cosmochim Acta 36:1131–1166
Piccoli F, Hermann J, Pettke T, Connolly JAD, Kempf ED, Duarte JFV (2019) Subducting serpentinites release reduced, not oxidized, aqueous fluids. Sci Rep 9:19573
Pollack HN, Chapman DS (1977) On the regional variation of heat-flow, geotherms, and lithospheric thickness. Tectonophysics 38:279–296
Rapp RP, Watson EB (1995) Dehydration melting of metabasalt at 8–32 kbar - Implications for continental growth and crust-mantle recycling. J Petrol 36:891–931

Rapp RP, Timmerman S, Lowczak J, Jaques AL (2017) Metasomatism of cratonic lithosphere by hydrous, silica-rich, fluids derived from recycled sediment: experimental insights at 5–7 GPa. International Kimberlite Conference: Extended Abstracts #11
Regier ME, Mišković A, Ickert RB, Pearson DG, Stachel T, Stern RA, Kopylova M (2018) An oxygen isotope test for the origin of Archean mantle roots. Geochem Perspect Lett 9:6–10
Richardson SH (1986) Latter-day origin of diamonds of eclogitic paragenesis. Nature 322:623–626
Richardson SH, Shirey SB (2008) Continental mantle signature of Bushveld magmas and coeval diamonds. Nature 453:910–913
Richardson SH, Gurney JJ, Erlank AJ, Harris JW (1984) Origin of diamonds in old enriched mantle. Nature 310:198–202
Richardson SH, Shirey SB, Harris JW, Carlson RW (2001) Archean subduction recorded by Re–Os isotopes in eclogitic sulfide inclusions in Kimberley diamonds. Earth Planet Sci Lett 191:257–266
Richardson SH, Pöml PF, Shirey SB, Harris JW (2009) Age and origin of peridotitic diamonds from Venetia, Limpopo Belt, Kaapvaal–Zimbabwe craton. Lithos 112:785–792
Robinson DN, Gurney JJ, Shee SR (1984) Diamond eclogite and graphite eclogite xenoliths from Orapa, Botswana. *In*: Kimberlites, II The Mantle and Crust-Mantle Relationships. Kornprobst J, (ed) Elsevier, Amsterdam, p 11–24
Rohrbach A, Schmidt MW (2011) Redox freezing and melting in the Earth's deep mantle resulting from carbon-iron redox coupling. Nature 472:209–212
Rudnick RL, Fountain DM (1995) Nature and composition of the continental crust: A lower crustal perspective. Rev Geophys 33:267–309
Rudnick RL, McDonough WF, Chappell BW (1993) Carbonatite metasomatism in the northern Tanzanian mantle: Petrographic and geochemical characteristics. Earth Planet Sci Lett 114:463 - 475
Rudnick RL, Donough WL, Orpin A (1994) Northern Tanzanian peridotite xenoliths: a comparison with Kaapvaal peridotites and inferences on metasomatic interactions. *In*: Kimberlites, Related Rocks and Mantle Xenoliths. Vol 1/A. Meyer HOA, Leonardos OH, (eds). CPRM Spec Publ Jan/94, Brasilia, p 336–353.
Rüpke LH, Morgan JP, Hort M, Connolly JAD (2004) Serpentine and the subduction zone water cycle. Earth Planet Sci Lett 223:17–34
Rustioni G, Audetat A, Keppler H (2021) The composition of subduction zone fluids and the origin of the trace element enrichment in arc magmas. Contrib Mineral Petrol 176:51
Schmädicke E, Okrusch M, Rupprecht-Gutowski P, Will TM (2011) Garnet pyroxenite, eclogite and alkremite xenoliths from the off-craton Gibeon Kimberlite Field, Namibia: A window into the upper mantle of the Rehoboth Terrane. Precambrian Res 191:1–17
Schmidt MW, Poli S (2014) Devolatilization during subduction. *In*: Treatise on Geochemistry 2nd Edition—The Crust. Holland HD, Turekian KK, Rudnick RL, (eds). Elsevier/Pergamon, Amsterdam, p 669-701
Schulze DJ (1989) Constraints on the abundance of eclogite in the upper mantle. J Geophys Res-Solid Earth Planets 94:4205–4212
Schulze DJ (2003) A classification scheme for mantle-derived garnets in kimberlite: a tool for investigating the mantle and exploring for diamonds. Lithos 71:195–213
Schulze DJ, Harte B, Valley JW, Brenan JM, Channer DMD (2003) Extreme crustal oxygen isotope signatures preserved in coesite in diamond. Nature 423:68–70
Scott Smith BH, Danchin RV, Harris JW, Stracke KJ (1984) Kimberlites near Orroroo, South Australia. *In*: Kimberlites I: Kimberlites and related rocks. Kornprobst J, (ed) Elsevier, Amsterdam, p 121–142
Sharma M, Wasserburg GJ (1996) The neodymium isotopic compositions and rare earth patterns in highly depleted ultramafic rocks. Geochim Cosmochim Acta 60:4537–4550
Sharp WE (1966) Pyrrhotite: a common inclusion in South African diamonds. Nature 211:402–403
Shatskiy A, Arefiev AV, Podborodnikov IV, Litasov KD (2019) Origin of K-rich diamond-forming immiscible melts and CO_2 fluid via partial melting of carbonated pelites at a depth of 180–200 km. Gondwana Res 75:154–171
Shchukina EV, Agashev AM, Pokhilenko NP (2017) Metasomatic origin of garnet xenocrysts from the V. Grib kimberlite pipe, Arkhangelsk region, NW Russia. Geosci Front 8:641–651
Shimizu N (1975) Rare earth elements in garnets and clinopyroxenes from garnet lherzolite nodules in kimberlites. Earth Planet Sci Lett 25:26–32
Shimizu N, Richardson SH (1987) Trace element abundance patterns of garnet inclusions in peridotite-suite diamonds. Geochim Cosmochim Acta 51:755–758
Shirey SB, Richardson SH (2011) Start of the Wilson Cycle at 3 Ga shown by diamonds from subcontinental mantle. Science 333:434–436
Shirey SB, Harris JW, Richardson SH, Fouch MJ, James DE, Cartigny P, Deines P, Viljoen KS (2002) Diamond genesis, seismic structure, and evolution of the Kaapvaal-Zimbabwe craton. Science 297:1683–1686
Shirey SB, Wagner LS, Walter MJ, Pearson DG, van Keken PE (2021) Slab transport of fluids to deep focus earthquake depths - thermal modeling constraints and evidence from diamonds. AGU Adv 2:e2020AV000304
Shu Q, Brey GP (2015) Ancient mantle metasomatism recorded in subcalcic garnet xenocrysts: Temporal links between mantle metasomatism, diamond growth and crustal tectonomagmatism. Earth Planet Sci Lett 418:27–39

Simon NSC, Carlson RW, Pearson DG, Davies GR (2007) The origin and evolution of the Kaapvaal cratonic lithospheric mantle. J Petrol 48:589–625
Smart KA, Heaman LM, Chacko T, Simonetti A, Kopylova M, Mah D, Daniels D (2009) The origin of high-MgO diamond eclogites from the Jericho Kimberlite, Canada. Earth Planet Sci Lett 284:527–537
Smart KA, Chacko T, Stachel T, Tappe S, Stern RA, Ickert RB, EIMF (2012) Eclogite formation beneath the northern Slave craton constrained by diamond inclusions: Oceanic lithosphere origin without a crustal signature. Earth Planet Sci Lett 319:165–177
Smit KV, Stachel T, Stern RA (2014a) Diamonds in the Attawapiskat area of the Superior craton (Canada): evidence for a major diamond-forming event younger than 1.1 Ga. Contrib Mineral Petrol 167:1–16
Smit KV, Stachel T, Creaser RA, Ickert RB, DuFrane SA, Stern RA, Seller M (2014b) Origin of eclogite and pyroxenite xenoliths from the Victor kimberlite, Canada, and implications for Superior craton formation. Geochim Cosmochim Acta 125:308–337
Smit KV, Shirey SB, Hauri EH, Stern RA (2019a) Sulfur isotopes in diamonds reveal differences in continent construction. Science 364:383–385
Smit KV, Stachel T, Luth RW, Stern RA (2019b) Evaluating mechanisms for eclogitic diamond growth: An example from Zimmi Neoproterozoic diamonds (West African craton). Chem Geol 520:21–32
Smit KV, Timmerman S, Aulbach S, Shirey SB, Richardson SH, Phillips D, Pearson DG (2022) Geochronology of diamonds. Rev Mineral Geochem 88:567–636
Smith D (1988) Implications of zoned garnets for the evolution of sheared lherzolites: Examples from northern Lesotho and the Colorado Plateau. J Geophys Res: Solid Earth 93:4895–4905
Smith D, Griffin WL, Ryan CG (1993) Compositional evolution of high-temperature sheared lherzolite PHN 1611. Geochim Cosmochim Acta 57:605–613
Smith EM, Shirey SB, Nestola F, Bullock ES, Wang JH, Richardson SH, Wang WY (2016) Large gem diamonds from metallic liquid in Earth's deep mantle. Science 354:1403–1405
Snyder GA, Taylor LA, Crozaz G, Halliday AN, Beard BL, Sobolev VN, Sobolev NV (1997) The origins of Yakutian eclogite xenoliths. J Petrol 38:85–113
Sobolev NV (1977) Deep-seated inclusions in kimberlites and the problem of the composition of the upper mantle. (Translated from the Russian edition, 1974). AGU, Washington
Sobolev NV (1985) Ultramafic and eclogitic types of paragenesis of diamonds. Conference on Native Elements Formation in Endogenic Processes, Extended Abstracts. Acad Sci USSR, Siberian Division, Yakutsk, (not paginated)
Sobolev NV, Lavrent'ev YG, Pospelova LN, Sobolev VC (1969) Chrome pyrope from Yakutian diamonds. Doklady Akademii Nauk SSSR 189:133–136
Sobolev NV, Lavrent'ev YG, Pokhilenko NP, Usova LV (1973) Chrome-rich garnets from the kimberlites of Yakutia and their paragenesis. Contrib Mineral Petrol 40:39–52
Sobolev NV, Logvinova AM, Efimova ES (2009) Syngenetic phlogopite inclusions in kimberlite-hosted diamonds: implications for role of volatiles in diamond formation. Russ Geol Geophys 50:1234–1248
Spandler C, Pirard C (2013) Element recycling from subducting slabs to arc crust: A review. Lithos 170:208–223
Spencer LJ (1924) An inclusion of magnetite in diamond. Mineral Mag 20:245–247
Spetsius ZV, Taylor LA (2002) Partial melting in mantle eclogite xenoliths: Connections with diamond paragenesis. Int Geol Rev 44:973–987
Stachel T (2014) Diamond. Mineralogical Association of Canada Short Course Series 44:1–28
Stachel T, Harris JW (1997) Diamond precipitation and mantle metasomatism - evidence from the trace element chemistry of silicate inclusions in diamonds from Akwatia, Ghana. Contrib Mineral Petrol 129:143–154
Stachel T, Harris JW (2008) The origin of cratonic diamonds—Constraints from mineral inclusions. Ore Geol Rev 34:5–32
Stachel T, Luth RW (2015) Diamond formation — Where, when and how? Lithos 220–223:200–220
Stachel T, Viljoen KS, Brey G, Harris JW (1998) Metasomatic processes in lherzolitic and harzburgitic domains of diamondiferous lithospheric mantle: REE in garnets from xenoliths and inclusions in diamonds. Earth Planet Sci Lett 159:1–12
Stachel T, Aulbach S, Brey GP, Harris JW, Leost I, Tappert R, Viljoen KS (2004) The trace element composition of silicate inclusions in diamonds: a review. Lithos 77:1–19
Stachel T, Banas A, Muehlenbachs K, Kurszlaukis S, Walker EC (2006) Archean diamonds from Wawa (Canada): samples from deep cratonic roots predating cratonization of the Superior Province. Contrib Mineral Petrol 151:737–750
Stachel T, Chacko T, Luth RW (2017) Carbon isotope fractionation during diamond growth in depleted peridotite: Counterintuitive insights from modelling water-maximum CHO fluids as multi-component systems. Earth Planet Sci Lett 473:44–51
Stachel T, Harris JW, Hunt L, Muehlenbachs K, Kobussen AF, EIMF (2018a) Argyle diamonds: How subduction along the Kimberley Craton edge generated the world's biggest diamond deposit. *In*: Geoscience and Exploration of the Argyle, Bunder, Diavik, and Murowa Diamond Deposits. Vol 20. Davy AT, Smith CB, Helmstaedt H, Lynton Jaques A, Gurney JJ, (eds). Society of Economic Geologists, p 145–167

Stachel T, Banas A, Aulbach S, Smit KV, Wescott P, Chinn IL, Kong J (2018b) The Victor Mine (Superior Craton, Canada): Neoproterozoic lherzolitic diamonds from a thermally-modified cratonic root. Mineral Petrol 112:325–336
Stachel T, Cartigny P, Chacko T, Pearson DG (2022) Carbon and nitrogen in mantle-derived diamonds. Rev Mineral Geochem 88:809–876
Stagno V, Ojwang DO, McCammon CA, Frost DJ (2013) The oxidation state of the mantle and the extraction of carbon from Earth's interior. Nature 493:84–88
Stagno V, Frost DJ, McCammon CA, Mohseni H, Fei Y (2015) The oxygen fugacity at which graphite or diamond forms from carbonate-bearing melts in eclogitic rocks. Contrib Mineral Petrol 169:16
Stalder R, Foley SF, Brey GP, Horn I (1998) Mineral-aqueous fluid partitioning of trace elements at 900–1200°C and 3.0–5.7 GPa: new experimental data for garnet, clinopyroxene, and rutile, and implications for mantle metasomatism. Geochim Cosmochim Acta 62:1781–1801
Stosch HG, Lugmair GW (1986) Trace element and Sr and Nd isotope geochemistry of peridotite xenoliths from the Eifel (West Germany) and their bearing on the evolution of the subcontinental lithosphere. Earth Planet Sci Lett 80:281–298
Streckeisen A (1976) To each plutonic rock its proper name. Earth Sci Rev 12:1–33
Sun S-S, McDonough WF (1989) Chemical and isotopic systematics of oceanic basalts: implications for mantle compositions and processes. *In*: Magmatism in the ocean basins. Vol 42. Saunders AD, Norry MJ (eds) Geol Soc Spec Publ, p 313–345
Sutton JR (1907) The relationship between diamonds and garnets. Nature 75:488–488
Sutton JR (1921) Inclusions in diamond from South Africa. Mineral Mag 19:208–210
Sverjensky DA, Huang F (2015) Diamond formation due to a pH drop during fluid–rock interactions. Nature Communications 6:8702
Syracuse EM, van Keken PE, Abers GA (2010) The global range of subduction zone thermal models. Phys Earth Planet Sci 183:73–90
Tappe S, Foley SF, Kjarsgaard BA, Romer RL, Heaman LM, Stracke A, Jenner GA (2008) Between carbonatite and lamproite - Diamondiferous Torngat ultramafic lamprophyres formed by carbonate-fluxed melting of cratonic MARID-type metasomes. Geochim Cosmochim Acta 72:3258–3286
Tavernier JB (1676) Travels in India. Translated from French original by V. Ball, 1889. Macmillan and Co., London
Taylor WR (1998) An experimental test of some geothermometer and geobarometer formulations for upper mantle peridotites with application to the thermobarometry of fertile lherzolite and garnet websterite. N Jb Miner Abh 172:381–408
Taylor LA, Neal CR (1989) Eclogites with oceanic crustal and mantle signatures from the Bellsbank kimberlite, South Africa. 1. Mineralogy, petrography and whole rock chemistry. J Geol 97:551–567
Thomassot E, Cartigny P, Harris JW, Lorand JP, Rollion-Bard C, Chaussidon M (2009) Metasomatic diamond growth: A multi-isotope study (^{13}C, ^{15}N, ^{33}S, ^{34}S) of sulphide inclusions and their host diamonds from Jwaneng (Botswana). Earth Planet Sci Lett 282:79–90
Thomson AR, Walter MJ, Kohn SC, Brooker RA (2016) Slab melting as a barrier to deep carbon subduction. Nature 529:76–79
Timmerman S, Koornneef JM, Chinn IL, Davies GR (2017) Dated eclogitic diamond growth zones reveal variable recycling of crustal carbon through time. Earth Planet Sci Lett 463:178–188
Tomlinson EL, Kamber BS (2021) Depth-dependent peridotite–melt interaction and the origin of variable silica in the cratonic mantle. Nat Commun 12:1082
Uenver-Thiele L, Woodland AB, Seitz H-M, Downes H, Altherr R (2017) Metasomatic processes revealed by trace element and redox signatures of the lithospheric mantle beneath the Massif Central, France. J Petrol 58:395–422
Ulmer P (1989) Partitioning of high field strength elements among olivine, pyroxenes, garnet and calc-alkaline picrobasalt: Experimental results and application. Inter J Mass Spectrom Ion Phys 1989:42–47
Viljoen KS, Harris JW, Ivanic T, Richardson SH, Gray K (2014) Trace element chemistry of peridotitic garnets in diamonds from the Premier (Cullinan) and Finsch kimberlites, South Africa: Contrasting styles of mantle metasomatism. Lithos 208–209:1–15
Viljoen KS, Perritt SH, Chinn IL (2018) An unusual suite of eclogitic, websteritic and transitional websteritic-lherzolitic diamonds from the Voorspoed kimberlite in South Africa: Mineral inclusions and infrared characteristics. Lithos 320–321:416–434
Vitale Brovarone A, Tumiati S, Piccoli F, Ague JJ, Connolly JAD, Beyssac O (2020) Fluid-mediated selective dissolution of subducting carbonaceous material: Implications for carbon recycling and fluid fluxes at forearc depths. Chem Geol 549:119682
Wagner PA (1914) The diamond fields of Southern Africa. Transvaal Leader, Johannesburg
Walter MJ (1999) Melting residues of fertile peridotite and the origin of cratonic lithosphere. *In*: Mantle Petrology: Field Observations and High Pressure Experimentation: A tribute to Francis R (Joe) Boyd. Vol 6. Fei Y, Bertka CM, Mysen BO, (eds). The Geochemical Society, Houston, p 225–239
Walter MJ, Thomson AR, Smith EM (2022) Geochemistry of silicate and oxide inclusions in sublithospheric diamonds. Rev Mineral Geochem 88:393–450

Wang H, van Hunen J, Pearson DG (2018) Making Archean cratonic roots by lateral compression: A two-stage thickening and stabilization model. Tectonophysics 746:562–571
Wang W (1998) Formation of diamond with mineral inclusions of ''mixed'' eclogite and peridotite paragenesis. Earth Planet Sci Lett 160:831–843
Waters FG, Erlank AJ (1988) Assessment of the vertical extent and distribution of mantle metasomatism below Kimberley, South Africa. J Petrol Spec Vol:185–204
Watson EB, Brenan JM, Baker DR (1990) Distribution of fluids in the continental mantle. *In*: Continental Mantle. Vol 16. Menzies MA (ed) Oxford Monographs on Geology and Geophysics, p 111–125
Weiss Y, Goldstein SL (2018) The involvement of diamond-forming fluids in the metasomatic "cocktail' of kimberlite sources. Mineral Petrol 112:149–167
Weiss Y, Griffin WL, Bell DR, Navon O (2011) High-Mg carbonatitic melts in diamonds, kimberlites and the sub-continental lithosphere. Earth Planet Sci Lett 309:337–347
Weiss Y, Griffin WL, Navon O (2013) Diamond-forming fluids in fibrous diamonds: The trace-element perspective. Earth Planet Sci Lett 376:110–125
Weiss Y, Kiflawi I, Davies N, Navon O (2014) High-density fluids and the growth of monocrystalline diamonds. Geochim Cosmochim Acta 141:145–159
Weiss Y, McNeill J, Pearson DG, Nowell GM, Ottley CJ (2015) Highly saline fluids from a subducting slab as the source for fluid-rich diamonds. Nature 524:339–342
Weiss Y, Cazs J, Navon O (2022) Fluid inclusions in fibrous diamonds. Rev Mineral Geochem 88:475–532
Welke HJ, Allsopp HL, Harris JW (1974) Measurements of K, Rb, U, Sr, and Pb in diamonds containing inclusions. Nature 252:35–36
White WM, Klein EM (2014) Composition of the oceanic crust. *In*: Treatise on Geochemistry 2nd Edition. Vol 2. Holland HD, Turekian KK, Carlson RW (eds) Elsevier Pergamon, Amsterdam, p 457–496
Wiggers de Vries DF, Pearson DG, Bulanova GP, Smelov AP, Pavlushin AD, Davies GR (2013) Re–Os dating of sulphide inclusions zonally distributed in single Yakutian diamonds: Evidence for multiple episodes of Proterozoic formation and protracted timescales of diamond growth. Geochim Cosmochim Acta 120:363–394
Wijbrans CH, Klemme S, Berndt J, Vollmer C (2015) Experimental determination of trace element partition coefficients between spinel and silicate melt: the influence of chemical composition and oxygen fugacity. Contrib Mineral Petrol 169:45
Williams AF (1932) The genesis of the diamond. Ernest Benn Limited, London
Wolff-Boenisch B (1994) Aufbau der Analytik zur Messung der Osmium-Isotopie sowie die Strontium-, Neodym- und Osmium-Systematik eines Hoch-Temperatur-Granat-Lherzoliths (J4) von Jagersfontein (Südafrika). Dipl Thesis, University of Mainz (Germany)
Workman RK, Hart SR (2005) Major and trace element composition of the depleted MORB mantle (DMM). Earth Planet Sci Lett 231:53–72
Wyllie PJ (1987) Metasomatism and fluid generation in mantle xenoliths. *In*: Mantle Xenoliths. Nixon PH (ed) John Wiley & Sons Ltd., Chichester, p 609–621
Wyllie PJ (1992) Experimental petrology: Earth materials science. *In*: Understanding Earth. Brown GC, Hawkesworth CJ, Wilson RCL, (eds). Cambridge University Press, Cambridge, p 67–87
Wyllie PJ, Huang W-L (1976) Carbonation and melting reactions in the system CaO–MgO–SiO_2–CO_2 at mantle pressures with geophysical and petrological applications. Contrib Mineral Petrol 54:79–107
Wyllie PJ, Ryabchikov ID (2000) Volatile components, magmas, and critical fluids in upwelling mantle. J Petrol 41:1195–1206
Yaxley GM (1993) Carbonatite metasomatism in the mantle: sources and roles of carbonate in metasomatic enrichment processes in the lithosphere. PhD thesis University of Tasmania
Yaxley GM, Green DH (1998) Reactions between eclogite and peridotite: Mantle refertilisation by subduction of oceanic crust. Schweizerische Mineralogische und Petrographische Mitteilungen 78:243–255
Zedgenizov DA, Kagi H, Shatsky VS, Sobolev NV (2004) Carbonatitic melts in cuboid diamonds from Udachnaya kimberlite pipe (Yakutia): evidence from vibrational spectroscopy. Mineral Mag 68:61–73
Zhang C, Duan ZH (2010) GFluid: An Excel spreadsheet for investigating C–O–H fluid composition under high temperatures and pressures. Computers Geosci 36:569–572
Zhu J, Zhang L, Tao R, Fei Y (2020) The formation of graphite-rich eclogite vein in S.W. Tianshan (China) and its implication for deep carbon cycling in subduction zone. Chem Geol 533
Ziaja K, Foley SF, White RW, Buhre S (2014) Metamorphism and melting of picritic crust in the early Earth. Lithos 189:173–184
Ziberna L, Klemme S, Nimis P (2013) Garnet and spinel in fertile and depleted mantle: insights from thermodynamic modelling. Contrib Mineral Petrol 166:411–421